NEUTRON-NEUTRON SCATTERING PARAMETERS

FROM THE

^{3}He(d,t)2p AND ^{3}H(d,^{3}He)2n REACTIONS

Thesis by

Harold Theodore Larson

In Partial Fulfillment of the Requirements

For the Degree of

Doctor of Philosophy

California Institute of Technology

Pasadena, California

1970

(Submitted September 18, 1969)

ii

ACKNOWLEDGEMENTS

It is my sincere pleasure to acknowledge the constant encouragement and patience given by Dr. T. A. Tombrello; without his help this study would neither have begun nor have been completed. Two others have also been essential to this research, and I am deeply indebted to them for their efforts: to Dr. A. D. Bacher for his instruction and guidance in the experimental phases of this work, and to Dr. K. Nagatani for his tutoring and aid in the theoretical aspects of this research.

Thanks are given to the entire Kellogg Radiation Laboratory faculty and staff for their support and aid. Particular thanks are given to Mrs. B. A. Zimmerman for her assistance with many computational problems and to Dr. R. J. Spiger for his counsel on the ways of handling tritium.

The continuing support of the California Institute of Technology is gratefully acknowledged. This research has been supported in part by the Office of Naval Research and the National Science Foundation.

Above all, I thank my wife, Donna, for her never-ending help.

ABSTRACT

The energy spectra of tritons and Helium-3 nuclei from the reactions $^3\text{He}(d,t)2p$, $^3\text{H}(d,^3\text{He})2n$, $^3\text{He}(d,^3\text{He})pn$, and $^3\text{H}(d,t)pn$ were measured between 6° and 20° at a bombarding energy of 10.9 MeV. An upper limit of 5 μb/sr. was obtained for producing a bound di-neutron at 6° and 7.5°. The $^3\text{He}(d,t)2p$ and $^3\text{H}(d,^3\text{He})2n$ data, together with previous measurements at higher energies, have been used to investigate whether one can unambiguously extract information on the two-nucleon system from these three-body final state reactions. As an aid to these theoretical investigations, Born approximation calculations were made employing realistic nucleon-nucleon potentials and an antisymmetrized final state wave function for the five-particle system. These calculations reproduce many of the features observed in the experimental data and indicate that the role of exchange processes cannot be ignored. The results show that previous attempts to obtain information on the neutron-neutron scattering length from the $^3\text{H}(d,^3\text{He})2n$ reaction may have seriously overestimated the precision that could be attained.

TABLE OF CONTENTS

LIST OF TABLES

I. INTRODUCTION

In recent years a number of reactions involving three strongly interacting particles in the final state have been used to determine low energy scattering parameters. This thesis describes an investigation of one of these reactions, $^3H(d,{}^3He)2n$, for making such a determination. The study was motivated by the desire both to learn something of the processes involved in this reaction and to determine to what extent these processes might affect measuring the neutron-neutron scattering parameters.

The neutron-neutron effective range parameters remain a missing link in the study of the low energy nucleon-nucleon system. A precise determination of these parameters would be helpful in confirming the charge symmetry of nuclear forces and in understanding the finer details of the nucleon-nucleon interaction. While it has been known for a long time that nuclear forces are nearly charge symmetric and, to a large extent, charge independent, small deviations from isospin conservation are to be expected. These symmetry-breaking forces, mostly attributable to electro-magnetic effects, are related to our basic understanding of nuclear interactions. An accurate measurement of the neutron-neutron effective range parameters would be helpful in making the electromagnetic corrections necessary for understanding these finer details.

The low energy nucleon-nucleon system has certain advantages in studying small departures from isospin conservation. At very low energies, only S waves contribute significantly to the scattering; accordingly, very accurate phase shift analyses can be made. Since a short range nuclear force dominates the interaction, the energy dependence of the phase shift can very nearly be expressed in a potential-independent way with the effective range expansion. Furthermore, because the ^1S_o state is almost bound, the scattering length is a sensitive measure of the nuclear interaction. Moravcsik (1964) has shown that for the nucleon-nucleon system a relative change in the scattering length is about ten times greater than the corresponding relative change in the potential. (For a review of isospin conservation that emphasizes the low energy nucleon-nucleon system, see the article of Henley, 1968).

The main problem in determining the neutron-neutron effective range parameters has been to find a suitably measureable neutron-neutron interaction. Direct scattering, the best way to make the measurement, has, as yet, not been feasible because of experimental limitations. There are no neutron sources available with the high flux required for a colliding beam experiment, and nuclear explosions have many practical problems to overcome before they could be used. Consequently, only indirect methods have been available for

determining the scattering parameters.

The desirability of measuring the neutron-neutron scattering length, coupled with the inability to use direct scattering, has prompted the development of the final state interaction approach to measuring a_{nn}. It has been recognized for a long time that interactions among the particles emerging from a nuclear reaction may strongly alter the measured spectra and cross sections. A familiar example of this effect is the influence of the Coulomb interaction on β-decay spectra. For β^--decay the number of low energy electrons in the spectrum is increased by the attractive Coulomb force between the daughter nucleus and the electron, while, for β^+-decay, the number is reduced by the repulsive force.

In interpreting the results of early pion-nucleon experiments, it was recognized that final state interactions profoundly influenced the observed spectra (Brueckner, 1951; Watson and Brueckner, 1951). Watson and Stuart (1951) proposed using the $D(\pi^-, \gamma)2n$ reaction to study the neutron-neutron scattering. They discussed how the interaction between the two neutrons in the final state would distort the γ-ray spectrum and gave a prescription for extracting the S-wave phase shift. In a later paper Watson (1952) gave a more general discussion of final state interactions. Migdal (1955) published a similar theory suitable for

nuclear reactions with three strongly interacting particles in the final state. In recent attempts to determine the nucleon-nucleon scattering parameters, the Watson-Migdal theory, or variations of it, has commonly been used to make the extraction from the observed spectra.

In 1961 Ilakovac, et al. observed a pronounced peak in the small-angle proton spectrum from the $D(n,p)2n$ reaction. Interpreting this peak as an enhancement in the differential cross section due to a final state interaction between the neutrons, they determined the neutron-neutron scattering length to be -22 ± 2 F. This apparent violation of the charge symmetry of nuclear forces helped to spark new interest in the low energy neutron-neutron system.

Since 1961 there have been a number of determinations of a_{nn} from $D(n,p)2n$ and other reactions with three strongly interacting particles in the final state. These experiments have measured widely different values of a_{nn}. Currently there is no adequate theory for reactions with three strongly interacting particles in the final state, and the approximations necessary for extracting a_{nn} are unreliable. It has been found that, for a given spectrum, the extracted a_{nn} depends critically upon assumptions made about the reaction's mechanism. Unless these assumptions are proven to be valid, the extracted value of a_{nn} must be considered unreliable.

Van Oers, et al. (1965) have proposed comparing mirror reactions as a method for eliminating the uncertainty in extracting a_{nn} from multinucleon reactions. The mirror reactions should be studied under conditions as similar as possible in order to match reaction mechanisms. This procedure would supposedly test the analysis used to determine a_{nn}, since the proton-proton effective range parameters are accurately known from direct scattering.

Baumgartner, et al. (1966) used the comparison procedure to determine $a_{nn} = -16.1 \pm 1$ F and the neutron-neutron effective range $r_{nn} = 3.2 \pm 1.6$ F from the $^3H(d,^3He)2n$ reaction. Use of the Watson-Migdal approximation was justified on the basis that it gave $a_{pp} = -7.69 \, ^{+0.61}_{-0.67}$ F from the $^3He(d,t)2p$ reaction, in agreement with the value determined from proton-proton scattering. While a_{nn} has also been determined from the $D(\pi^-,\gamma)2n$ reaction, the only experimental information known about r_{nn} is from the experiment of Baumgartner, et al.

Although the use of the Watson-Migdal approximation by Baumgartner, et al. appears to be successful, there are reasons for having reservations about the results. The approximation is only successful in extracting a_{pp} from the $^3He(d,t)2p$ reaction at very forward angles. The method fails for other, presumably simpler, proton-proton final state reactions like $D(p,n)2p$ and $^3He(p,d)2p$ and even

for the ^{3}He(d,t)2p reaction at more backward angles.
Because of the approximation's limited success, one wonders
if it is only by chance that the Watson-Migdal prediction
agrees with the ^{3}He(d,t)2p forward angle triton spectra.

This thesis describes a study of the ^{3}He(d,t)2p
and ^{3}H(d,^{3}He)2n reaction mechanisms and the applicability
of the Watson-Migdal approximation for determining the
neutron-neutron effective range parameters from the
^{3}H(d,^{3}He)2n reaction. Part II discusses the Watson-Migdal
approximation and summarizes some previous experimental
measurements of the proton-proton scattering length used
to test the theoretical analysis. Part III describes
experimental measurements of triton and ^{3}He spectra from
the ^{3}He(d,t)2p, ^{3}H(d,^{3}He)2n, ^{3}He(d,^{3}He)pn, and ^{3}H(d,t)pn
reactions which provide empirical evidence for a complex
reaction mechanism that would violate the assumptions of the
Watson-Migdal approximation. Part IV describes a plane wave
Born approximation calculation of all the first order con-
tributions to the transition amplitude of the ^{3}He(d,t)2p
and ^{3}H(d,^{3}He)2n reactions. The results of the calculation
show that reaction processes ignored in justifying the
Watson-Migdal approximation for very forward angles may
make important contributions to the reaction cross section.
At the same time, the calculated spectra for the very
backward angles are in substantial agreement with the

experimental observations. Part V discusses the applicability of the comparison method for the reactions studied and shows that the method is of limited value in determining the effective range parameters. Part VI summarizes the results of this study and concludes that values of the neutron-neutron effective range parameters determined from the ^{3}He(d,t)2p and ^{3}H(d,^{3}He)2n reactions are much more uncertain than previously believed.

II. FINAL STATE INTERACTIONS

The indirect method of measuring the neutron-neutron scattering length has partially been prompted by the development of easily applied theories. However, because of assumptions made in analyzing the observed spectra, the results of these measurements are often of questionable value. In this Part we briefly review the Watson-Migdal approximation, its limitations, and experimental results that illustrate some of the problems in its application. We also consider the plane wave Born approximation as an alternative model for analysis. The theoretical models are discussed by first introducing the concept of sequential reactions and indicating how this concept can be used to obtain an exact expression for the transition amplitude which includes the final state interaction.

A. Sequential reactions

Reactions with a two-nucleon final state interaction are often assumed to occur in two steps:

$$(1) \quad 1 + 2 \longrightarrow 3 + (N + N)$$
$$(2) \quad (N + N) \longrightarrow N + N$$
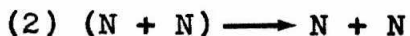
In Step (1), a primary reaction mechanism produces particle 3 and a virtual di-nucleon (N + N). Then in Step (2), a very short time later, the virtual di-nucleon decays into

the two nucleons, N and N. This process is indicated schematically in Figure 1. In order for this sequential assumption to be valid, the interaction between particle 3 and either of the nucleons must be much weaker than the interaction between the nucleons. This condition is often met in practice if the relative energy between particle 3 and the di-nucleon state is sufficiently high.

From an argument due to Watson (1952), we can intuitively see that a strong, attractive nucleon-nucleon final state interaction can significantly increase the transition probability for the reaction. Consider the reaction to be occurring in the time-reversed sense; then (referring to Figure 1) the attractive nucleon-nucleon interaction U causes the incident nucleons to momentarily "cling together" in the di-nucleon state until particle 3 interacts with them to produce particles 1 and 2. Thus, we would expect the amplitude for producing particles 1 and 2 to be enhanced if the relative energy in the nucleon-nucleon system is close to the resonance energy of the di-nucleon. We would also expect that the probability for the reaction to occur is roughly proportional to the nucleon-nucleon scattering cross section. Therefore, from detailed balancing, we would expect the corresponding three-body break-up reaction to be enhanced.

FIGURE 1

Schematic diagram of the sequential reaction mechanism.
Incident particles 1 and 2 interact via the primary process
V producing particle 3 and a virtual di-neucleon. The di-
nucleon decays via the final state interaction U into
nucleons N and N.
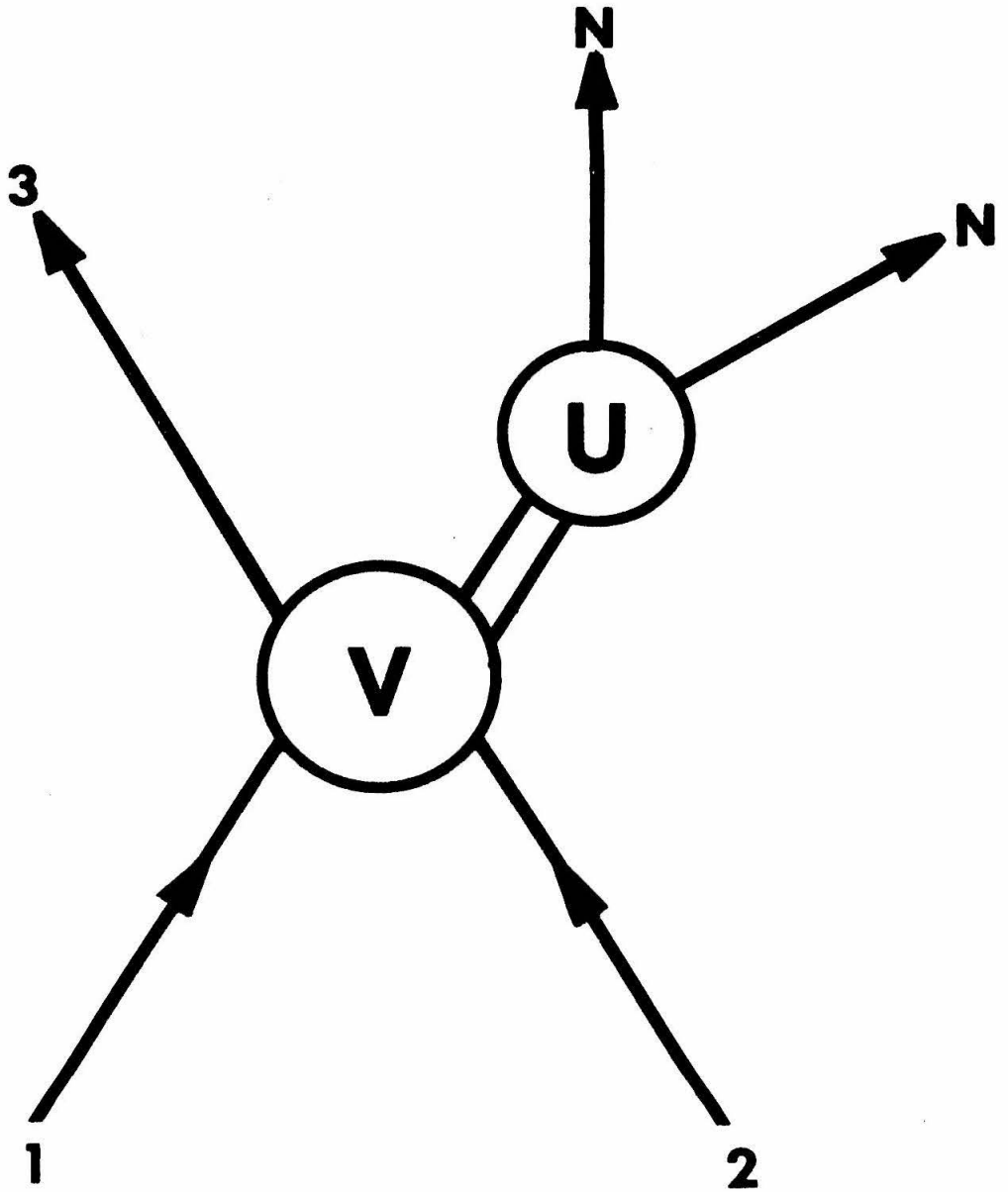
FIGURE 1

These qualitative ideas indicate how potential theory can incorporate final state interactions. Since derivations of the exact transition amplitude have been given elsewhere (see, for example, Watson (1952), Goldberger and Watson (1964), or Gillespie (1964)), we shall only summarize the results in the following discussion.

From standard perturbation theory the expression for the differential cross section for transitions into the continuum is

$$d\sigma = 2\pi \left| T_{fi} \right|^2 \rho(E)/\hbar v_i \qquad (3)$$

where v_i is the relative velocity of the incident and target particles, $\rho(E)$ is the density of final states, and T_{fi} is the transition amplitude between the initial and final states.

Equation (3) can be rewritten to allow a comparison with the experimentally observed energy spectra. From van Oers and Slaus (1967), the center-of-mass differential cross section for detecting only one particle in the final state (which we have labeled particle 3) is given by

$$\frac{d^2\sigma}{dE_3 d\Omega_3} = \frac{\mu_3 \mu k_3 k}{\hbar^5 v_i} \int \left| T_{fi} \right|^2 d\Omega \qquad (4)$$

The integration over $d\Omega$ can be made immediately if we

restrict the energy of the relative motion of the unobserved nucleons to less than 5 MeV so that they can be described by an S-state wave function. The expression in the brackets then becomes the absolute square of the transition amplitude, $|T_{fi}|^2$, which includes an average over initial spin substates.

The transition amplitude, as shown in formal scattering theory, is given by

$$T_{fi} = \langle \phi_f | V_t | \Psi_i^{(+)} \rangle \tag{5}$$

for an interaction $H = H_o + V_t$. Here H_o represents the unperturbed Hamiltonian, V_t the total perturbing interaction, and ϕ_f a plane-wave final state. $\Psi_i^{(+)}$ is the solution to the integral equation

$$\Psi_i^{(+)} = \phi_i + \frac{1}{E - H_o + i\epsilon} V_t \Psi_i^{(+)} \tag{6}$$

with outgoing spherical waves of energy E.

In the first paper explicitly dealing with final state interactions, Watson considered processes which could be described by a Hamiltonian with two separable potentials, $H = H_o + V + U$. As motivated by his qualitative discussion of sequential processes which we just presented above, V was taken to describe the production process, while U was

assumed to occur only between two particles in the final
state. He showed that the transition matrix of Equation (5)
could be written

$$T_{fi} = \langle \chi_f^{(-)} | V | \Psi_i^{(+)} \rangle + \langle \chi_f^{(-)} | U | \phi_i \rangle \qquad (7)$$

where $\Psi_i^{(+)}$ is defined in Equation (6), $\chi_f^{(-)}$ is the
scattering state function of the particles interacting in
the final state and is defined by

$$\chi_f^{(-)} = \phi_f + \frac{1}{E - H_o - i\epsilon} U \chi_f^{(-)} \qquad (8)$$

Here ϕ_i and ϕ_f satisfy the Schrodinger equations

$$\begin{aligned} H_o \phi_i &= E_i \phi_i \\ H_o \phi_f &= E_f \phi_f \end{aligned} \qquad (9)$$

in the initial and final states, respectively. The second
term of Equation (7) is usually neglected in final state
formalisms, since it is assumed that the final state inter-
action U does not connect initial and final states. The
analysis can be extended for rearrangement collisions,
following Gell-Mann and Goldberger (1953), with the result

$$T_{f'i} = \langle \chi_{f'}^{(-)} | V | \Psi_i^{(+)} \rangle \tag{10}$$

where

$$\Psi_i^{(+)} = \frac{1}{E - H_o - U + i\epsilon} V \Psi_i^{(+)} \tag{11}$$

and

$$\chi_{f'}^{(-)} = \phi_{f'} + \frac{1}{E - H_o' - i\epsilon} U \chi_{f'}^{(-)} \tag{12}$$

Here H_o' represents the rearranged Hamiltonian of the final state.

Expression (7) or (10) is the starting equation for the approximate theories used in interpreting experimental spectra. Two different approaches have frequently been taken in evaluating the transition amplitude. The most straightforward approach is to explicitly calculate the transition matrix by assuming sufficiently tractable forms for the wave functions and potentials. This has been the approach of the Born approximation calculations which will be discussed in Section C. The other approach is that of Watson. He recognized that for some reactions the effects of the final state interaction would completely dominate

the observed spectra, so that the important part of the total transition amplitude would be the amplitude for scattering between the interacting pair of the final state. We shall describe Watson's approximation in the next section.

B. Watson-Migdal Approximation

If particle 3 does not interact with either of the nucleons in the final state, then the final state wave function has the form

$$\chi_f^{(-)} = \phi(r_3, r) \, \phi(r_3) \, \bar{\phi}(r) \, \eta_f \tag{13}$$

where $\phi(r_3, r)$ represents the wave function of the relative motion of particle 3 with respect to the center-of-mass of the two nucleons; $\phi(r_3)$ represents the bound state wave function of particle 3; $\bar{\phi}(r)$ represents the two-nucleon scattering wave function; and η_f represents the spin wave function. Using Equation (13), the spatial representation of the transition amplitude becomes

$$T_{fi} = \int \phi(r_3, r) \, \phi(r_3) \, \bar{\phi}(r) \, \eta_f V \, \Psi_i^{(+)} d\tau \tag{14}$$

In the Watson approximation, $\bar{\phi}(r)$ is assumed to have approximately the same momentum dependence as its asymptotic

form throughout the spatial region of integration defined by the finite range of V in Equation (14). Furthermore, the momentum dependence is assumed to be factorable from the radial dependence. The validity of these assumptions is crucial to the Watson-Migdal approximation, and we shall discuss them in the next few paragraphs.

Suppose the nucleon-nucleon interaction is of range b. Then, for $r \geq b$, the asymptotic form of $\bar{\phi}(r)$ is

$$\bar{\phi}(k,r) = e^{-i\delta}(f_o \cos(\delta) + g_o \sin(\delta))/kr \qquad (15)$$

where $\delta = \delta(k)$ is the ^1S_o phase shift. For an n-n or n-p system

$$f_o = \sin(kr)$$
$$g_o = \cos(kr)$$

and for the p-p system

$$f_o = F_o(kr)$$
$$g_o = G_o(kr)$$

where $F_o(kr)$ and $G_o(kr)$ are the regular and irregular S-wave Coulomb functions, respectively. Now for $r \leq b$, the radial shape of $\bar{\phi}(r)$ is insensitive to the value of k for the nucleon-nucleon energy range of interest. Physically, this is because k at most corresponds to an

energy of 4 MeV, which is small compared to a nucleon-nucleon well depth of the order of 50 MeV. Inside the range b the momentum dependence approximately becomes a normalizing factor for the radial dependence so that we can write

$$\phi(k,r) \approx N(k)v(r) \tag{16}$$

This fact is born out by the numerical solutions to the Schrodinger equation for a nucleon-nucleon interaction.

A similar factorization occurs for the region $r \geq b$ if $kr \ll 1$. To see this, assume $kr \ll 1$, so that if

$$f_0 = \sin(kr) \approx kr - (kr)^3/3! + \ldots$$

or

$$= F_0(kr) \approx C(\eta)kr(1 + r/2R) + \ldots$$

and

$$g_0 = \cos(kr) \approx 1 - (kr)^2/2! + \ldots \tag{17}$$

or

$$= G_0(kr)$$

where

$$\approx (1 + ((r/R)(\ln(r/R) + h(\eta) + 2\gamma - 1) + \ldots))/C(\eta)$$

$$C(\eta) = (2\pi\eta/(\exp(2\pi\eta) - 1))$$
$$h(\eta) = \eta^2 \sum_{n=1}^{\infty} \{1/(n(n^2 + \eta^2))\} - \ln\eta - 0.57722$$
$$R = \hbar^2/2me^2 = 28.8 \text{ F} \tag{18}$$
$$\eta = me^2/2\hbar^2 k$$
$$\gamma = 0.57722$$

Using Equation (16), the effective range expansion for the phase shift (Jackson and Blatt, 1950)

$$C^2(\eta)k\cot(\delta) + h(\eta)/R = -1/a + (1/2)r_0 k^2 + \ldots \tag{19}$$

and neglecting terms of order $(kr)^2$, $\frac{r}{R}$, we obtain from Equation (15)

$$\phi(k,r) = \frac{e^{-i\delta}\sin(\delta)}{C(\eta)k}(1 - r/a + r_0 k^2 r/2 + \ldots)/r$$

$$= \frac{e^{-i\delta}\sin(\delta)}{C(\eta)k}f(r) \qquad (20)$$

so that the momentum dependence is approximately factored from the radial dependence. This result also holds for the n-n and n-p systems if we replace $C(\eta)$ by 1.

If we arbitrarily assume the normalization $v(b) = 1$, we find from Equation (20) that for $r \leq b$

$$N(k) = \frac{e^{-i\delta}\sin(\delta)}{C(\eta)k}(1 - b/a + r_0 bk^2/2 + \ldots)/b \qquad (21)$$

Then, using Equations (20) and (21), we have from Equation (14)

$$T_{fi} = \frac{e^{-i\delta}\sin(\delta)}{C(\eta)k}\left[(1/b)(1 - b/a + r_0 bk^2/2 + \ldots)\eta_f \iint_0^b \phi(r_3,r)\phi(r_3)v(r)V\Psi_i^{(+)}d^3r d\tau' \right.$$
$$\left. + \eta_f \iint_b^\infty (1/r)(1 - r/a + r_0 rk^2/2 + \ldots)\phi(r_3,r)\phi(r_3)V\Psi_i^{(+)}d^3r d\tau' \right] \qquad (22)$$

where the integration is divided into two parts: an inner core region of $r \leq b$ and an outer region of $r \geq b$. If the factor in the square brackets is independent of k, we obtain the Watson-Migdal approximation

$$T_{fi} = \frac{e^{-i\delta}\sin(\delta)}{C(\eta)\,k}\,T_0 \qquad (23)$$

where T_0 gives the amplitude for three-particle break-up, and $e^{-i\delta}\sin(\delta)/(C(\eta)k)$ is an enhancement factor due to the final state interaction. Except for the negative sign of the

phase shift in the exponential, this enhancement factor is the S-wave scattering amplitude between the final state nucleons. The essential feature of the Watson-Migdal approximation is the replacement of the momentum dependence of $\phi(r)$ with what amounts to the NN scattering amplitude. Since the NN scattering amplitude is simply related to the phase shifts and cross sections, it is easy to use in analyzing experimental data.

The conditions required for the validity of the Watson-Migdal approximation can be determined from the factor in square brackets of Equation (22). For nucleon-nucleon final state energies under consideration ($0 \leq E_{NN} \leq 4$ MeV), the factorization will always be valid in the inner core region, since kb is always significantly less than 1. However, for the Watson-Migdal approximation to be valid in the outer region, the function $V\Psi_i^{(+)}$ must fall rapidly enough to cut off terms of order $r_0 r k^2$ and higher. Interpreting calculations due to Haybron (1968), we find that the range of $V\Psi_i^{(+)}$ must be less than 5 F. This condition is not often met in practice, as will be shown in Section D.

Using the transition amplitude given by Equation (23) in Equation (4), the Watson-Migdal prediction for the differential cross section per unit energy can be written in the form

$$\frac{d^2\sigma}{dE_3 d\Omega_3} = \frac{C(\boldsymbol{\eta})k_3 k \left|T_o\right|^2}{(-1/a + r_o k^2/2 - h(\boldsymbol{\eta})/R)^2 + C^2(\boldsymbol{\eta})k^2} \tag{24}$$

For the n-n or n-p system we replace $C(\boldsymbol{\eta})$ by 1 and set $h(\boldsymbol{\eta}) = 0$. In practice, Equation (24) is used to fit the experimentally observed spectra with $\left|T_o\right|^2$, a, and r_o as arbitrary parameters.

C. Plane Wave Born Approximation

The purpose of this Section is to direct attention to the plane wave Born approximation (PWBA) as an alternative method of analysis of reactions with final state interactions. The method has an even longer history of application to multiparticle final state reactions than the Watson-Migdal approximation. The PWBA has been used, for example, by:

Wu and Ashkin, 1948
Gluckstern and Bethe, 1951
Frank and Gammel, 1954
Heckrotte and MacGregor, 1958
Koehler and Mann, 1964; Koehler, 1965
Yu and Meyerhof, 1966
Henley, Richards, and Yu, 1967
van Oers and Slaus, 1967

These calculations have brought out the complexity of the total mechanism involved in reactions among the light nuclei. To make the calculations tractable, most PWBA calculations have included additional simplifications beyond that of plane waves. Some calculations have employed zero-range interactions to separate the coordinates

in the overlap integrals. Others have assumed a dominant reaction mechanism such as a pickup process or a charge exchange mode and have neglected the other possible contributions. It is not by accident that the most complicated processes are the ones that are neglected. Only the calculation for the simplest system (the D(n,p)2n reaction) by Koehler and Mann includes all the possible processes with realistic interactions.

In contrast to the Watson-Migdal approximation, the PWBA includes the effect of the primary reaction mechanism on the predicted spectra via the function $V\Psi_i^{(+)}$ in Equation (14). This allows study of the contributions of different reaction processes to the total reaction mechanism and provides a way to investigate possible interferences among these different processes.

Of course, the PWBA also has severe limitations. The approximation is questionable at low energies where distortion effects in the incident and exit channels should be appreciable. However, for reactions among light nuclei, the interaction which causes a given reaction is generally a large part of the interaction which causes the elastic scattering. Thus, the distorted wave Born approximation (DWBA) is not such a good approximation, either, and the PWBA may be somewhat better for lighter nuclei than for heavier ones. The neglect of many-body forces is another

limitation of the PWBA. While calculations are now being made based on the exact three-body equations of Fadeev (1960), they also require simplifying assumptions about the nuclear force. The effects of these assumptions are not thoroughly understood; therefore, it would be somewhat premature to use the method as a reliable analytical tool.

Despite its limitations, the PWBA is a logical first step toward understanding the total reaction mechanism among light nuclei. Unfortunately, the difficulty of realistic PWBA calculations for even the simplest systems has greatly diminished its appeal.

D. Comparison with Experiment

The Watson-Migdal approach to evaluating the transition amplitude is most reliable when applied to reactions involving short range primary interactions such as $D(\pi^-, \gamma)2n$. In such reactions, it is to be expected that the function $V\Psi_i^{(+)}$ will vanish sufficiently fast to separate the momentum dependence from the spatial integration. Furthermore, the observed particle cannot interact strongly with the interacting pair of the final state, thus eliminating a major source of uncertainty. Bander (1964) has estimated the theoretical uncertainty in the value of a_{nn} determined from the $D(\pi^-, \gamma)2n$ reaction to be ± 1 F. Several determinations have been made using this reaction:

Phillips and Crowe, 1954
Ryan, 1964
Haddock, et al., 1965
Nygren, 1968
Butler, et al., 1968

Haddock, et al. found $a_{nn} = -16.4 \pm 1.3$ F, in agreement with the calculations of Heller, et al. (1964), which were based on the charge symmetry of nuclear forces and the low energy p-p scattering results. However, re-analysis of the data of Haddock, et al. by Nygren gives $a_{nn} = -18.4 \pm 1.5$ F. The most recent measurement by Butler, et al. finds $a_{nn} = -13.1 {}^{-3.4}_{+2.4}$ F.

The application of the Watson-Migdal approximation to nuclear reactions having three strongly interacting particles in the final state is much more uncertain. In some reactions the observed spectra can be fitted with the approximation. Bacher (1966) has found that the high energy region of the proton spectra from ${}^3\text{He}({}^3\text{He},p){}^5\text{Li}$ can be fitted with the Watson-Migdal approximation and the known ${}^5\text{Li}$ ground state phase shifts. A noteworthy feature of these proton spectra is that the enhancement due to the ${}^5\text{Li}$ ground state break-up is prominent over a wide range of angles (20° to 160°) and incident energies (3 to 18 MeV). Thus, the observed spectra are not sensitive to the primary interaction mechanism. On the other hand, the Watson-Migdal approximation fails completely to predict the shape of the neutron and deuteron spectra from the $D(p,n)2p$ and ${}^3\text{He}(p,d)2p$ reactions with the known p-p effective range

parameters (van Oers and Slaus, 1967; Tombrello and Bacher, 1965).

There has been growing evidence that a detailed knowledge of each of the possible processes which contribute to the total reaction mechanism is needed to reliably apply the Watson-Migdal approximation. Phillips (1964), using the impulse approximation, has shown that the proton and neutron spectra from the D(n,p)2n and D(p,n)2p reactions may be markedly different from the Watson-Migdal prediction if the reactions occur through a long range charge-exchange process. Without recourse to specific models, we see that a long range interaction corresponds to the function $V\Psi_i^{(+)}$ falling too slowly to justify Watson's approximation. A PWBA analysis of the data of Jakobsen, et al. (1965) for the ^{3}He(d,t)2p reaction by Henley, et al. has shown that the experimental angular distribution can be qualitatively explained by assuming different reaction mechanisms in the forward and backward hemispheres. For forward angles, a simple stripping mechanism was assumed, while, for backward angles, a charge exchange process was assumed to dominate. Extending their analysis to the DWBA (admittedly question-able for such light nuclei), they found that both processes contributed significantly at all c.m. angles. The applica-bility of the Watson-Migdal approximation to the ^{3}He(d,t)2p reaction has been studied by Morton, et al. (1968), where

triton spectra were measured for laboratory angles 5° and 180° at a center-of-mass energy of 20 MeV. For the 5° spectrum, the Watson-Migdal prediction agreed, but at 180° (measured using $D(^3He,t)2p$ at 0° with the appropriate ^3He incident energy), the measured spectrum was much narrower than predicted. Re-interpreting their 180° spectrum using the charge exchange mechanism formulated by Henley, et al., Morton, et al. obtained much better agreement.

The above-mentioned studies using p-p final state interactions demonstrate that it is difficult to know a priori if the Watson-Migdal approximation (or any approximation that ignores the primary mechanism) will be applicable to a multinucleon final state reaction. To remove the uncertainty in extracting n-n effective range parameters from such reactions, it has been proposed that the mirror reaction be studied under as identical conditions as possible (van Oers, et al., 1965; van Oers and Slaus, 1967). Thus, the theoretical analysis could be tested using the known p-p effective range parameters.

Using this method of comparative analysis, Baumgartner, et al. (1966) studied the mirror reactions $^3He(d,t)2p$ and $^3H(d,^3He)2n$ to determine the n-n scattering length. Using the Watson-Migdal approximation to analyze a ^3He spectrum measured at 6° with an incident deuteron energy of 32.5 MeV, they found $a_{nn} = -16.1 \pm 1.0$ F. The use

of the Watson-Migdal approximation was justified on the basis that it also gave $a_{pp} = -7.69 \, ^{+0.61}_{-0.67}$ F for the mirror reaction (in agreement with the results of low energy p-p scattering).

In the next Part we describe measurements of the ^{3}He and triton spectra from the ^{3}H(d,^{3}He)2n, ^{3}He(d,t)2p, ^{3}H(d,t)pn, and ^{3}He(d,^{3}He)pn reactions at several forward angles for a deuteron energy of 10.91 MeV. These measurements were undertaken to determine if the Watson-Migdal approximation could fit the observed spectra and, if so, what values of a_{nn} would be required.

III. ENERGY SPECTRUM MEASUREMENTS

In this Part we describe measurements of the triton
and ^{3}He energy spectra at very forward angles from the
^{3}He(d,t)2p, ^{3}H(d,^{3}He)2n, ^{3}He(d,^{3}He)pn, and ^{3}H(d,t)pn
reactions. Accurate measurements were made to test how
well the Watson-Migdal approximation fitted the observed
spectra at seven laboratory angles between 6° and 20 °. As
discussed in Part II, a rapid variation in the observed
spectrum shape would indicate that the conditions necessary
for the validity of the Watson-Migdal approximation would
not be met. Additionally, accurate measurements of the
spectra would permit study of the value of the scattering
length extracted as a function of the energy region of the
spectra fitted.

In this experiment gaseous tritium and ^{3}He targets
were bombarded with 11 MeV deuterons. Mass-three nuclei
from the nuclear reactions were detected by an array of
counters placed along the focal plane of a 61 cm double-
focusing magnetic spectrometer. Section A of this Part
describes the apparatus used in this experiment, while
Section B discusses the experimental procedures and data re-
duction. Section C presents the results of the experiment.

A. Apparatus

    1. Deuteron Beam

The beam of 11 MeV deuterons used in this experiment
was obtained from the ONR-CIT tandem van de Graaff accele-
rator (for a description of the production and acceleration
of ion beams in tandem accelerators, see the review article
by Rose, 1967). A negatively charged deuteron beam,
typically about 10 microamperes, was produced in a negative
ion source and injected in the machine. After acceleration,
the energy of the beam was measured by passing the beam
through a 90° uniform-field analyzing magnet. The beam was
then passed through collimating slits and into the target
chamber of the spectrometer. Figure 2 shows the relation-
ship of the incident beam to the chamber's gas target cell
and to the position of the spectrometer. After passing
through the target gas, the beam was stopped by the walls
of the target cell (held at + 300 V), and the resulting
current was integrated. An Eldorado model CI-110 current
integrator was employed, and leakage current was held to a
very small fraction of the beam current. The beam current
on the target cell ranged between 100 and 400 nanoamperes,
depending upon the spectrometer's angle of observation and
the amount of acceptable dead time in the detection system.
The beam energy at the center of the target cell was cal-
culated to be 10.91 MeV using the stopping curves of
Whaling (1958). The beam's energy uncertainty was
± 17 keV.

FIGURE 2

A horizontal section of the tritium target cell as it appears
when placed in the spectrometer. The numbered items of the
figure correspond to those listed below:

(1) Spectrometer Target Chamber

(2) Gas Target Cell

(3) Extension Tube

(4) Primary Collimating Slit

(5) Entrance Foil

(6) Exit Foil
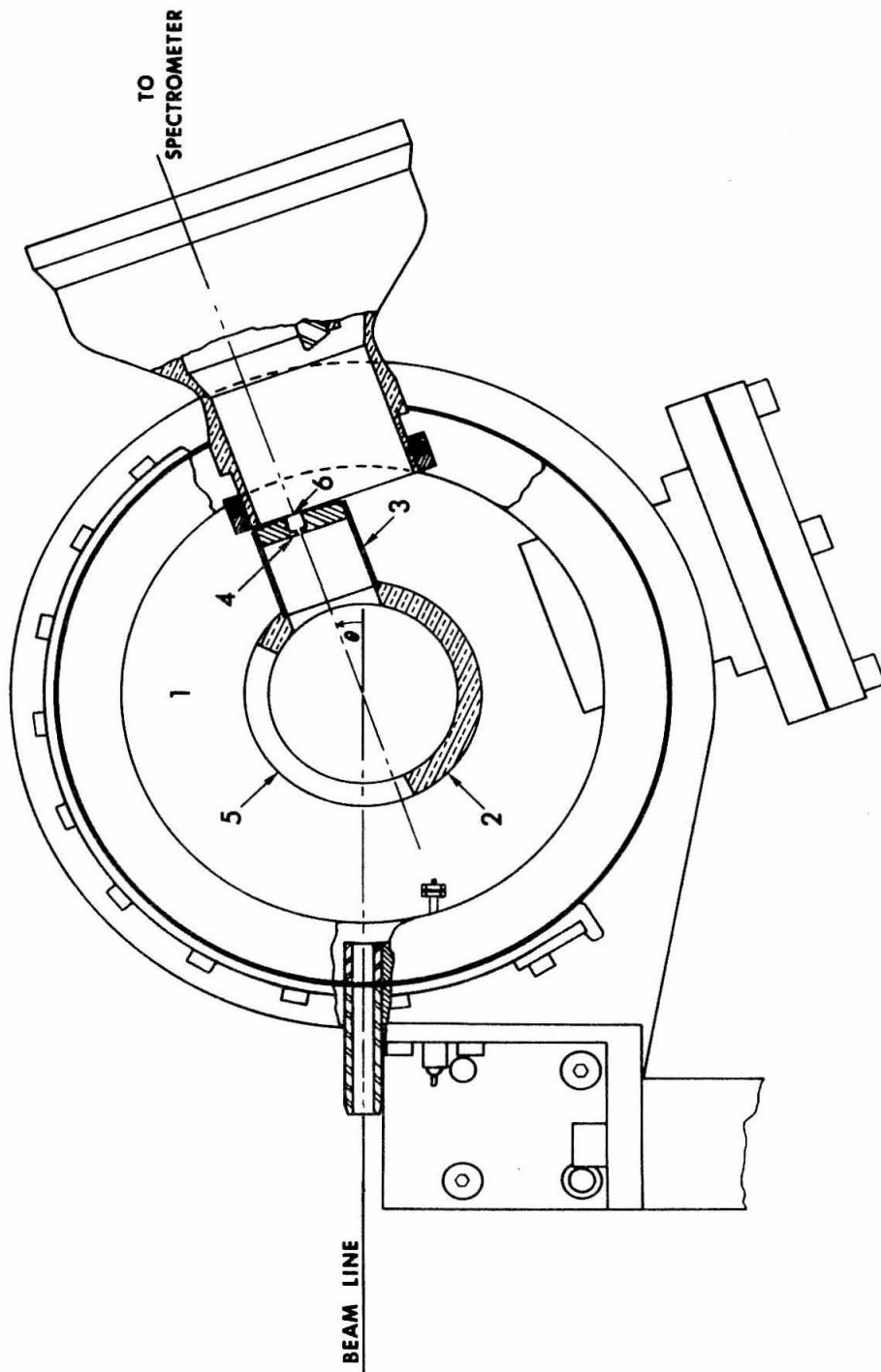
FIGURE 2

2. Target Gases

The tritium target gas presented two additional problems not encountered with the ^{3}He gas. First, since it is an isotope of hydrogen, tritium readily exchanges with the normal hydrogen with which it comes in contact. Therefore, tritium easily contaminates and is easily contaminated by any hydrogenous material. We attempted to minimize contaminating the tritium by using hydrogen-free materials in constructing those parts of the apparatus with which the tritium came in contact. Second, because of its radioactivity, tritium is a serious health hazard and has to be handled carefully. Ordinary laboratory radiation detectors cannot be used with tritium since the β-decay energy is so low the emitted electrons cannot penetrate the detector's windows. Because of the gas's properties, special techniques had to be employed in working with the tritium. The methods used in this experiment were essentially those employed by Spiger (1967), and Appendix C of his thesis should be consulted for a more complete description of how the gas was handled.

The tritium and ^{3}He gases were used in the same target system so that the measurements of the mirror reactions were made under as identical conditions as possible. Only two cubic centimeters of tritium (STP) were used in the experiment to limit the activity to approximately five Curies.

The tritium was obtained from the Oak Ridge National Laboratory, Oak Ridge, Tennessee. The ^{3}He target gas was obtained from the Mound Laboratory, Miamisburg, Ohio, with an analyzed purity of 99.36%. The ^{3}He gas, of course, presented none of the experimental difficulties associated with the tritium.

3. Spectrometer Target System

Previously built gas targets for the spectrometer were not suitable for tritium, and a new system had to be constructed. The new spectrometer target system had to meet several requirements set by the purpose of the experiment, the properties of the tritium target gas, and the existing apparatus. The design had to: (1) minimize hazards to the laboratory equipment and personnel; (2) be compatable with the target chamber and slit system of the spectrometer; (3) allow measurements at very forward laboratory angles; (4) minimize contamination of the tritium target with hydrogen; and (5) be easily tested and safely stored. The system built to satisfy these requirements is described in the following paragraphs.

From previous experiments with the tritium target system of Spiger, target cell foils of the thickness required for this experiment were found to be quite stable for long periods of time. Because of this past experience, it was felt that a simple, straightforward design would be the

best approach for safely using a tritium target in the spectrometer. Figure 3 is a sectional view of the completed target system as it would appear in use with the spectrometer.

The system was built around a Lucite disk that served as the lid to the spectrometer target chamber. The disk insulated the target cell from the spectrometer so that the cell could be used as a beam stop. The disk also made the connection between chamber vacuum and the system's gas manifold. Attached to the top of the disk was an aluminum frame that supported the system's gas manifold, tritium reservoir, differential pressure gauge, and interconnecting plumbing.

A small-volume, brass target cell with internal dimensions of 2.54 cm high by 5.08 cm in diameter was attached to the underside of the Lucite lid. The small volume of the cell minimized the amount of tritium required for a useable target density. However, the internal dimensions of the cell were still of sufficient size in relation to the collimating slits that particles scattered from the walls, top, and bottom of the cell were prevented from entering the spectrometer. The cell had $\frac{1}{4}$ inch thick walls that provided structural rigidity for the relatively long beam entrance window and that also provided part of the heat sink required for the foil soldering when the

FIGURE 3

A vertical section of the tritium target system as it
appears when placed in the target chamber of the spectro-
meter. The numbered items of the figure correspond to
those listed below:

    (1) Spectrometer Target Chamber

    (2) Gas Target Cell

    (3) Extension Tube

    (4) Primary Collimating Slit

    (5) Entrance Foil

    (6) Exit Foil

    (7) Insulating Teflon Block

    (8) Manifold

    (9) Nupro Valve

  (10) Tritium Reservoir

  (11) Uranium tritide

  (12) Metering Valve

  (13) Differential Pressure Gauge

  (14) Aluminum Frame

  (15) Lucite Chamber Lid
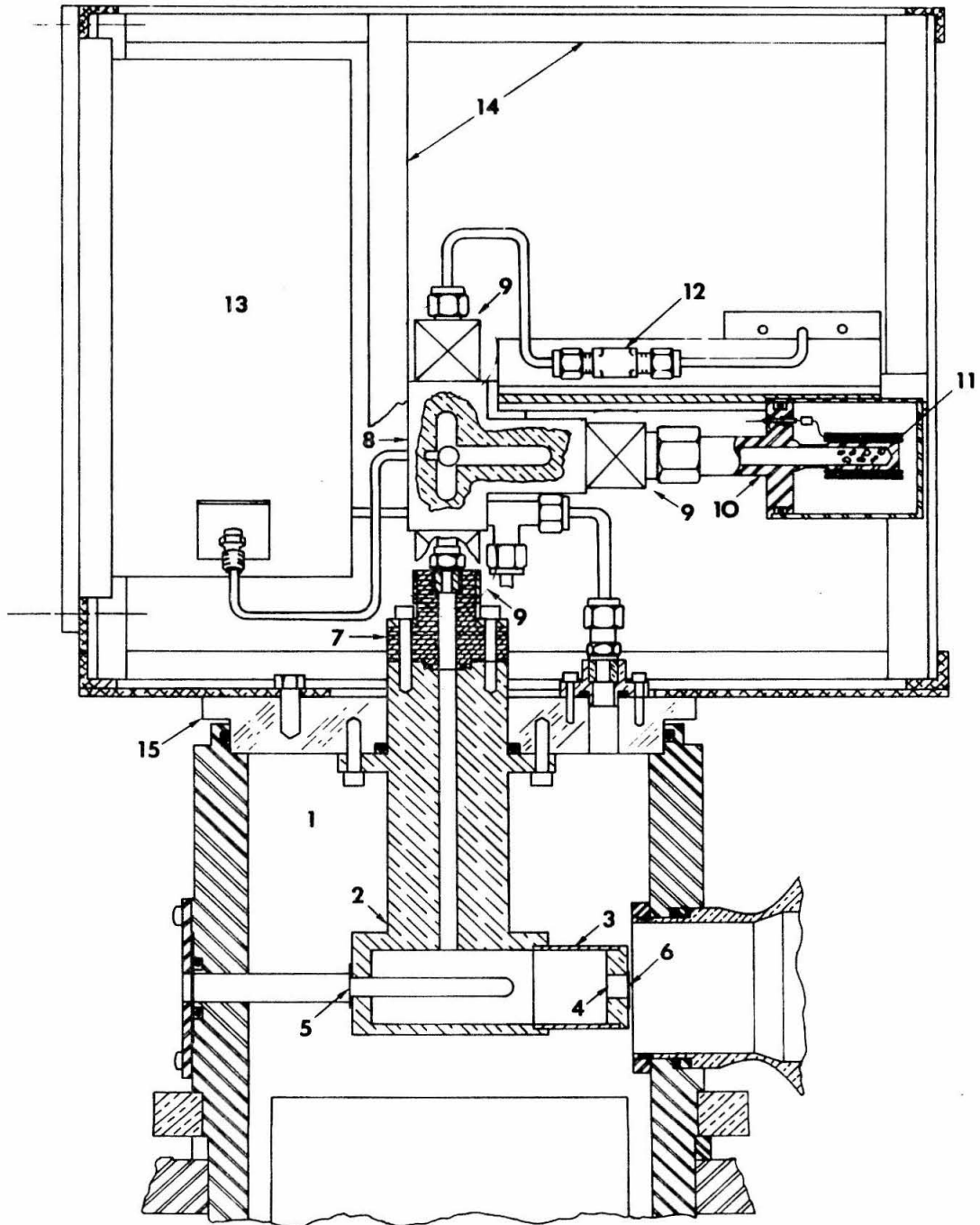
FIGURE 3

cell was constructed. The beam entrance window was made by
milling a $\frac{1}{4}$ inch slot through a 140° angular range in one
side of the cell and covering the slot with a 1/10 mil
Havar foil (obtained from Precision Metals Division,
Hamilton Watch Company, Lancaster, Pennsylvania). The
comparatively thick Havar was chosen because the entrance
window's large area required a strong material that was easy
to handle. At 11 MeV the incident beam only suffered a 1%
energy loss in passing through the Havar foil. Protruding
from the side of the cell was an extension tube that was
part of the target collimating system for the spectrometer.
A 1/16 inch vertical slot recessed in the end of the tube
served as the first collimating slit. The extension tube
increased the distance between the first slit and the target
region in the gas, thus permitting measurements at very
forward angles without unduly increasing the cell's volume.
The cell's exit window was a 6,150 $\overset{\circ}{A}$ foil (obtained from the
Chromium Corporation of America, Waterbury, Connecticut),
soldered over the end of the extension tube. The exit foil
was as thin as possible (consistent with safety) to minimize
the ^{3}He ions' energy loss and straggle in passing through
the foil. For the spectra at very forward angles, the
major contribution to the energy resolution came from the
energy straggle in the exit foil (see Table I). Figure 2
shows the relationship between the entrance window,

TABLE I

The experimental energy resolution (FWHM) for each angle of

each reaction.

TABLE I

Reaction	Angle (deg)	Resolution (keV)	Reaction	Angle (deg)	Resolution (keV)
^{3}H(d,^{3}He)2n	6	55	^{3}He(d,t)2p	6	43
	7.5	64		7.5	54
	10	143		10	136
	12.5	171		12.5	167
	15	199		15	193
	17.5	234		17.5	218
	20	254		20	244
^{3}H(d,^{3}H)pn	6	43	^{3}He(d,^{3}He)pn	6	56
	7.5	55		7.5	65
	10	136		10	174
	15	194		15	196
	20	244		20	245

extension tube, and exit window.

Both the entrance and exit foils were soldered to the cell to eliminate adhesive joints that would have contained hydrogen. The entrance foil was soldered with commercial 50/50 solder that melted around 360° F. The exit foil was soldered with Cerrobend (obtained from the Cerro de Pasco Corporation, New York, New York). Cerrobend is a bismuth based eutectic alloy that melts at 158° F. It was chosen because of its much lower melting temperature than the 50/50 solder; thus, the exit foil could be soldered to the cell without endangering the seal of the previously soldered entrance foil. Tests proved that Cerrobend could provide a satisfactory seal, even though it is not normally used as a solder. As a safety precaution against peeling, all the soldered foil joints were coated externally with epoxy cement.

The target cell was connected to the gas handling system through an insulating teflon block. Figure 4 is a schematic diagram of the gas handling system. The gas manifold interconnected the major components of the system: the gas target cell, the tritium reservoir, the differential pressure gauge, and the Helium inlet metering valve. The manifold was fitted with three special all-metal bellows-sealed valves (Nuclear Products Company, Cleveland, Ohio, valve model B-4H) for handling the tritium. One of the

FIGURE 4

A schematic diagram of the tritium target gas handling system. The numbered items correspond to those listed below:

(1) Spectrometer Target Chamber

(2) Gas Target Cell

(3) Manifold

(4) Tritium Reservoir

(5) Differential Pressure Gauge

(6) Nupro Valve

(7) Metering Valve

(8) Safety Vacuum Pump-out Valve
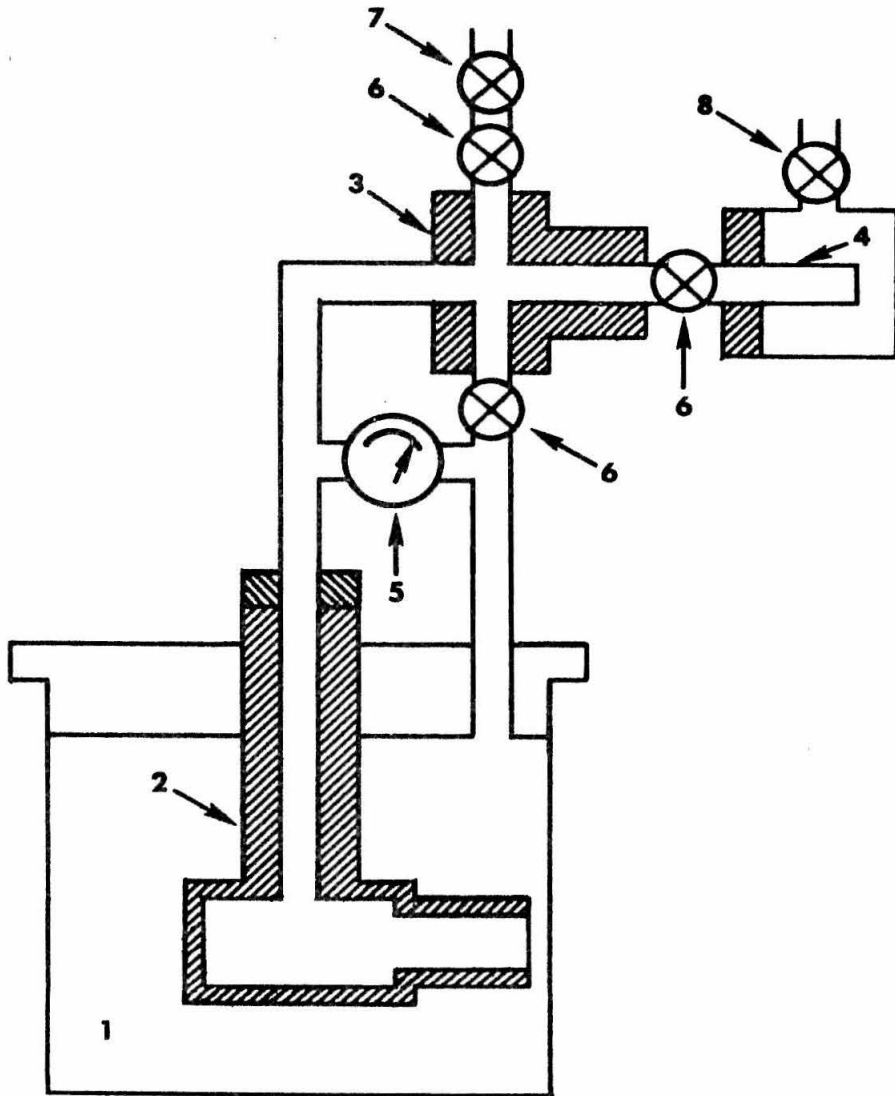
FIGURE 4

Nupro valves led to a metering valve that admitted the
target ^{3}He gas or the ^{4}He gas used in leak testing. A
second valve led to the tritium reservoir. The third
valve led to the spectrometer target chamber and the vacuum
side of the differential pressure gauge. One side of the
differential pressure gauge (a low volume aneroid type
obtained from Wallace and Tierman, Inc., Belleville, New
Jersey, model FA-141, pressure range 0 - 50 mm) was connect-
ed directly to the manifold and gas cell, while the other
side was connected to the spectrometer target chamber.
Thus, the gauge always indicated the pressure on the cell's
foil windows. All the joints of the system were either
soldered or sealed with teflon to minimize contaminating
the tritium. The gas lines were kept short and were of
small diameter to minimize the volume of the gas handling
system.

The tritium reservoir is similar to the one used by
Spiger. For safety and convenience in storage and in
handling, the tritium was kept in the reservoir in the form
of uranium tritide. Around the reservoir was wound a
nichrome-wire heater coil. When it was desired to fill the
target cell, the reservoir was heated, decomposing the
uranium tritide and releasing the tritium. Later the cell
could be emptied by re-exposing the tritium to the cooled
uranium.

A concerted effort insured that the target system was leak-free. The system was tested many times with a Helium leak detector at a pressure three times that which would be obtained with tritium. No detectable leak was acceptable, and several sets of foils were tried until a leak-free system was obtained.

4. Particle Collimation

For a gas target, a pair of collimating slits **are** needed to define the target region seen by the spectrometer, since, in a gas target, scatterings and reactions occur along every point of the beam path. Figure 5 illustrates how the geometrical configuration of the collimating slits defines the target thickness seen by the spectrometer.

When extracting differential cross sections from the measured particle yields, it was convenient to use the "G_o-factor", a geometrical quantity defined as the product of the observed target thickness and the solid angle subtended by the detection system. To first order this factor is given by

$$G_o = I_{\theta_3} \Omega_{det} = \left[\frac{w_1 R}{d \sin(\theta_3)} \right] \left[\frac{w_2 h}{R^2} \right] = \frac{w_1 w_2 h}{R d \sin(\theta_3)} \tag{25}$$

Here

$$\Omega_{det} = \text{solid angle subtended by the detection system}$$

FIGURE 5

A schematic diagram of the collimation geometry for the magnetic spectrometer. The target region along the beam path which illuminates the spectrometer is defined by the primary collimating slit and the detection aperture. The diagram shows the parameters for determining the detection solid angle and target thickness discussed on pages 42 and 45.
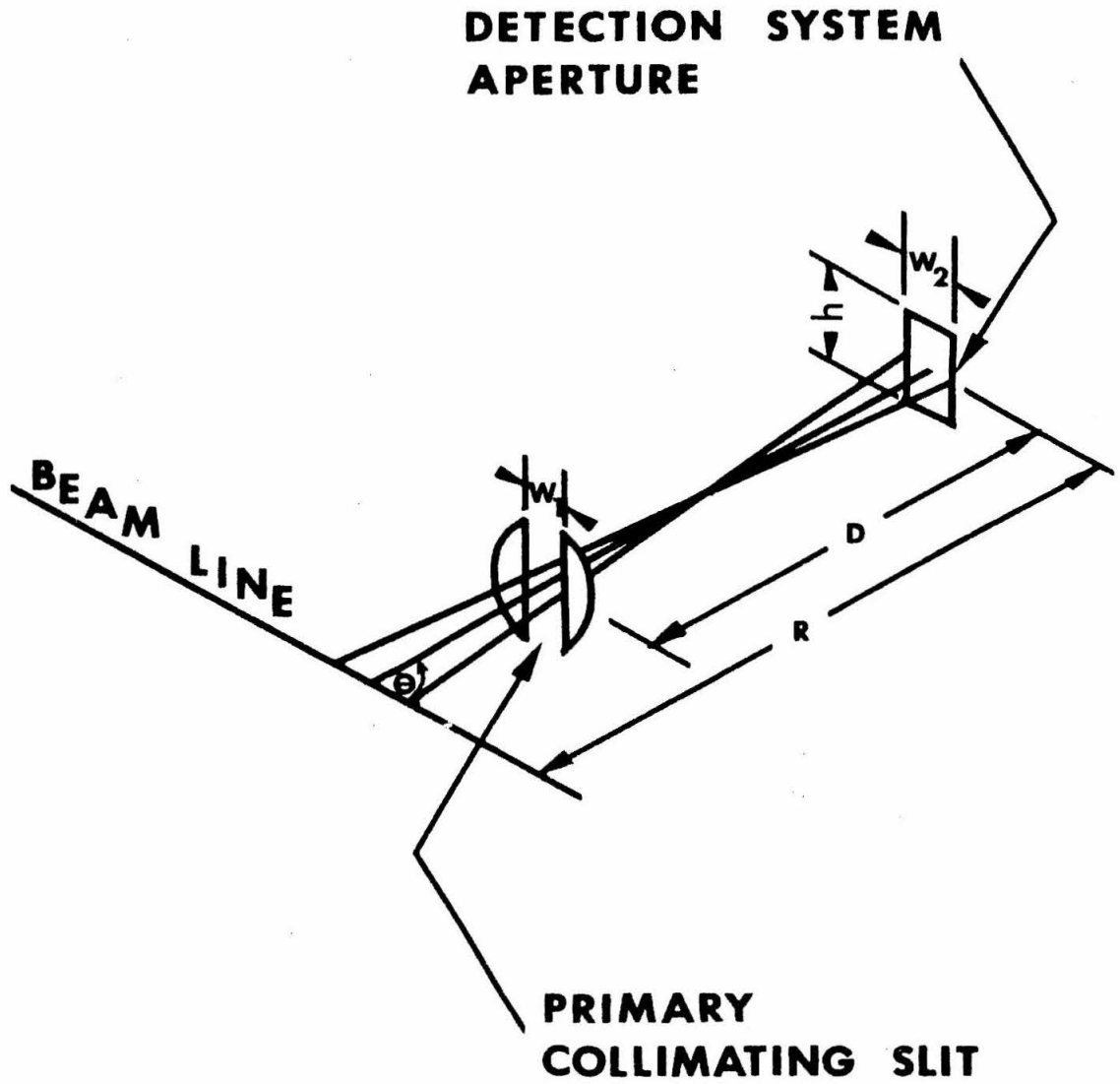
FIGURE 5

$$= \frac{w_2 h}{R^2}$$

For the spectrometer, the detection system aperture width, w_2, is determined by the Θ slit; the height, h, is determined by the Φ slit; and R is the distance from the center of the target chamber to the entrance slits.

and

l_{θ_3} = target thickness seen at the laboratory angle θ_3

$$= \frac{w_1 R}{d \sin(\theta_3)}$$

where w_1 = width of the first collimation slit, and d = separation between the first slit and the detection aperture.

A more exact treatment which includes effects due to the finite beam size and variation of the differential cross section over the collimation angle has been given by Silverstein (1959).

B. Procedure

    1. Data Acquisition

For a gas target, the differential cross section per unit energy averaged over the energy and angular resolution factors for the experimental configuration, at an angle θ and energy E, is given by

$$(d^2\sigma/(dE\, d\Omega))_{av} = Y(E,\theta)/(\xi \cdot N_b \cdot N_t \cdot l\Delta\Omega \cdot \Delta E) \qquad (26)$$

where

ξ = the detection efficiency

N_b = the number of incident particles

N_t = the number of target nuclei per cm^3

$l\Delta\Omega$ = the target thickness times the solid angle

ΔE = the energy resolution of spectrometer

$Y(E,\theta)$ = the number of particles observed in the intervals $\Delta\Omega$ and ΔE

Since current theories for final state interactions do not predict the absolute value of the differential cross section, only a relative consistency between points in the spectrometer scans was required to study the shapes of the spectra. Nevertheless, it is valuable to have a good estimate of the absolute value to set a limit on the cross section for producing a bound di-neutron and for more refined calculations of the future. Therefore, a reasonable degree of care was taken in the measurements required for determining each of the parameters of Equation (26). The procedure used in acquiring these data with the previously described apparatus will be outlined in the following paragraphs.

The measurements were scheduled so that two consecutive days were available with the spectrometer to minimize handling the target system. To insure the correct positioning of the gas cell required for collimation, the

system was aligned optically with respect to the spectrometer. With the magnet set at 90°, the beam line through the target chamber was established with a transit by aligning the beam entrance hole and the center of the 90° access port in the side of the target chamber. The gas cell was then positioned in the target chamber so that a reference index (scribed at 90° with respect to the cell's exit slit) coincided with the beam line. With this procedure, the observation angle was determined to the same precision as the spectrometer could be set, $\pm 0.1^{\circ}$.

Several safety precautions were taken when tritium was used in the target cell. To protect the laboratory, a closed liquid-nitrogen-cooled Zeolite trap was attached to the exhaust port of the spectrometer's mechanical fore-pump. In the event of a tritium leak, this trap would have prevented contamination of the laboratory. The target room was continuously monitored with a tritium "sniffer" (Johnston Laboratories, Inc., Baltimore, Maryland; model 755B). Also, the pressure of the gas target cell was continuously monitored from the accelerator control room using closed-circuit television.

The energy spectra of the mass-three nuclei were measured with the CIT 61 cm magnetic spectrometer and 16 counter array. The magnetic spectrometer provided both the energy resolution and the particle discrimination required

for the measurements. Good energy resolution was important for accurately measuring the spectrum shape needed for testing the Watson-Migdal final state interaction theory. Particle discrimination was important for measurements at very forward angles, since the large number of elastically scattered deuterons would have smothered the mass-three particles without the separation of particle species. Even with the spectrometer, regions of the 6°, 7.5°, and 10° spectra were obscured by the elastically scattered deuterons coming through the magnet. Groce (1963) has given a detailed description of the construction and operation of the magnetic spectrometer.

The spectrometer has a slow data accumulation rate because it only measures a small segment of the energy spectrum at a given magnetic field setting. This disadvantage was offset somewhat by using an array of 16 Au-Si surface barrier semiconductor detectors mounted in the focal plane of the spectrometer. A detailed description of the design and use of this array and its associated electronics has been given by McNally (1966) and by Moss (1968). **Most of the data were taken with the array.**

The spectrometer measurements were made by starting well above the kinematic three-body end point (the maximum energy available to the observed particle) and then slowly working downward in energy. The settings of the magnet

were made (using an NMR probe) so that the spectrometer
scans would overlap by 50%. This overlapping of scans
averaged out uncertainties in the spectrum introduced by
differences in the counters. When the triton spectra were
measured, a thin (.00636 mm) aluminum foil was placed in
front of the array. This was necessary because tritons
and (^{3}He$^+$) ions analyzed by the spectrometer at a fixed
field setting have equal energies. The aluminum foil
lowered the (^{3}He$^+$) ions' energy relative to the triton
energy, thus separating the particles.

The angular aperture of the spectrometer entrance
slits was on the order of $\Delta\Theta = \pm 1^{\circ}$ and $\Delta\Phi = \pm 2^{\circ}$. A slit
in front of each counter defined the relative energy
resolution $\frac{\Delta E}{E}$ to be about 1/400. The total experimental
resolution, due to energy straggling in the entrance and
exit foils of the cell and the finite energy and angular
resolutions of the spectrometer, is summarized in Table I
for each angle of each reaction measured.

A different electronics system was used for the
^{3}H(d,^{3}He)2n three-body end point scans at 6° and 7.5° and
for the ^{3}H(d,t)pn scans at 6°. For these measurements,
eight counters of the array were selected and fed into two
RIDL 400 channel pulse height analyzers, each operated
in the 4 x 100 channel mode. The increase from 64 to 100
channels improved the analysis of the detector pulses.

Also, the system was felt to be more reliable than the standard system using the Nuclear Data 160 analyzer because of the improved pulse routing. Since the three-body end-point scans were used to set a limit on the cross section for producing a bound di-neutron, it was important to minimize stray counts.

The number of deuterons incident on the target was determined from the charge accumulated by the gas cell. Each scan with the spectrometer was terminated when the charge reached a preset limit. After each scan, the temperature and pressure of the target gas was measured. About 15 mm of Hg pressure was used on all runs. The temperature of the target gas was measured by assuming that it was in equilibrium with the cell. (Localized heating of the gas along the beam path was expected to be small because of the small energy loss of the beam in the gas.) An accurate thermometer ($\pm$ 0.05° C) was attached to the top of the gas cell to monitor the temperature. From the temperature and pressure data, the number of target nuclei per cm^3 was determined.

2. Data Reduction

In reducing the data, corrections were made for: changes in target thickness due to slight changes in temperature and pressure; energy loss of the incident beam and detected particles in the foils and target gas; dead time

of the electronics system; variations in the effective area
and efficiency of the counters; and the effective radial
position of each counter in the spectrometer. The correc-
tions for the variations between the counters was made with
correction factors determined by requiring agreement with
the spectrum shape observed with the central counter of
the array. Several sets of correction factors were measur-
ed, and the sets were in agreement to within 5%. An array
data reduction computer program was written (largely by
Dr. A. D. Bacher) to make the above corrections. This
program is described in Appendix A.

In calculating the energy spectra with Equation (26),
the yield, $Y(E,\theta)$, and energy resolution, ΔE, were handled
as a single quantity. For the magnetic spectrometer, the
relative energy resolution $\Delta E/E$ is constant so that the
quantity $Y(E,\theta)/\Delta E$ can be written as $Y(E,\theta)/(R_E E)$ with
$R_E = \Delta E/E$. Since the particle energy E is proportional to
f^2 where f is the frequency measured with the NMR probe,
the spectra are proportional to $Y(E,\theta)/f^2$. It is this
quantity that the computer program mentioned above calcu-
lates.

A portion of each forward angle triton spectrum, in
the energy region around 7 MeV, is obscured by the tail of
the intense group of elastically scattered deuterons. In
these regions, the deuteron background was substracted as

reliably as possible, but many of the data points had to be eliminated. This difficulty remains for the lower energy regions of the 6° triton spectra. This problem does not occur for the ^{3}He spectra because the $(^{3}He^{++})$ ions have an energy greater than the deuterons for a given field setting of the spectrometer.

As discussed in Section III-A-4, the target thickness times the solid angle is given to first order by the geometrical factor, G_o. G_o was calculated from the previously measured dimensions of the spectrometer, but, since the zero settings of the entrance slits of the spectrometer were not recalibrated, the geometrical factors had the largest uncertainty of any of the parameters required for calculating the absolute cross section. The calculated value of the absolute cross section was checked by measuring the differential cross section for ^{3}He elastic scattering from ^{3}He(d,^{3}He)d at 33.3°. This calibration measurement was made under the same conditions as the energy spectra measurements so that differences due to the experimental configuration would be minimized. The calibration elastic scattering cross section agreed to within 6% with the previously measured value of Tombrello, et al. (1967) --- well within the combined uncertainties of the two experiments.

C. Results and Comparison with the Watson-Migdal Prediction

The measured spectra for the $^3\text{He}(d,t)2p$, $^3\text{H}(d,^3\text{He})2n$, $^3\text{He}(d,^3\text{He})pn$, and $^3\text{H}(d,t)pn$ reactions at laboratory angles $6°$, $10°$, $15°$, and $20°$ are shown in Figures 6, 7, 8, and 9, respectively. The data points are shown as filled circles, and the scatter in the points is indicative of their uncertainty. The smooth curves are calculated spectra which will be discussed below. The vertical scales in each figure are in arbitrary units and are not related to one another. The horizontal scales give the energy of the observed particle and have been corrected for energy loss in the target gas and exit foil. For the $^3\text{He}(d,t)2p$ and $^3\text{H}(d,^3\text{He})2n$ reactions, spectra were also measured at $7.5°$, $12.5°$, and $17.5°$, and for the $^3\text{He}(d,^3\text{He})pn$ and $^3\text{H}(d,t)pn$ reactions at $7.5°$. Figure 10 shows all the measured spectra plotted together on the same vertical scale. Each division on this scale corresponds to a differential cross section per unit energy of 52.5 millibarn/MeV-sterradian. These curves, shown alternately solid and dashed for greater clarity, were obtained by drawing smooth curves through the data points.

Some general remarks can be made about these spectra. For each reaction, the high-energy region of the spectra at forward angles is enhanced over what one would predict from three-body phase space with a constant transition matrix. At $6°$ and at $7.5°$, the enhancements are about equal, but

56

FIGURE 6

The triton energy distributions from $^3He(d,t)2p$ for laboratory angles 6° 10°, 15°, and 20° at an incident deuteron energy of 10.91 MeV. The vertical scales are arbitrary and are not related to one another for the four spectra shown. The horizontal scale is the energy the triton had at the center of the target cell. The arrows on the forward angle spectra indicate a region of the spectrum that is obscured by the intense group of elastically-scattered deuterons. The solid curves shown are calculated with the Watson-Migdal approximation using a_{pp} = -7.75 F, while the dashed curves at 6° indicate the sensitivity of the calculated shape to a $\pm$ 1 F change in the p-p scattering length. The scatter in the points indicate the statistical spread in the data.

FIGURE 6

58
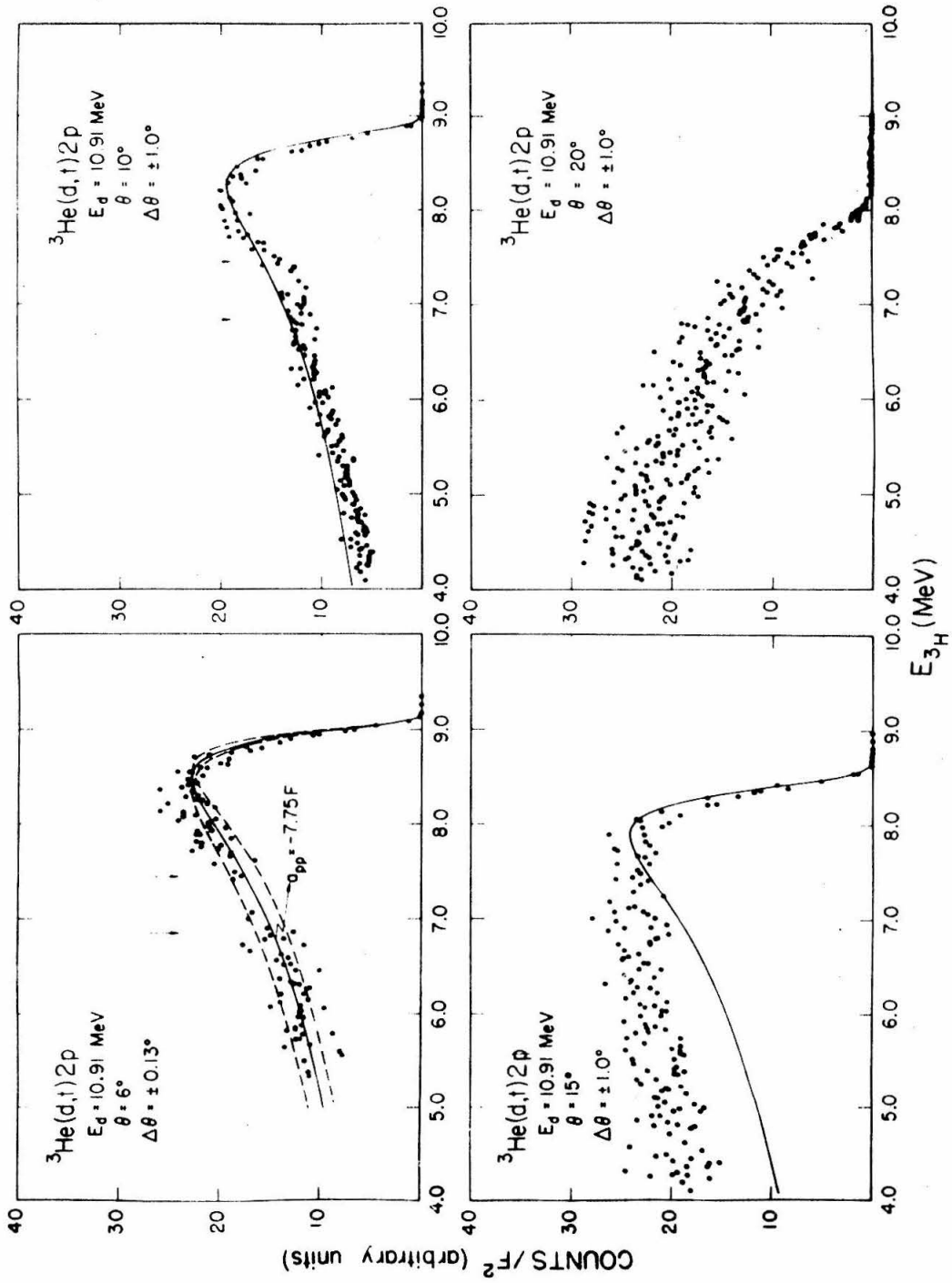
FIGURE 7

The ^{3}He energy distribution from ^{3}H(d,^{3}He)2n for the same angles and incident energy of Figure 6. The solid curves are again calculated from the Watson-Migdal formula using the n-n scattering length (-16.4 F) obtained from Haddock, et al., (1965). The dashed line on the 6° and 10° curves show the same calculation except that a_{nn} = -20.4 F has been used.
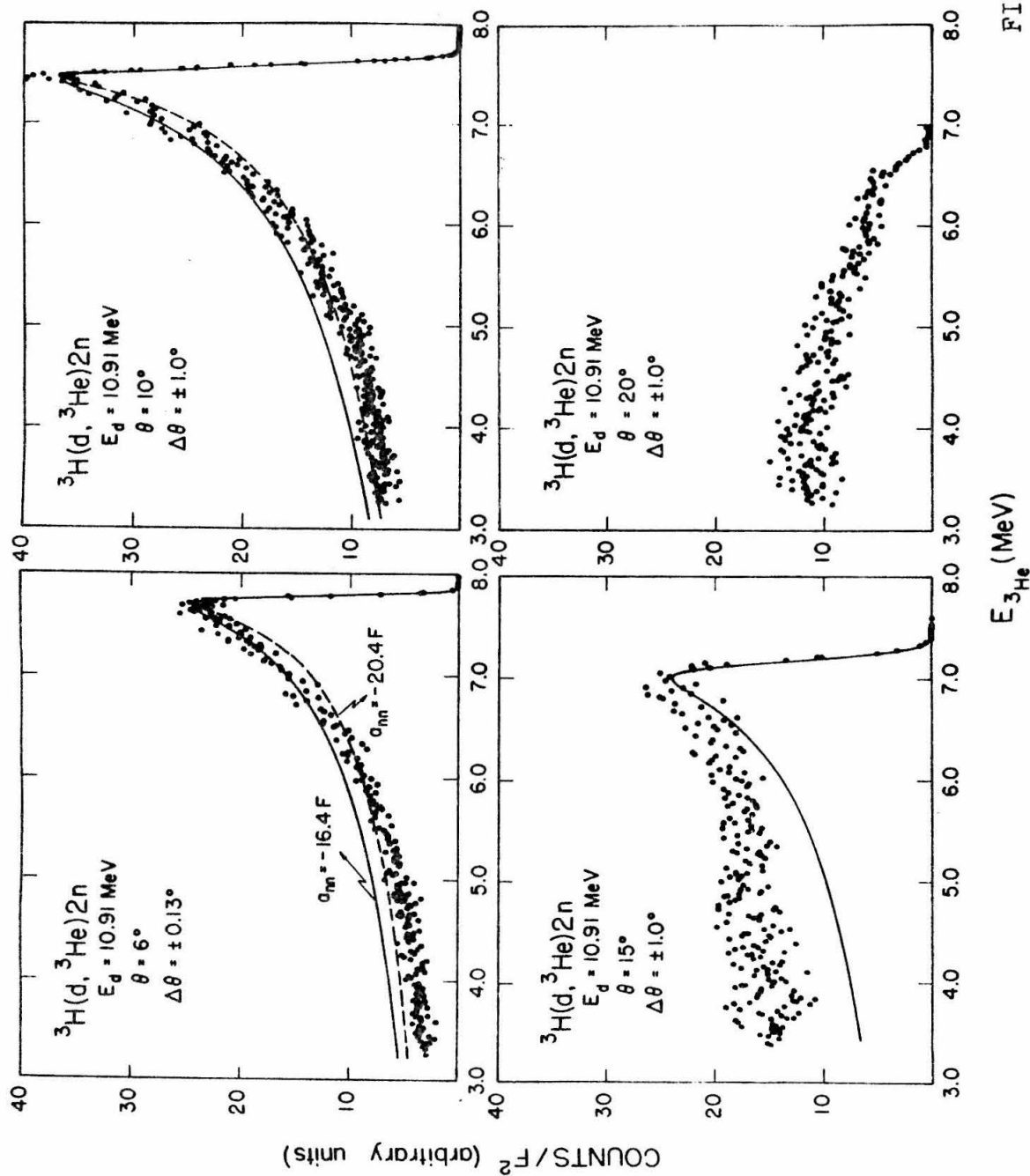
FIGURE 7

FIGURE 8

The ^{3}He energy distribution from ^{3}He(d,^{3}He)pn for the same angles and incident energies of Figure 6. The solid curves are calculated with the Watson-Migdal approximation using a_{np} = -23.7 F.
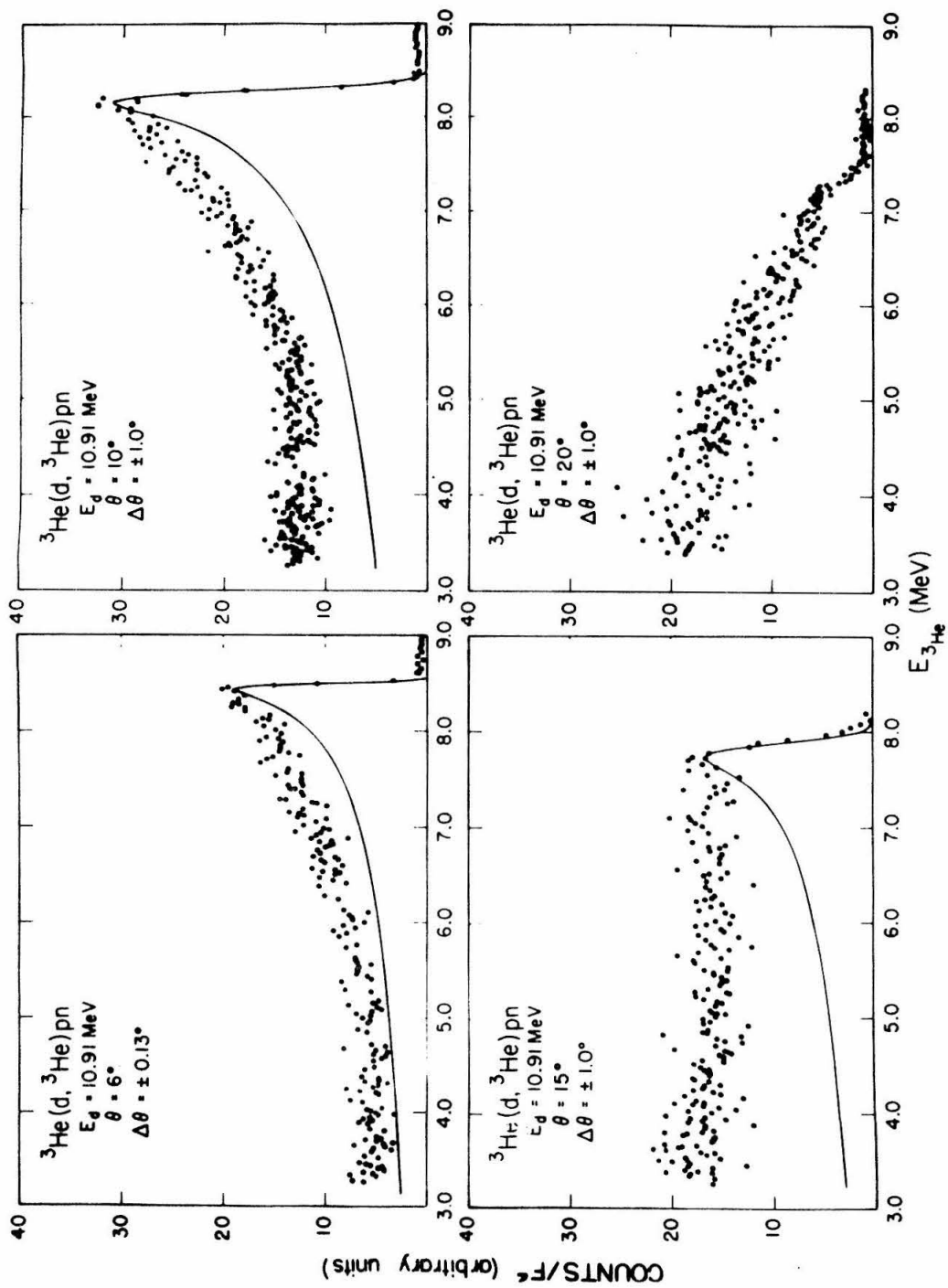
FIGURE 8

FIGURE 9

The ^{3}H energy distribution from ^{3}H(d,t)pn for the same angles and incident energy as Figure 6. The solid curves are calculated in the same way as Figure 8.
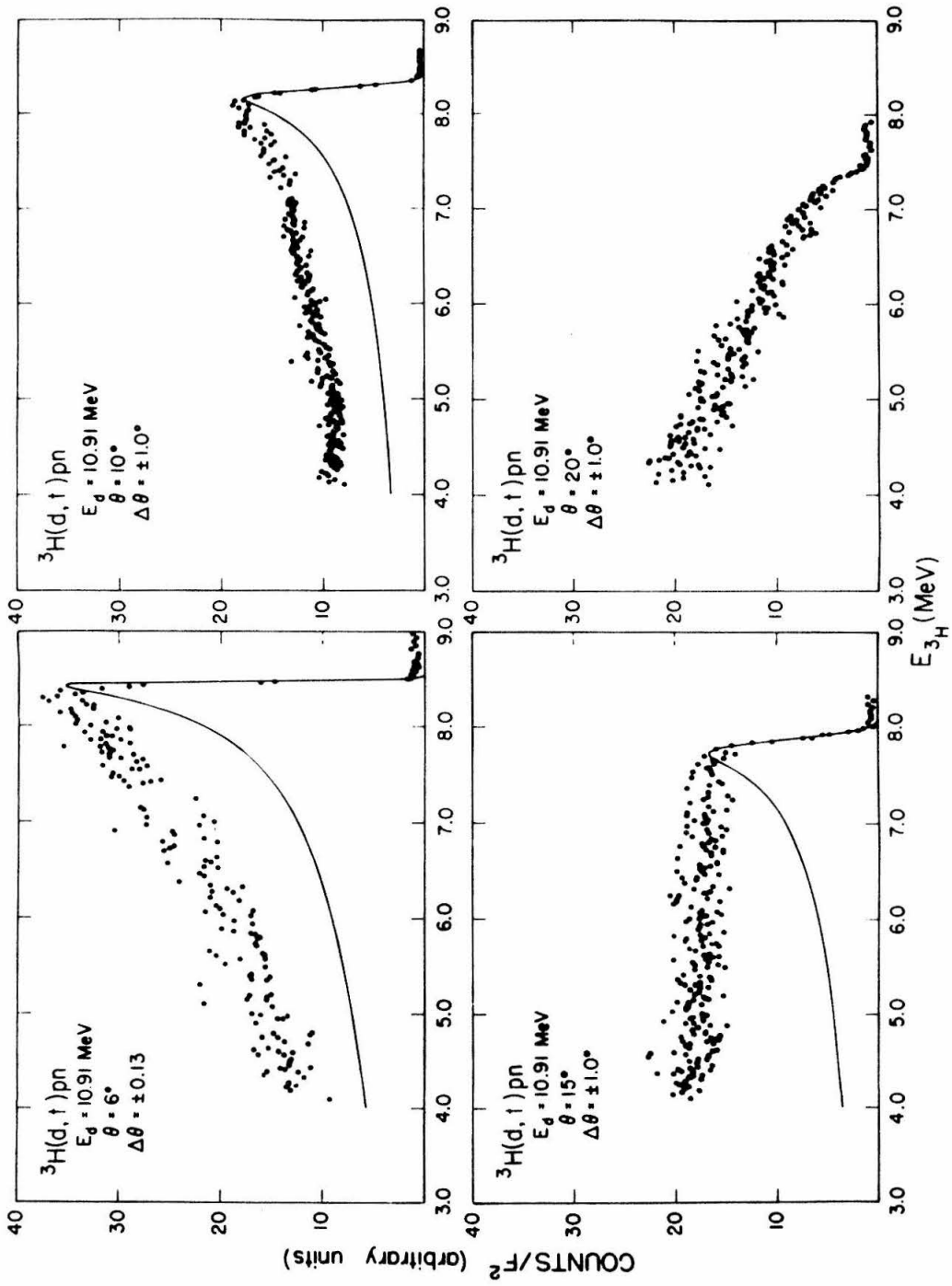
FIGURE 9

FIGURE 10

Results of all the measurements plotted on the same vertical scale; each division corresponds to a differential cross section of 52.5 millibarn/MeV-sterradian. These curves, shown alternately solid and dashed for greater clarity, were obtained by drawing smooth curves through the data points.
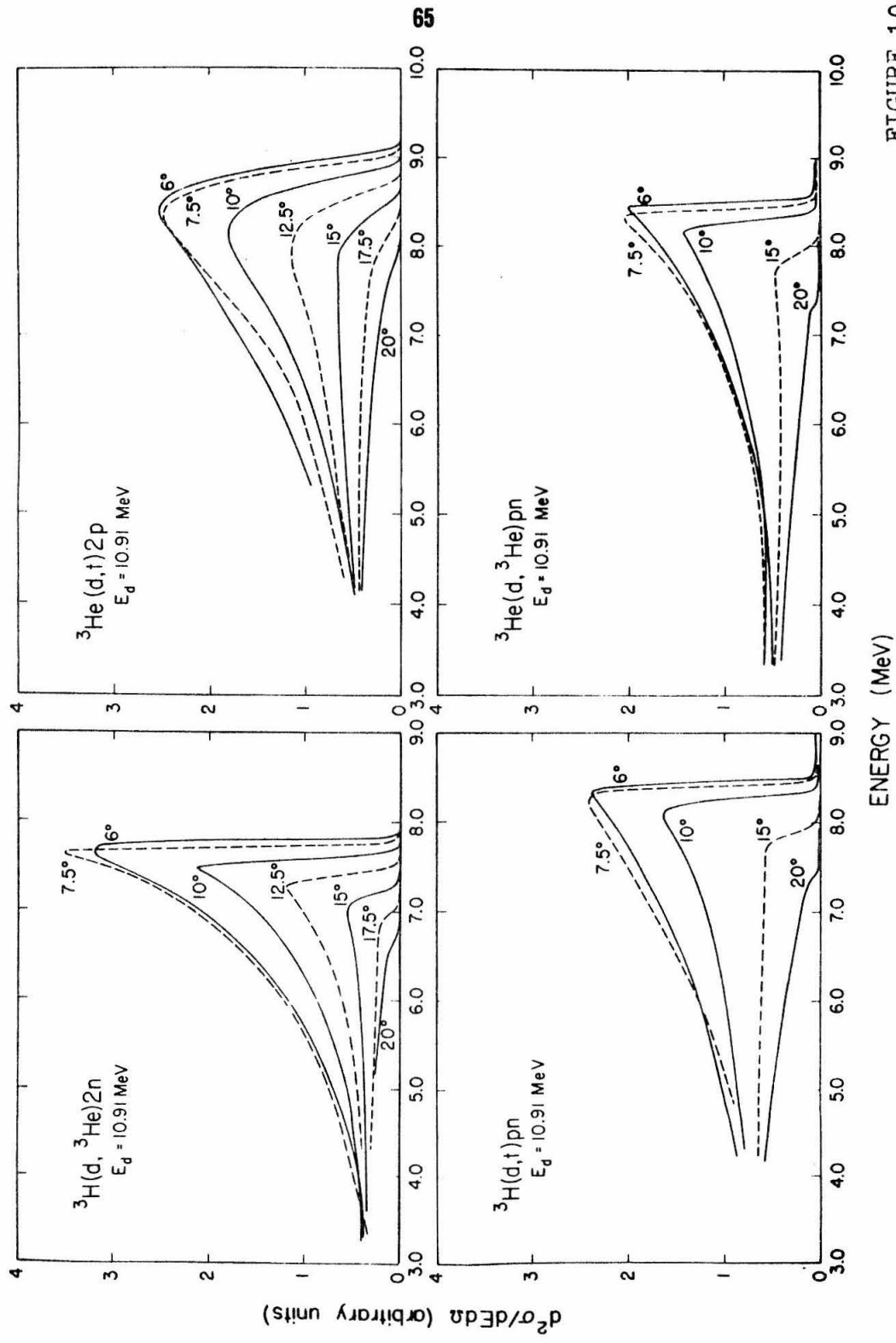
FIGURE 10

they rapidly diminish with laboratory angle and have nearly disappeared at 20°. In the ^{3}H(d,^{3}He)2n spectra, the sharp peaking at forward angles, due to the n-n final state interaction, is quite pronounced. The ^{3}He(d,t)2p spectra, on the other hand, are broadened and reduced in peak height by the repulsive Coulomb interaction between the final state protons. The additional triplet p-n state is the likely cause of the broader energy spectra observed in the ^{3}He(d,^{3}He)pn and ^{3}H(d,t)pn reactions. For these reactions, one expects from isospin algebra that the part due to the ^{1}S$_{o}$ p-n interaction should be half the size of the n-n and p-p cross sections. Strong evidence for the hypothesis that the enhancements are due to the ^{1}S$_{o}$ nucleon-nucleon final state interaction is the absence of the effect in the kinematically similar reaction, ^{4}He(d,α)pn (Tombrello and Bacher, 1965). Isospin conservation should strongly inhibit the s-wave, singlet p-n final state interaction in this reaction.

The curves shown in Figures 6, 7, 8, and 9 are fits to the data made with the Watson-Migdal approximation. The curves were calculated by using Equation (24), converting to the laboratory system, and folding in a Gaussian resolution function that corresponded to the total of the experimental energy resolutions listed in Table I. Each curve was normalized to the maximum of the spectrum. The values of the effective range parameters for the p-p and

and p-n systems were taken from Preston (1962).

For the ^{3}He(d,t)2p reaction at 6°, 10°, and 15°, the solid curves were calculated with the Watson-Migdal approximation using a_{pp} = -7.75 F (see Figure 6). At 6° and 10° the observed spectra appear to be adequately described by the approximation down to a triton energy of 6 MeV, although the prediction does not quite fit the leading edges. The 6 MeV triton energy corresponds to an excitation energy greater than 3 MeV in the p-p final state system. The dashed lines on the 6° data indicate the sensitivity of the Watson-Migdal prediction to a change of $\pm$ 1 F in the p-p scattering length.

For the ^{3}H(d,^{3}He)2n reaction at 6°, 10°, and 15°, the solid curves were calculated with the Watson-Migdal approximation using a_{nn} = -16.4 F, the value of the n-n scattering length determined by Haddock, et al. from the $D(\pi^-,\gamma)$2n reaction. The dashed curve shows the same calculation using a_{nn} = -20.4 F. If one arbitrarily limits the region of fitting to include only points below an n-n relative energy of 1 MeV, then the former value gives a quite adequate fit. However, if the entire spectrum is used, then the shape of the prediction is no longer adequate, and the best compromise fit is for a value of a_{nn} = -18 $\pm$ 2 F. This same uncertainty in the value of a_{nn} is found for the ^{3}He spectra for laboratory angles of 7.5^O and 12.5^O, although the exact

value of a_{nn} required is somewhat more negative at 7.5° and is less negative at 12.5°.

The solid curves in Figures 8 and 9 were calculated with the Watson-Migdal approximation using $a_{np} = -23.7$ F. For the $^{3}He(d,^{3}He)pn$ and $^{3}H(d,t)pn$ reactions, the presence of the additional triplet p-n interaction is apparent even at the most forward angles.

The measurements included a search for evidence of a bound di-neutron. Figure 11 shows the results of a scan of the region above the three-body end point for the $^{3}H(d,^{3}He)2n$ reaction at a laboratory angle of 7.5°. The solid curve is a Watson-Migdal fit to the data using $a_{nn} = -16.4$ F. This scan covers an n-n relative energy range down to about -675 keV and determines a cross section limit on the production of a bound di-neutron of 5 μb/sr. The same limit was also set with data taken at 6°.

D. Discussion

The measurements show that at very forward angles ($\theta_3 \leq 12.5^{\circ}$) the two-nucleon final state interaction plays an important role in determining the energy distribution of the mass-three nuclei. For angles greater than 12.5°, however, the effect of the final state interaction diminishes and other processes become important. The reaction mechanism changes rapidly over a small angular interval,

FIGURE 11

The measurement of the region above the three-body end points for $^{3}H(d,^{3}He)2n$ at a laboratory angle of 7.5^{o}. The solid dots and curve show the data and corresponding fit up to a 2n excitation energy of about 800 keV. The open circles and the dashed curve give a one hundred fold expansion of the vertical scale. The vertical error bars represent the statistical uncertainty in the individual points, and the horizontal bars indicate the experimental energy resolution of 59 keV.
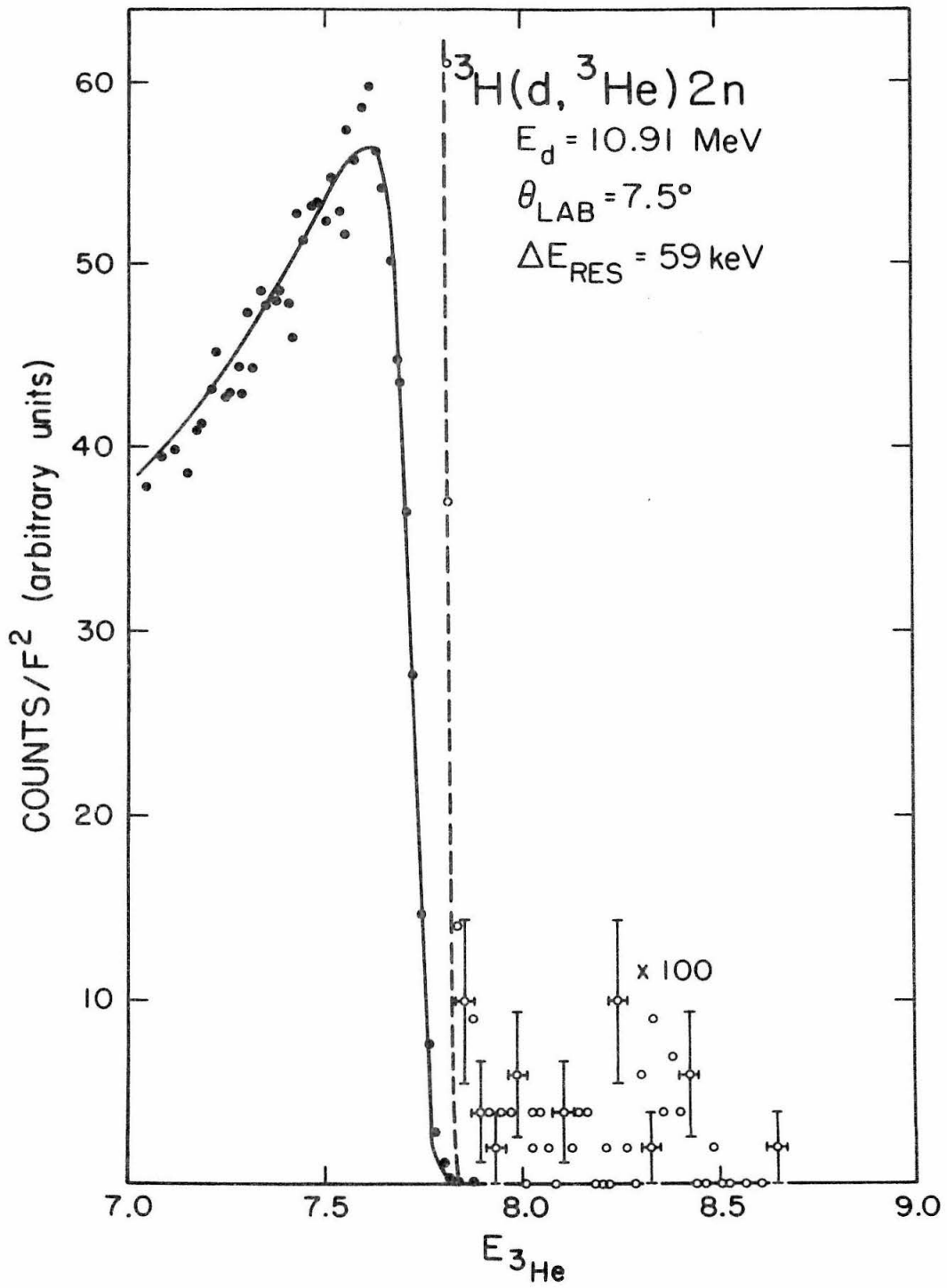
FIGURE 11

indicating an interference between the final state inter-
action and the primary mechanism which initiates the
reaction.

The observed behavior of the spectra leads one to
question the applicability of the Watson-Migdal approxi-
mation at very forward angles even though its predictions
agree with the measured spectra. As discussed in Part II,
the Watson-Migdal approximation is based on the assumption
that the primary interaction is isolated from the final
state interaction. The observations, on the other hand,
indicate that the interactions are not separated over the
limited angular range measured. Thus, the theoretical
assumptions necessary for the Watson-Migdal approximation
may not be justified, and perhaps it is merely fortuitous
that the forward angle spectra and the Watson-Migdal
predictions are in agreement. What one needs is a better
understanding of the total mechanism occuring in these
reactions. In Part IV we describe a calculation that pro-
vides additional information regarding this question.

IV.   PLANE WAVE BORN APPROXIMATION CALCULATIONS

In Part III we have seen that the quality of the
Watson-Migdal fits to the observed spectra rapidly decreases
with increasing laboratory angle.   Except for effects due
to phase-space kinematics, the Watson-Migdal approximation
predicts no change of shape in the spectra with laboratory
angle.   Furthermore, each predicted spectrum must be norma-
lized at each angle.   Thus, the Watson-Migdal approximation
does not give a systematic description of the observations.

As indicated in Section II-C, Born approximation cal-
culations provide a way to study the contribution of the
primary interaction to the reaction mechanism.   Predictions
are possible for both spectra and angular distributions.
An understanding of the primary interaction's contribution
to the ^{3}He(d,t)2p and ^{3}H(d,^{3}He)2n reaction mechanisms is
interesting both for its own sake and, as we have seen, for
the proper application of final state interaction theories
used to extract nucleon-nucleon scattering parameters.

Two PWBA calculations for the ^{3}He(d,t)2p and
^{3}H(d,^{3}He)2n reactions are described in this Part.   The
calculation described in Section A assumes that the reaction
proceeds via a direct neutron pickup process.   This process
was postulated by Henley, et al. (1967) in their calculation
of triton angular distributions from the ^{3}He(d,t)2p reaction
at forward angles.   While the results of our first

calculation are in qualitative agreement with our observed
spectra, the more extensive calculation described in
Section B shows that such simple models for the primary
reaction mechanism are not justified.

A. Neutron Pickup Calculation

The calculation presented in this Section is intended
to illustrate the results obtainable with the direct neutron
pickup model (Bilaniuk and Slobodrian, 1963, Jakobsen,
et al., 1965; Henley, et al., 1967) and to provide a com-
parison for the results obtained with the calculation of
Section B. Since the calculation methods used very closely
follow those described by Banerjee (1960), we shall, in the
interest of brevity, only sketch the calculation.

The reaction was assumed to proceed as a direct pick-
up of the neutron of the ^{3}He target by the incident deute-
ron, producing a triton and two interacting protons in the
final state. The interaction was assumed to occur between
the neutron and the deuteron as a whole. Exchange effects
and the spins of the particles were ignored. The ^{3}He wave
function was assumed to be factorable into a product of
two wave functions, one which described the two protons and
one which described the neutron. Similarly, the triton was
assumed to be a product of two wave functions, one describ-
ing the proton and neutron, the other describing the re-
maining neutron. In keeping with the assumed peripheral

nature of the pickup reaction mechanism, the wave functions
describing the neutron were taken to have the asymptotic
radial form. The final state interaction between the
protons was included by using the proton-proton scattering
wave function. In calculating the overlap integral, the
explicit potential dependence was eliminated using Green's
theorem. To approximate distortion effects, a cutoff radius
was applied to the integrals describing the transfer of the
neutron.

Figure 12 compares the calculated spectra with our
data. The curves are normalized with respect to the 6°
data. A cutoff radius of 3 F has been used. The effect of
this pickup process is very nearly to superimpose a Butler
type angular distribution on the Watson-Migdal spectrum
shape. The apparent difference in the shapes of the curves
would be removed if they were redrawn on different scales,
for the curves are almost congruent when their maxima's are
matched.

Figure 13 indicates the change in the angular distri-
bution with cutoff radius. The filled circles were obtained
by integrating the regions of the spectra corresponding to
relative energies in the final state p-p system from 0 to 2
MeV, while the barred lines correspond to the maximum value
of each spectrum. The shapes of the calculated spectra are
not sensitive to the cutoff radius for values less than 3 F.

FIGURE 12

The PWBA (direct neutron pickup) fits to our 6°, 10°, 15°, and 20° ^{3}He(d,t)2p data. All of the spectra are plotted on the same scale. The curves were calculated with the assumptions described in Section IV-A. They are arbitrarily normalized to the data at 6°. A cutoff radius of 3 F has been applied to the integrals describing the transfer of the neutron.
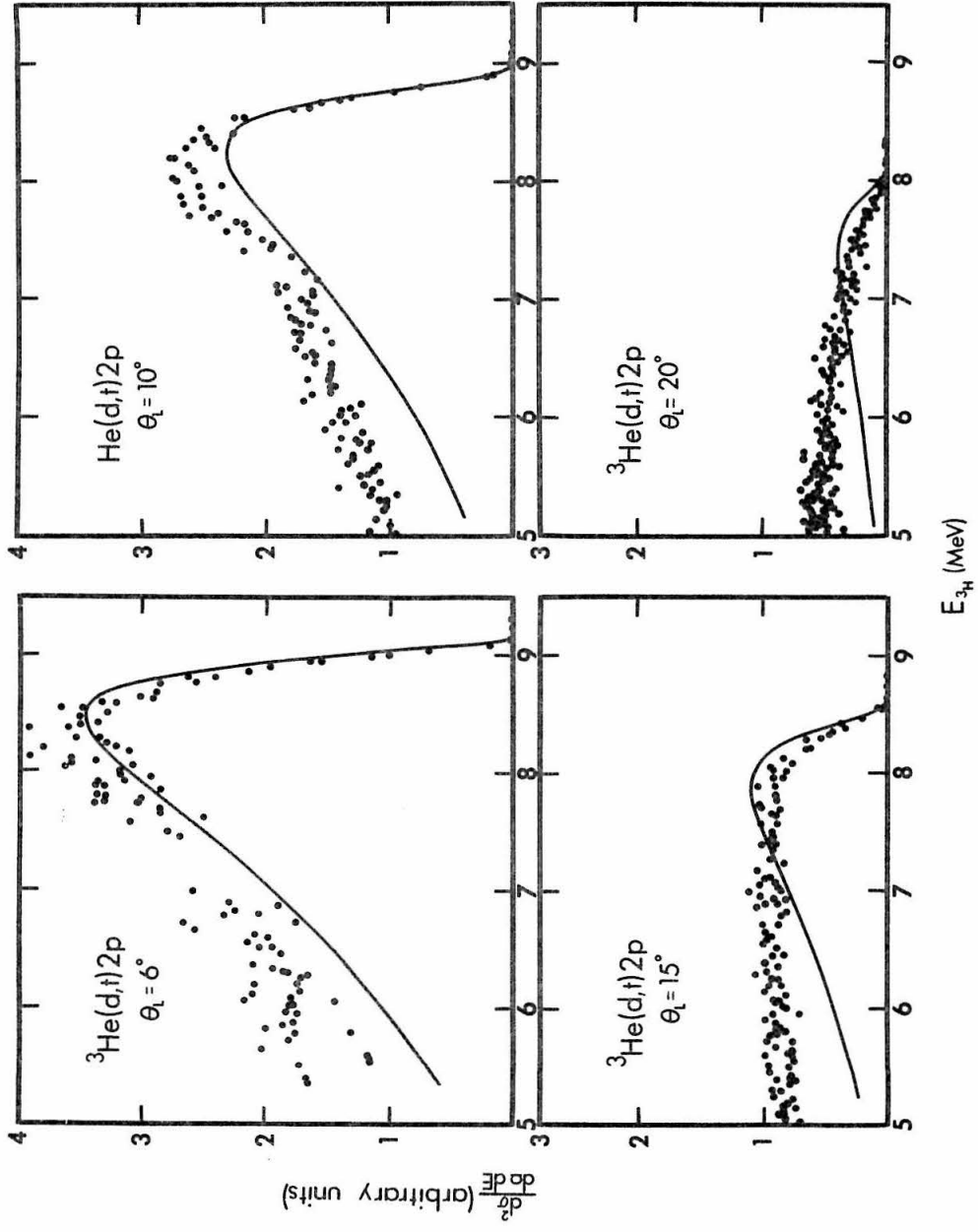
FIGURE 12

FIGURE 13

Comparison of PWBA (direct neutron pickup) calculated angular distributions with our ^{3}He(d,t)2p data. The filled circles indicate the angular distribution obtained by integrating the regions of the spectra corresponding to relative energies from 0 to 2 MeV in the final state proton-proton system. The barred lines indicate the angular distribution obtained by taking only the maxima of the spectra. The curves were calculated with the assumptions described in Section IV-A. Cutoff radii of 0.0, 1.5, and 3.0 F were applied to the integrals describing the transfer of the neutron. The best fit was obtained with the cutoff radius of 3.0 F.
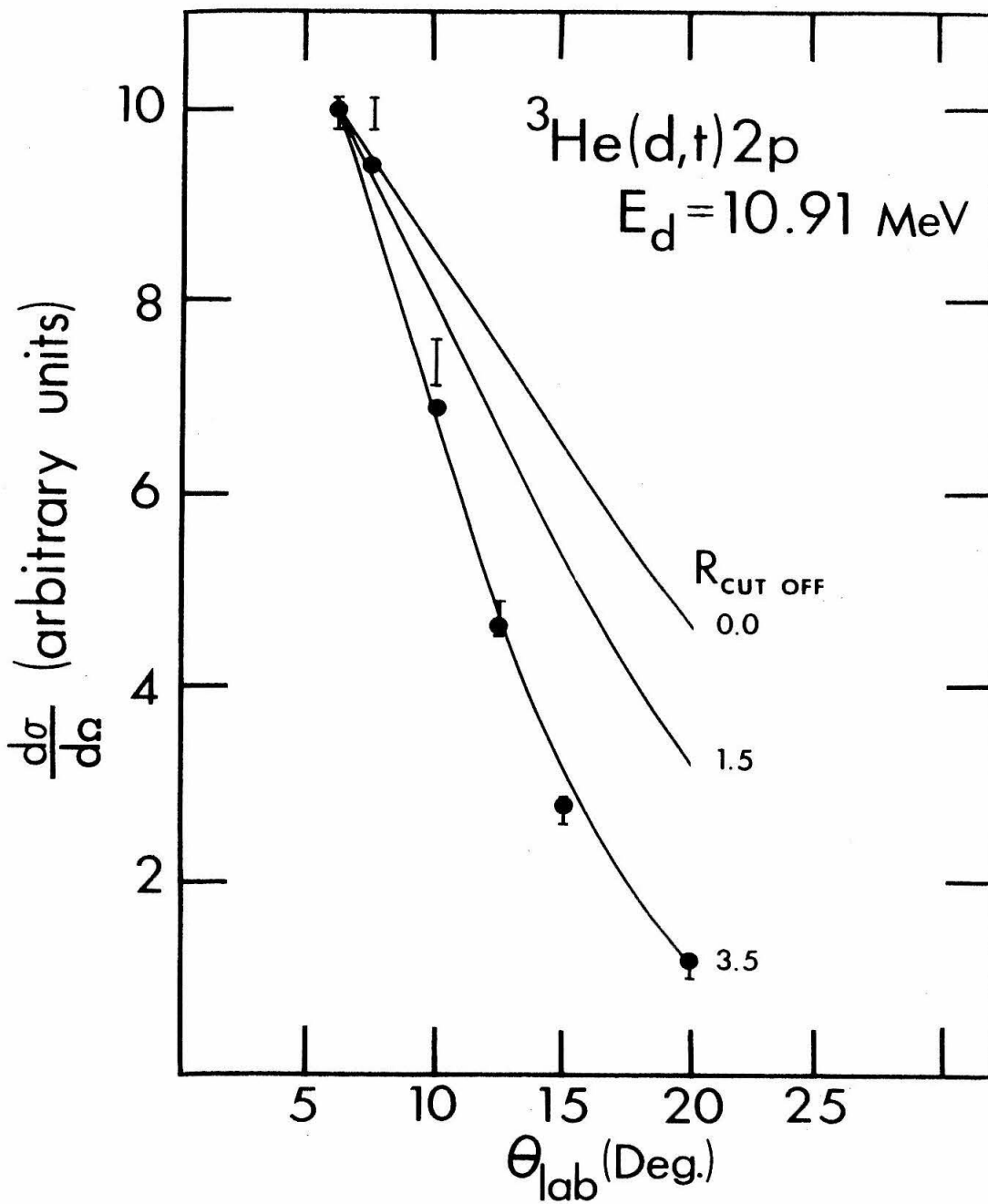
FIGURE 13

For cutoff radii greater than 3 F, the fits to the observed spectra rapidly deteriorate.

B. Antisymmetrized Calculation

Despite its qualitative agreement with the data, the calculation described in Section A fails in one respect. The assumed direct pickup mechanism cannot predict the observed change in spectrum shape at very forward angles because the final state interaction occurs as a multiplicative factor in the transition amplitude. This is true in both the PWBA and DWBA formulations and only depends upon the assumption that the wave functions are of the product form. Since we are calculating the collision of two loosely bound systems, exchange effects may be important. Other reaction processes may contribute, perhaps significantly, to the total transition amplitude, and an estimate should be made of their contributions. If the contributions of other processes were significant, they could interfere with the direct process and cause the rapid change in shape observed in the spectra.

Our calculations assume that the observed triton or ^{3}He ion does not interact with the nucleons of the final state. However, the influence of the p-^{3}H and n-^{3}He interactions upon the triton and ^{3}He spectra is unknown. These interactions should have their greatest effect somewhat below the mass-three three-body end point. While in most

studies these effects have not been observed, Jakobsen, et al. did find a statistically relevant "bump" at 6°, $E_{3_{He}} = 21$ MeV for the $D(^3He,t)2p$ reaction which occurred at the appropriate place in the triton spectrum. Since no other evidence of the $p-^3H$ resonance was observed, they chose not to attribute it to a $p-^3H$ final state interaction. Because such effects have not been observed by others or ourselves, we make the assumption in our calculations that the nucleons do not interact either individually or as a unit with the observed mass-three nucleus. Nevertheless, the effect may be important in the tail regions of the spectra, and it remains as another point on which to question the validity of the Watson-Migdal approximation as applied to this reaction.

In the following calculations, we included only two-body interactions and neglected three-body forces. We used an antisymmetrized final state wave function and a symmetrical, finite-range, spin-dependent, central interaction in evaluating the first order transition amplitudes. Thus, we included all of the possible first order contributions to the total matrix element. Our purpose was to estimate the relative importance of the processes that contribute to the total transition amplitude and to relate the $^3H(d,^3He)2n$ and $^3He(d,t)2p$ reaction cross sections in order to study the comparison method for determining a_{nn}.

Since the mathematical methods used were straight-forward, we shall only outline the calculations. Further-more, we shall only describe the calculation of the ^{3}He(d,t)2p reaction in any detail; the results for the ^{3}H(d,^{3}He)2n reaction are easily obtained by adjusting the Coulomb interactions between the nucleons.

1. ^{3}He(d,t)2p Reaction

   a. Description

   The five particle system was treated as if it were composed explicitly of three protons and two neutrons, designated as particles 1, 2, 4, and 3, 5, respectively. Explicitly keeping track of the protons and neutrons has the advantage that one can see how each process arises from the exchange nature of the interactions and the antisymmetrization of the final state wave function.

   With the PWBA, the expression for the total transition matrix, Equation (10), becomes

$$T_{f'i} = \langle \psi_f | V | \psi_i \rangle \tag{27}$$

where the initial and final state wave functions are defined as

$$\psi_i = (\frac{1}{2\pi})^{3/2} \exp(i\bar{K}_i \cdot \bar{R}_i) \psi_H(\bar{r}_1, \bar{r}_2, \bar{r}_3) \psi_d(\bar{r}_4, \bar{r}_5) \eta_i(12345)$$

$$\psi_f = A \left\{ (\frac{1}{2\pi})^{3/2} \exp(i\bar{K}_f \cdot \bar{R}_1) \psi_t(\bar{r}_3, \bar{r}_4, \bar{r}_5) \Phi_{pp}(\bar{r}_1, \bar{r}_2) \eta_f(12345) \right\} \tag{28}$$

with the operator A signifying the antisymmetrization of
the final state wave function with respect to the exchange
of all pairs of protons and the pair of neutrons. The
initial state plane wave describes the relative motion of
the incident deuteron (nucleons 4 and 5) with respect to
the target ^{3}He nucleus (nucleons 1, 2, and 3) with the
wave vector $\bar{K}_i$ and the displacement $\bar{R}_i$. Similarly, the
final state plane wave describes the relative motion of
the outgoing triton (nucleons 3, 4, and 5) and the p-p
system's center-of-mass with the wave vector $\bar{K}_f$ and the
displacement $\bar{R}_1$. The functions $\psi_H(\bar{r}_1,\bar{r}_2,\bar{r}_3)$, $\psi_d(\bar{r}_4,\bar{r}_5)$,
$\psi_t(\bar{r}_3,\bar{r}_4,\bar{r}_5)$ and $\Phi_{pp}(\bar{r}_1,\bar{r}_2)$ describe the spatial structure
of the ^{3}He, deuteron, triton, and singlet p-p state,
respectively. Each of these functions are assumed to be
spatially symmetric. The function $\eta_i(12345)$ describes
the initial spin state, while $\eta_f(12345)$ describes the
final spin state. The spin wave functions are taken to
be antisymmetric. After antisymmetrization, the final
state wave function can be written

$$\psi_f = \frac{1}{(2\pi)^{3/2}}\frac{1}{\sqrt{3}}\left[\exp(i\bar{K}_f\cdot\bar{R}_1)\psi_t(\bar{r}_1,\bar{r}_2,\bar{r}_3)\Phi_{pp}(\bar{r}_{12})\eta_f(12345)\right.$$
$$-\exp(i\bar{K}_f\cdot\bar{R}_2)\psi_t(\bar{r}_1,\bar{r}_3,\bar{r}_5)\Phi_{pp}(\bar{r}_{42})\eta_f(42315) \quad (29)$$
$$\left.-\exp(i\bar{K}_f\cdot\bar{R}_3)\psi_t(\bar{r}_2,\bar{r}_3,\bar{r}_5)\Phi_{pp}(\bar{r}_{14})\eta_f(14325)\right]$$

Here, in terms of the nucleon position vectors $\bar{r}_1$, $\bar{r}_2$, $\bar{r}_3$,
$\bar{r}_4$, and $\bar{r}_5$, the coordinate variables are defined as

$$\bar{r}_{ij} = \bar{r}_i - \bar{r}_j$$

$$\bar{R}_i = (\bar{r}_4 + \bar{r}_5)/2 - (\bar{r}_1 + \bar{r}_2 + \bar{r}_3)/3$$

$$\bar{R}_1 = (\bar{r}_1 + \bar{r}_2)/2 - (\bar{r}_3 + \bar{r}_4 + \bar{r}_5)/3$$

$$\bar{R}_2 = (\bar{r}_2 + \bar{r}_4)/2 - (\bar{r}_1 + \bar{r}_3 + \bar{r}_5)/3 \qquad (30)$$

$$\bar{R}_3 = (\bar{r}_1 + \bar{r}_4)/2 - (\bar{r}_2 + \bar{r}_3 + \bar{r}_5)/3$$

With the above definitions for the wave functions, the perturbing interaction is the sum of the remaining six nucleon-nucleon interactions

$$V = \sum_{i=1}^{3} \sum_{j=4}^{5} (V_{ij})$$

The nucleon-nucleon interaction $V(ij)$ is assumed to have the scalar form

$$V(ij) = V_N(r_{ij}) \ (w + bP_{ij}^{\sigma} + mP_{ij}^{r} + hP_{ij}^{r}P_{ij}^{\sigma}) + \epsilon_{ij}V_C(r_{ij}) \qquad (31)$$

where $V_N(r_{ij})$ and $V_C(r_{ij})$ describe the radial shapes of the nuclear and Coulomb potentials, respectively. This choice of nucleon-nucleon interaction conserves channel spin so that only singlet configurations in the entrance channel

contribute to the transition amplitude. P_{ij}^{σ} and P_{ij}^{r} are the spin and space exchange operators, respectively, while ϵ_{ij} is equal to one if i and j are protons and is equal to zero otherwise. The constants w, b, m, and h are the coefficients for the relative strengths of the Wigner, Bartlett, Majorana, and Heisenberg forces, respectively. They are normalized so that

$$w + b + m + h = 1 \qquad (32)$$

for the triplet interaction, and

$$w - b + m - h = .63 \qquad (33)$$

for the singlet interaction. The exact force mixture has not been established, but nucleon-nucleon scattering data require that it be close to a Serber mixture. The method of Thompson and Tang (1967) was used to vary the force mixture. With their method, the nucleon-nucleon potential was expressed in the form

$$V(ij) = yV_{serber} + (1 - y)V_{symmetric} \qquad (34)$$

where V_{serber} is the potential of Equation (31) with w = m and b = h, and $V_{symmetric}$ is the potential with m = 2b and h = 2w. The parameter y can then be varied to determine an intermediate force mixture, but y should not be too different from 1.

With the above assumptions and approximations and after a lengthy but straightforward calculation, the total matrix element for the reaction can be expressed as

$$
\begin{aligned}
T_{fi} = N\Big\{ &(2w + b - m - 2h)I_{14}(r_{14}) + (2w + b - m - 2h)I_{24}(r_{24}) \\
&- mI_{34}(r_{14}) - mI_{34}(r_{24}) + 2(w + m)I_{34}(r_{34}) + (2w + b)I_{15}(r_{15}) \\
&+ (2w + b)I_{25}(r_{25}) + 2(w - b + m - h)I_{35}(r_{35}) \\
&- (w + 2b - 2m - h)J_{14}(r_{14}) - (w - b + m - h)J_{24}(r_{24}) \\
&- wJ_{34}(r_{34}) + (2m + h)J_{15}(r_{14}) - (w + b + m + h)J_{15}(r_{15}) \\
&- wJ_{25}(r_{25}) - (w - b + m - h)J_{35}(r_{35}) - (w - b + m - h)K_{14}(r_{14}) \\
&- (w + 2b - 2m - h)K_{24}(r_{24}) - wK_{34}(r_{34}) - wK_{15}(r_{15}) \\
&+ (2m + h)K_{25}(r_{24}) - (w + b + m + h)K_{25}(r_{25}) \\
&- (w - b + m - h)K_{35}(r_{35}) - mL_{15}(r_{15}) - mL_{25}(r_{25}) \Big\}
\end{aligned}
\tag{35}
$$

where

$$
\begin{aligned}
I_{\mu\nu}(r_{kl}) = \int &\exp\left\{-i\bar{K}_f \cdot \bar{R}_1\right\} \Phi_{PP}^*(\bar{r}_{12}) \psi_t^*(\bar{r}_3,\bar{r}_4,\bar{r}_5) V_{\mu\nu}(r_{kl}) \\
&\exp\left\{i\bar{K}_i \cdot \bar{R}_i\right\} \psi_H(\bar{r}_1,\bar{r}_2,\bar{r}_3) \psi_d(\bar{r}_{45}) d\tau \\
J_{\mu\nu}(r_{kl}) = \int &\exp\left\{-i\bar{K}_f \cdot \bar{R}_2\right\} \Phi_{PP}^*(\bar{r}_{42}) \psi_t^*(\bar{r}_1,\bar{r}_3,\bar{r}_5) V_{\mu\nu}(r_{kl}) \\
&\exp\left\{i\bar{K}_i \cdot \bar{R}_i\right\} \psi_H(\bar{r}_1,\bar{r}_2,\bar{r}_3) \psi_d(\bar{r}_{45}) d\tau \\
K_{\mu\nu}(r_{kl}) = \int &\exp\left\{-i\bar{K}_f \cdot \bar{R}_3\right\} \Phi_{PP}^*(\bar{r}_{14}) \psi_t^*(\bar{r}_2,\bar{r}_3,\bar{r}_5) V_{\mu\nu}(r_{kl}) \\
&\exp\left\{i\bar{K}_i \cdot \bar{R}_i\right\} \psi_H(\bar{r}_1,\bar{r}_2,\bar{r}_3) \psi_d(\bar{r}_{45}) d\tau \\
L_{\mu\nu}(r_{kl}) = \int &\exp\left\{-i\bar{K}_f \cdot \bar{R}_i\right\} \Phi_{PP}^*(\bar{r}_{45}) \psi_t^*(\bar{r}_1,\bar{r}_2,\bar{r}_3) V_{\mu\nu}(r_{kl}) \\
&\exp\left\{i\bar{K}_i \cdot \bar{R}_i\right\} \psi_H(\bar{r}_1,\bar{r}_2,\bar{r}_3) \psi_d(\bar{r}_{45}) d\tau
\end{aligned}
\tag{36}
$$

and N is a normalization constant. The subscripts on the potentials indicate the interacting pair of particles.

Each of the above integrals can be classified as belonging to one of the seven schematic diagrams shown in Figure 14. The diagrams are only intended to represent the "topology" of the reaction mechanisms, and each diagram may correspond to a number of different physical processes. The lines in each diagram schematically represent the "paths" taken by the nucleons in going from the initial to the final state. There are three different patterns for these paths, corresponding as to whether none, one, or two nucleons are transferred from the ^{3}He nucleus to the deuteron. The ellipse represents the final state interaction between the protons. The dashed line represents the interaction between a particular nucleon of the target and of the projectile; it distinguishes the manner in which the transfer mechanism occurs. For example, Diagrams 1 and 2 both represent a neutron pickup process, but, in Diagram 1, the interactions do not include the neutron being transferred, while, in Diagram 2, they only include this neutron. Thus, we would refer to Diagram 2 as a direct pickup process and to Diagram 1 as an indirect or re-arrangement process. Listed below the diagrams are the integrals to which the diagrams correspond. Diagrams 3, 4, 5, and 6 represent reaction modes in which two nucleons

FIGURE 14

Schematic diagrams of the radial integrals of the transi-
tion matrix. The straight lines represent the "paths"
taken by the nucleon in going from the initial to the final
state; the dashed lines represent the perturbing nucleon-
nucleon interaction; the ellipses represent the final state
interaction between the protons. The functions listed
below each diagram indicate the radial integrals associated
with that diagram and are defined in the text.
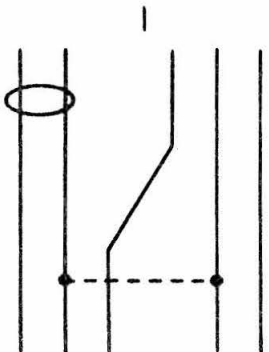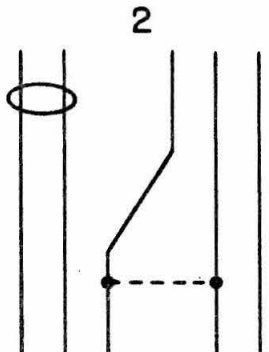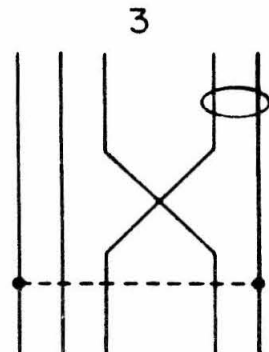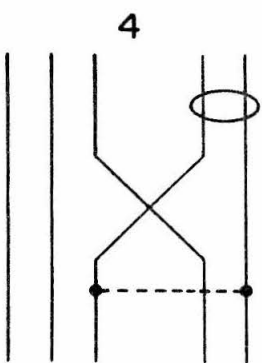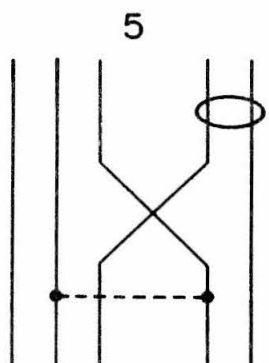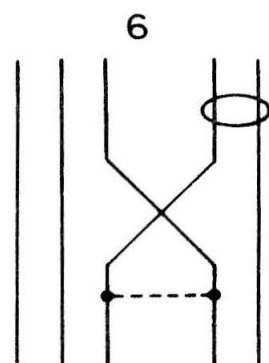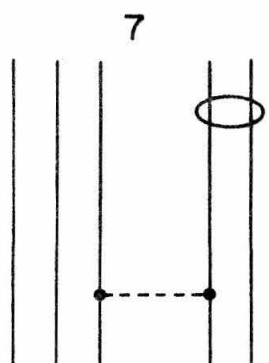
FIGURE 14

are transferred. Diagram 7 represents the case of no nucleons being transferred. This case can only occur through a Majorana exchange force and can be pictured, if one so desires, as a charge exchange process.

The evaluation of all of these integrals may be done analytically if Gaussians are used for each of the functions in the integrals. Therefore, it is convenient to express the bound state functions and the interaction potentials as sums of Gaussians. For the deuteron, we use the expansion

$$\psi_d(r) = \sum_{i=1}^{3} C_i \exp(-\alpha_i r^2) \tag{37}$$

where the parameters C_i and α_i are from van Oers (1967). They are:

i	C_i	α_i
1	.01388	.01691
2	.05583	.09018
3	.11784	.42836

For $r > 1$ F this function closely approximates the Hulthen wave function, and for $r < 1$ F it approaches the origin in a manner required by a hard-core potential. Gaussian, Irving, and Irving-Gunn wave functions (Griffy, et al., 1964) were used in the calculation to describe the mass-three nuclei in order to study the effect of the mass-three nuclei's spatial distribution on the predicted spectra.

Each of these wave functions only depends upon the sum of the squares of the separations between the particles. We may write this sum as

$$z^2 = (\bar{r}_1 - \bar{r}_2)^2 + (\bar{r}_1 - \bar{r}_3)^2 + (\bar{r}_2 - \bar{r}_3)^2 \tag{38}$$

With Equation (38) the Gaussian, Irving, and Irving-Gunn functions can be written

$$u_G(z) = \frac{3^{3/4}\gamma^3}{\pi^{3/2}}\exp(-\gamma^2 z^2/2)$$

$$u_I(z) = \frac{3^{3/4}\gamma^3}{\sqrt{120}\pi^{3/2}}\exp(-\gamma^2 z/2) \tag{39}$$

and

$$u_{IG}(z) = \frac{3^{3/4}\gamma^3}{\sqrt{2}\pi^{3/2}}\exp(-\gamma^2 z/2)/z$$

Gaussian expansions, defined by the equation

$$u(r) = \sum_{i=1}^{3} A_i \exp(-\delta_i r^2) \tag{40}$$

were made to the Irving and Irving-Gunn functions; their parameters, along with those of the Gaussian function, are listed in the following table:

i	Gaussian		Irving		Irving-Gunn	
	A_i	δ_i	A_i	δ_i	A_i	δ_i
1	1.0	0.1200	0.00450	0.06900	0.00526	0.05142
2			0.02444	0.22961	0.03681	0.22450
3			0.03727	1.34010	0.10072	0.99642

The fits of these expansions to the Irving and Irving-Gunn functions are neither unique nor probably the best possible fits obtainable with the method. Nevertheless, they are sufficiently accurate for the purposes of our calculation. As with the deuteron expansion, the fits only differ substantially from the functions in the region near the origin where the contributions to the integrals are small.

The spatial form of the nuclear interaction was taken to be a single Gaussian

$$V_N(r) = -V_o \exp(-\beta^2 r^2) \qquad (41)$$

where V_o is the strength and β is the inverse-range of the potential. As a convenience in studying the relative importance of the contribution of the Coulomb potential to the matrix element, the Coulomb part of the interaction was handled separately from the nuclear part. Thus, in calculating the total matrix element, there were six additional Coulomb terms corresponding to those integrals

which have interactions between protons. The Coulomb interaction

$$V_C(r) = \frac{e^2}{r} \tag{42}$$

was expanded in the same manner as the bound-state functions:

$$V_C = \sum_{i=1}^{4} B_i \exp(-\zeta_i r^2) \tag{43}$$

The parameters used were:

i	B_i	ζ_i
1	2.0454×10^{-3}	5.8174×10^{-4}
2	3.2967×10^{-3}	8.1899×10^{-3}
3	7.7669×10^{-3}	4.7414×10^{-2}
4	1.7965×10^{-2}	2.8663×10^{-1}

This expansion approximates the potential function between 2 and 38 F to better than $\pm$ 5%.

The singlet p-p scattering wave function $\Phi_{pp}(r)$ was obtained by numerically solving the corresponding Schrodinger equation with the boundary condition that the solution match the asymptotic Coulomb wave function. A Yukawa potential was used for the nuclear part of the p-p interaction. The solutions were checked by calculating the phase shift at each energy.

Because of the simple analytic forms and symmetries present in each of the terms of Equation (35), they could be analytically reduced to seven terms, each a product of a Gaussian function and a numerical integral over the separation distance between the two protons in the final state. These seven terms correspond to the seven diagrams of Figure 14. The terms corresponding to Diagrams 1, 3, and 4 also occur with the Coulomb force. For all of the terms except number 2, the integral over the final state interaction is explicitly dependent upon the initial and final momentum states.

A computer program was written to calculate the differential cross section from Equation (4) after determining the transition matrix from Equation (35) in the manner just outlined. After converting the energy spectra to the laboratory system, the experimental resolution was folded into the calculated curves for comparison with the experimental results. Except where noted, the calculated spectra were arbitrarily normalized at their maximum points to the data. Appendix B describes this computer program in more detail.

b. Comparison with Data

Besides the experimental work presented in this thesis, several others have measured the ^{3}He(d,t)2p and ^{3}H(d,^{3}He)2n reactions:

Morton, _et al._, 1968
Malanify, _et al._, 1967
Baumgartner, _et al._, 1966
Jakobsen, _et al._, 1965
Tombrello and Bacher, 1965
Conzett, _et al._, 1964
Bilaniuk and Slobodrian, 1963
Brolley, 1958

Most of these data consist of isolated spectra taken at various incident energies and at very forward angles. Most experiments have concentrated on measuring the shape of the spectra and have not determined absolute cross sections. Only one complete angular distribution has been reported (Jakobsen, _et al._).

Comparison of the results of this calculation with the data of Morton, _et al._ is of particular interest. Of all the measurements available, these were made at the highest incident energies, the energy region most valid for our PWBA calculation. They found that the Watson-Migdal prediction agrees with the forward angle spectra, but markedly disagrees with the backward angle spectra. Thus, the reaction occurs through different mechanisms at the very forward and backward angles. Henley, _et al._ (1967) postulated a simple neutron pickup mechanism for the forward hemisphere and a charge exchange mechanism for the backward hemisphere. As shall be shown, the assumptions of Henley, _et al._ are an over-simplification of the reaction mechanism that is occurring.

Figure 15 presents PWBA (antisymmetrized) calculated fits to the 5°, 36 MeV and 0°, 53 MeV data of Morton, et al. The curves were calculated with parameters of Thompson and Tang for the nucleon-nucleon potential and the mass-three Gaussian wave functions:

$$V_o = 72.98 \text{ MeV}$$
$$\beta^2 = 0.46 \text{ F}^{-2}$$
$$y = 1.0 \text{ (pure Serber force mixture)} \qquad (44)$$
$$\delta_1 = .12 \text{ F}^{-2}$$

The relative contribution of all the first order processes to the total transition amplitude is illustrated below the measured spectra in Figure 15. Each curve is labeled to correspond to the type of integral diagrammed in Figure 14; the signs enclosed in parentheses indicate the relative sign of each term.

As shown in Figure 15, our calculated spectrum for the 5°, 36 MeV data approximately agrees with the measured spectrum. If only the simple neutron pickup process (term 2) were included, our calculated spectrum would be the same as the Watson-Migdal predicted spectrum (neglecting the small dependence on the initial and final relative motion momentum states). However, other possible processes do influence the spectrum shape, and our spectrum is slightly narrower than the Watson-Migdal prediction. The simple

FIGURE 15

The upper diagrams present the data of Morton, et al.,
(1968) for the ^{3}He(d,t)2p reaction at $\theta_{Lab} = 5^O$ and the
D(^{3}He,t)2p reaction at $\theta_{Lab} = 0^O$. The incident energies
were chosen so that both reactions had approximately the
same center-of-mass energy (21.6 MeV). The dashed curves
indicate the Watson-Migdal fit ($a_{pp} = -7.7$ F) calculated by
Morton, et al., (1968), while the solid curves show the
results of the present PWBA (antisymmetrized) calculation.
The lower portions of the figure indicate the relative
contribution of each of the diagrams of Figure 14 to the
total matrix element. In this calculation the mass-three
wave function was assumed to be a single Gaussian; the
nucleon-nucleon interaction was taken to have a Serber mix-
ture whose range and depth were taken from Thompson and
Tang (1967).
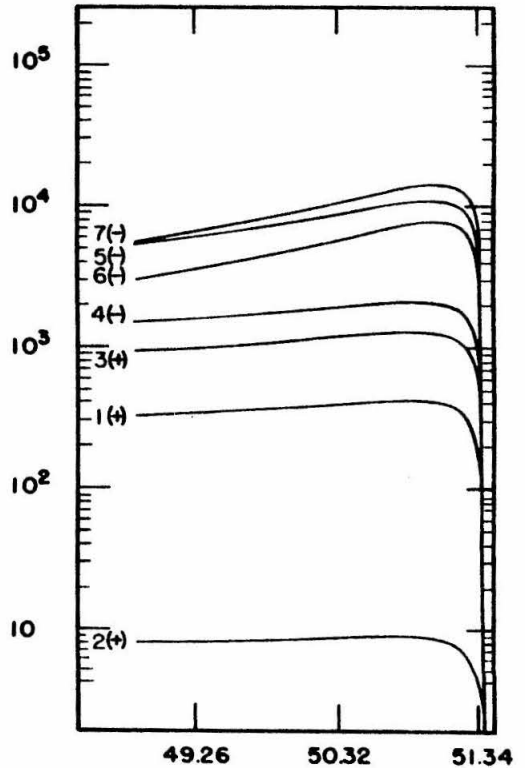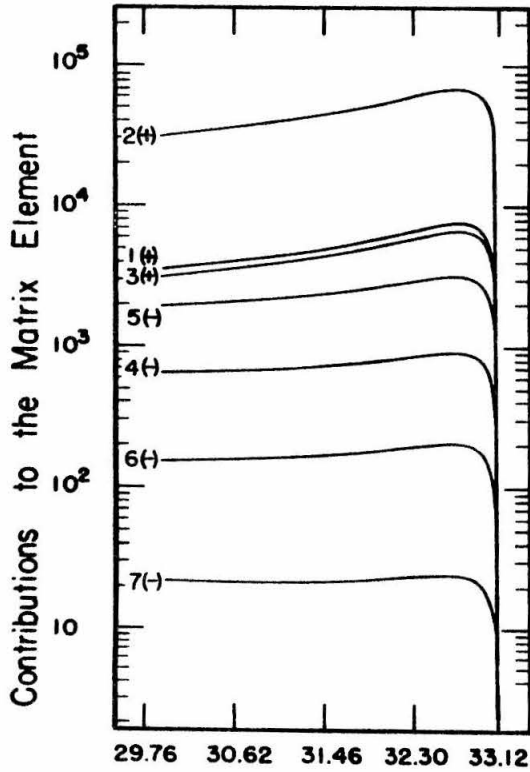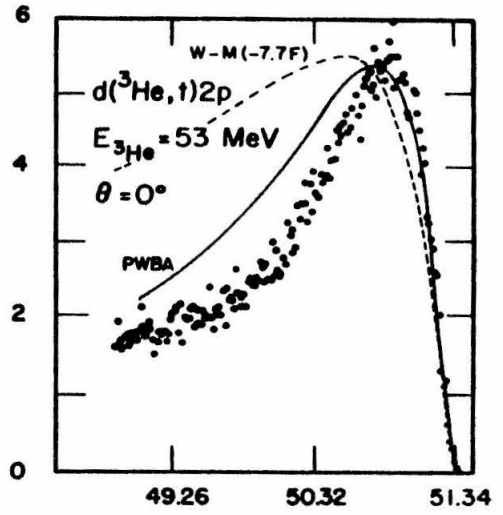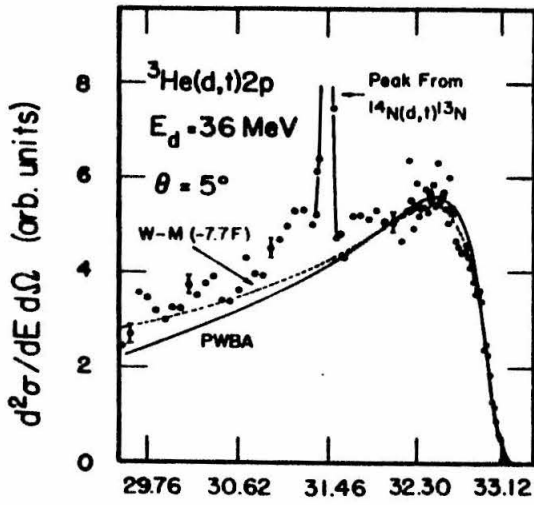
FIGURE 15

neutron pickup term is about a factor of ten more probable
than the other processes, but, including the other reaction
mechanisms, preferentially weights the transition amplitude
for the higher triton energy region. Consequently, we
obtain a somewhat narrower peak than the Watson-Migdal
prediction.

Although broader than the measured spectrum, our
calculated spectrum for the 0°, 53 MeV data of Morton,
et al. is considerably improved over the Watson-Migdal
prediction. Our calculation shows that important changes
have been made in the reaction mechanism. Except for term
5, the terms have inverted in importance when compared with
forward angle term contributions. In contrast to the for-
ward angle case, there is no dominant reaction mechanism
for the backward angle. Term 7 corresponds to the charge
exchange process assumed by Henley, et al.; it arises purely
from the Majorana interaction. Term 6 is very similar to
term 7, but it arises from a pure Wigner interaction, and,
in the limit of a zero range force, it becomes identical to
term 7. Term 5 is one of the more complicated rearrangement
terms; it corresponds to a neutron pickup reaction from
states generated by antisymmetrizing the system. The
dominant term in the forward angle spectrum makes a neglig-
ible contribution to the backward angle spectrum.

Similar results are obtained for the $0°$, 74 MeV data of Morton, et al. (see Figure 16), using the same calculation parameters. The fit to the data is better, perhaps indicating that the plane wave Born approximation is better at the higher incident energy. In comparison with the $0°$, 53 MeV calculation, term 5 is slightly suppressed with respect to term 7 and term 6, while term 2 has become even less important. The contributions of the terms are spread over a wider range of values than at $0°$, 53 MeV.

When the incident beam energy is lowered, the terms tend to bunch together. Calculations for our $6°$, 11 MeV data on the $^3He(d,t)2p$ reaction (see Figure 17) show that all the terms are within a factor of 150; whereas, for $5°$, 36 MeV, the terms are spread by a factor of 3000. At the lower energy, the negative terms have substantially increased in importance. These negative terms have two important effects. First, when they are subtracted from the positive terms, they make the predicted spectrum narrower than the observed spectrum. (The positive terms, by themselves, fit the data well.) Secondly, interference effects between the positive and negative terms will occur at more forward angles at the lower energy than at the higher energies.

The predicted spectra from our antisymmetrized PWBA model are compared with our data in Figure 18. The only

FIGURE 16

Watson-Migdal and PWBA (antisymmetrized) fits to the 74 MeV, D(^{3}He,t)2p data of Morton, <u>et al.</u>, (1968). The curves are calculated with the same assumptions listed in Figure 15.
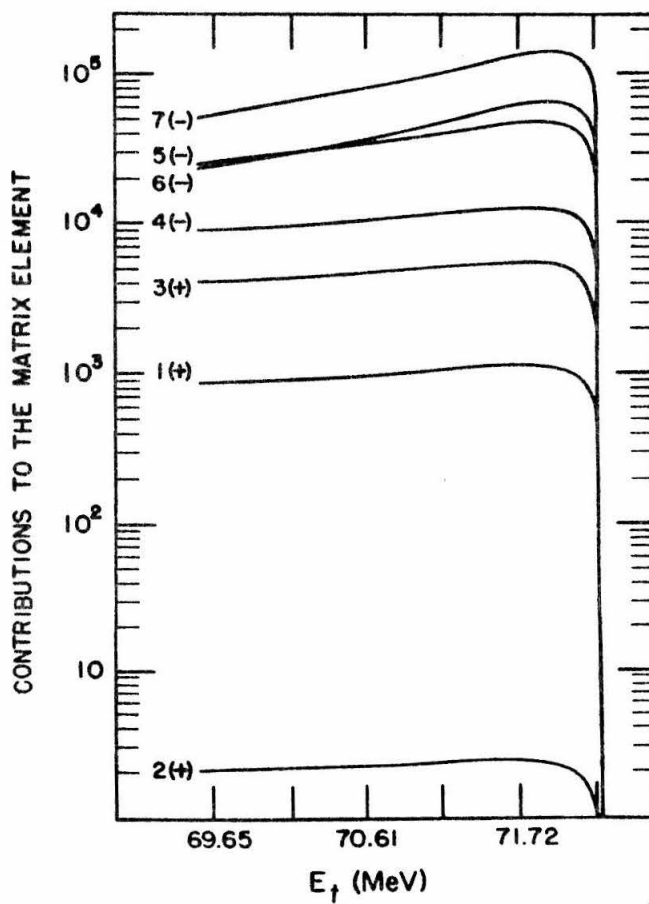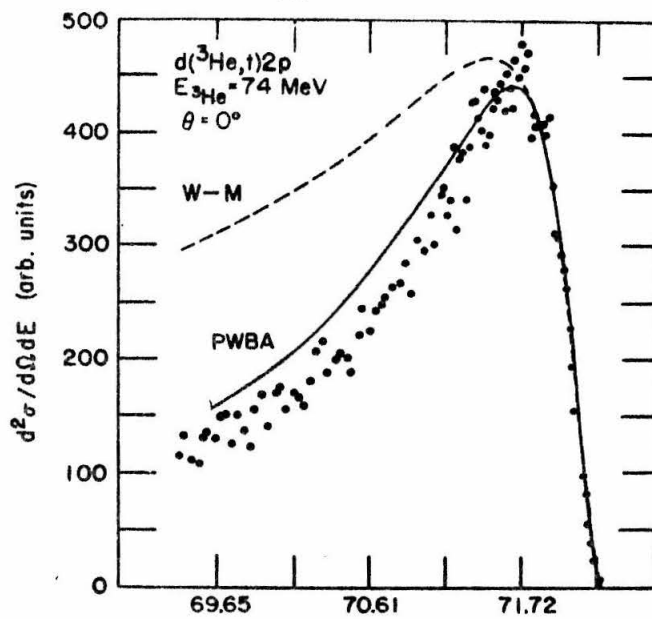
FIGURE 16

FIGURE 17

The PWBA (antisymmetrized) fit to our 6°, ^{3}He(d,t)2p data. The curves are calculated with the same assumptions listed in Figure 15.

FIGURE 17

104
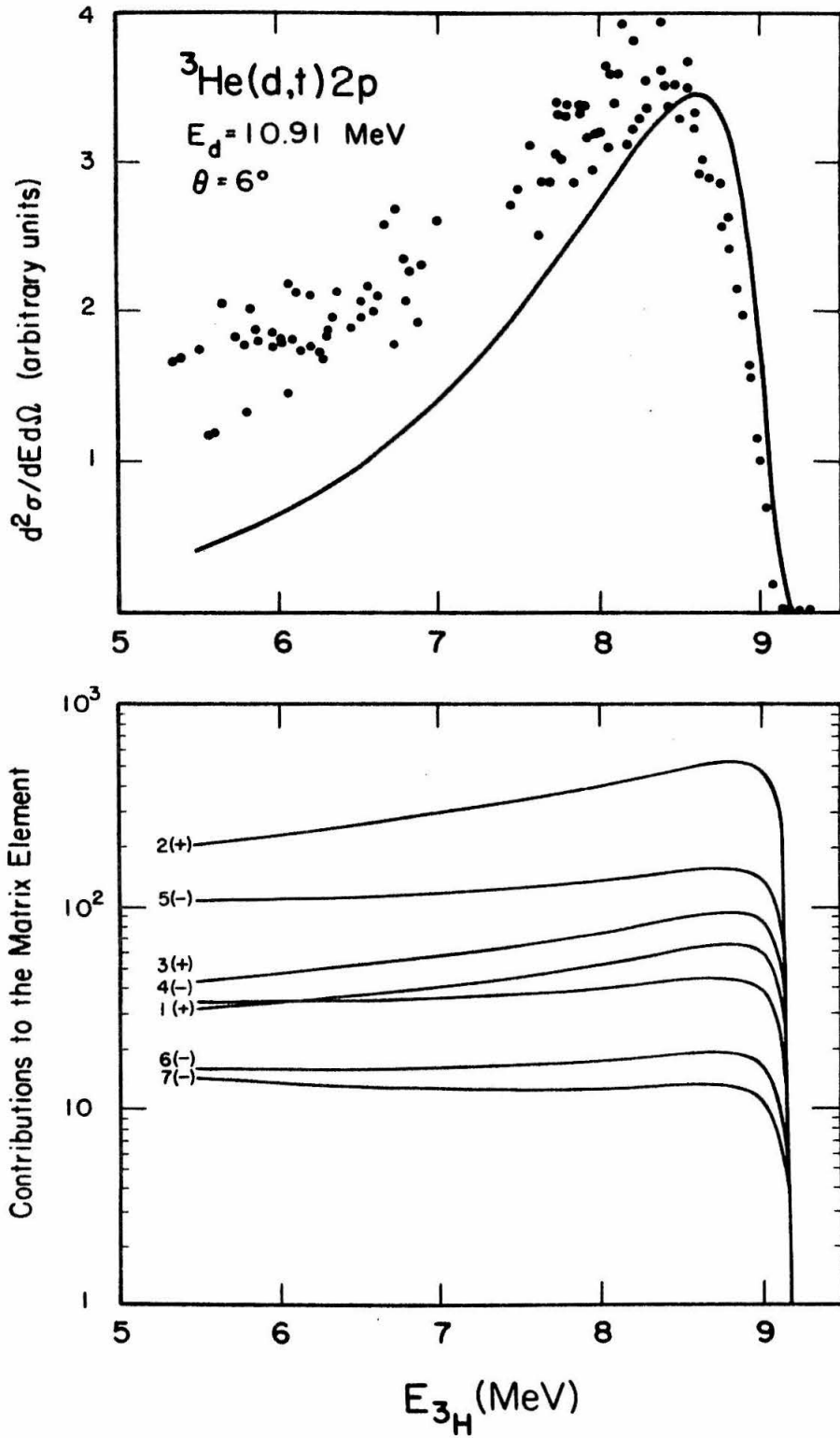
FIGURE 18

The PWBA(antisymmetrized)fits to our 6°, 10°, 15°, and 20° ^{3}He(d,t)2p data. All of the spectra are plotted on the same scale. The curves are calculated with the assumptions listed in Figure 15; the only arbitrary parameter is the normalization to the data at 6°.
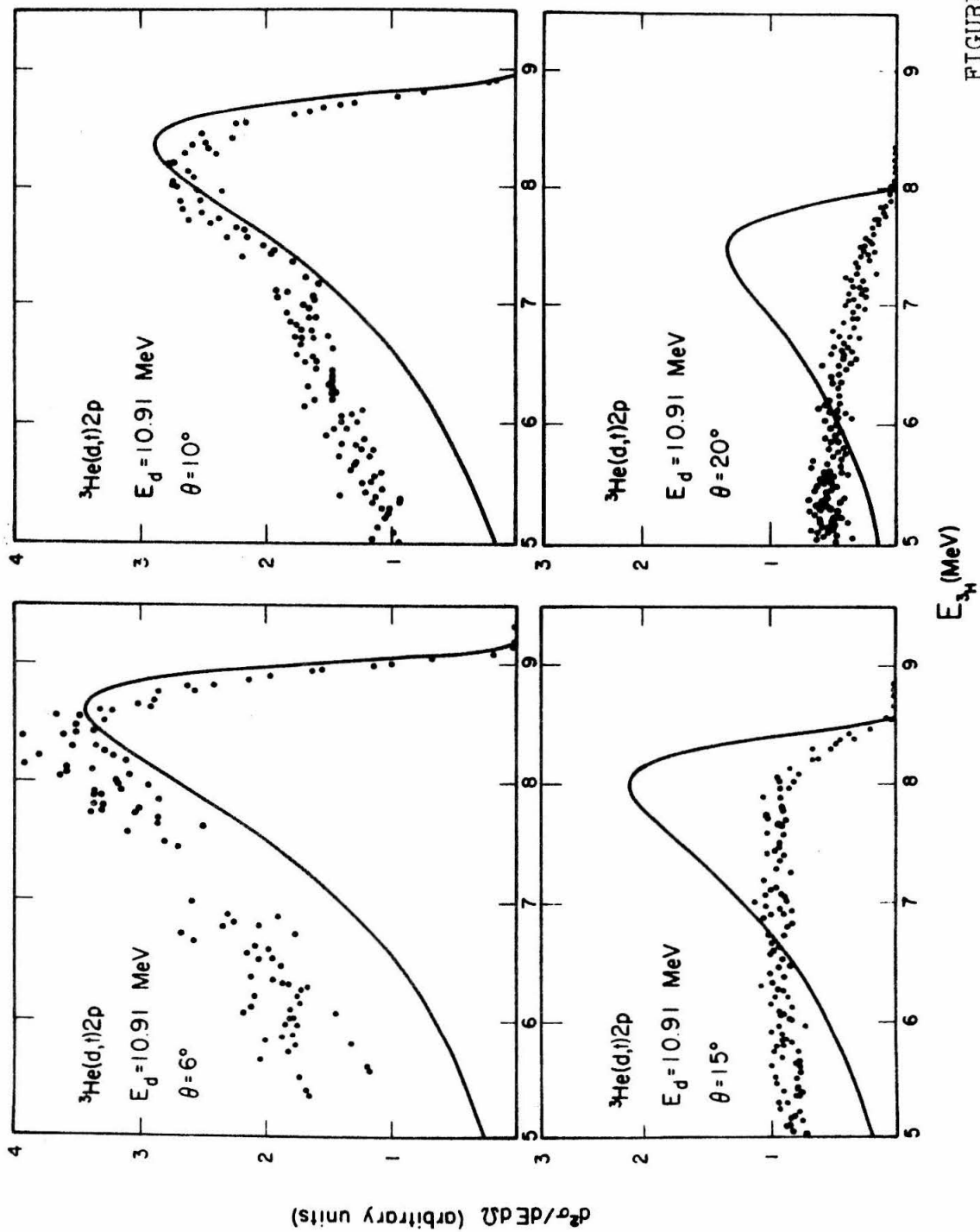
FIGURE 18

arbitrary parameter used in calculating these curves is the normalization to the data at 6°.

We do not approximate distortion effects by applying radial cutoff parameters to the integrals in our antisymmetrized calculation. That method makes evaluating most of the integrals very difficult. However, it is easy to apply radial cutoff parameters to terms 2 and 7. Henley, et al. has done so, and they have obtained qualitative fits to the angular distributions of Jakobsen, et al. with a cutoff radius of 5 F. But employing a cutoff parameter can markedly change the shape of the predicted spectra. How distortion effects would change the predicted spectrum shapes and interference effects remains the greatest uncertainty in our calculation. The angular distribution fit to the data of Jakobsen, et al. is poor using the present model (see Figure 19). The calculation does exhibit, however, the gross feature of the dominance of direct terms at forward angles and exchange terms at backward angles with about the correct relative magnitude for the cross sections. Despite its limitations, the present calculation indicates that complex rearrangement terms are important in determining the transition amplitude at lower incident energies and at intermediate angles.

We have studied the effects of changing: (1) the force mixture; (2) the potential parameters; and (3) the

107

FIGURE 19

The PWBA (antisymmetrized) fit to the ^{3}He(d,t)2p angular distribution of Jakobsen, et al., (1965) for a constant p-p relative energy of 1 MeV. The curve is calculated with the assumptions listed in Figure 15 and has been arbitrarily normalized to the data point at 13°.

C.M. ANGLE (Degrees)

$d\sigma/d\Omega$ (mb/sr)

FIGURE 19
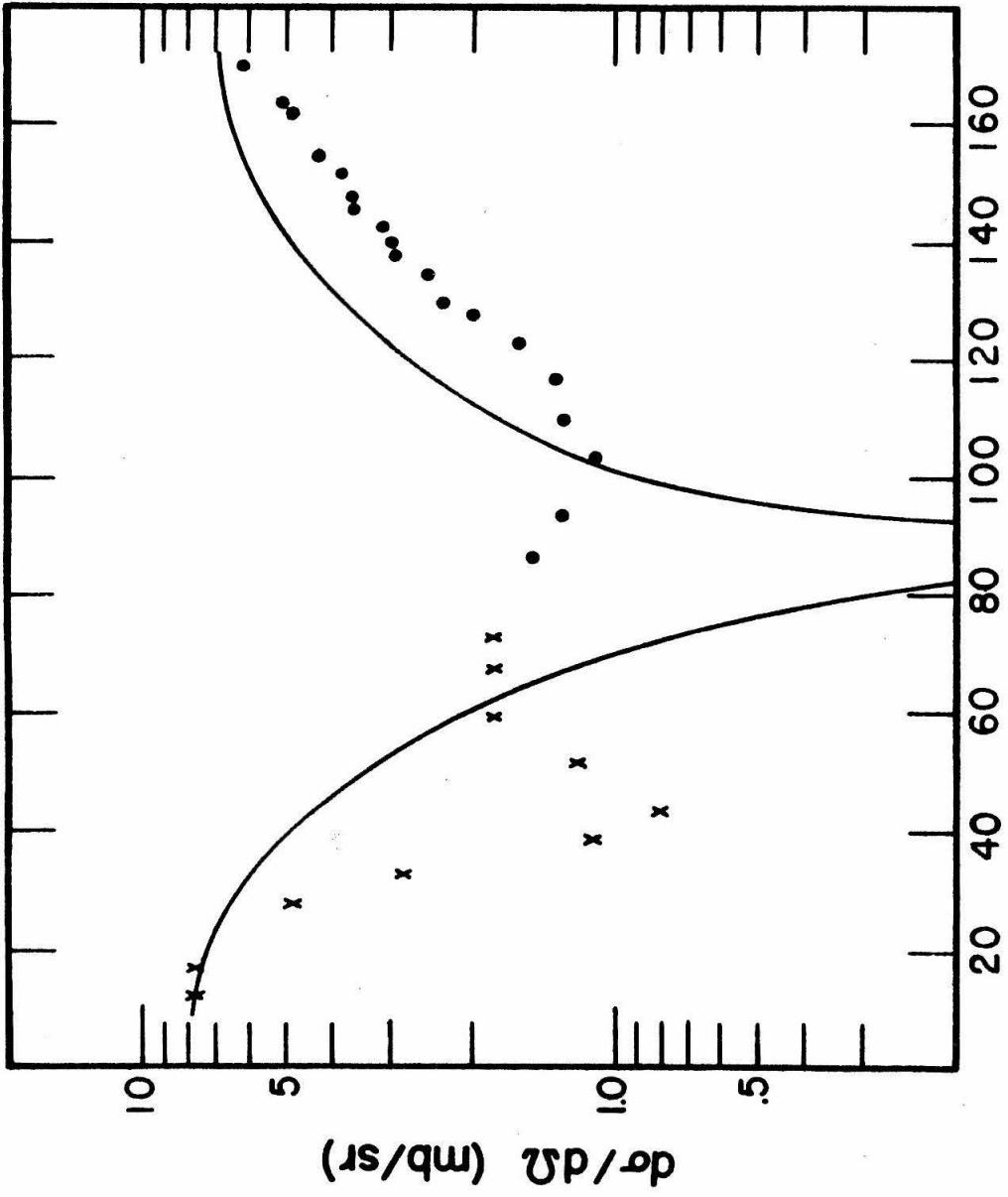
wave functions of the mass-three nuclei on the energy
spectra and the relative contributions of the reaction
processes.

There are two reasons why the results are not
strongly affected by changing the force mixture. First,
for terms 2, 4, and 5, the coefficients w, b, m, and h
appear in groups that are simple combinations of the sing-
let and triplet interactions. Since the ratio of the
singlet to triplet interaction is taken to be fixed, these
terms are not affected by changing the Serber-symmetric
force ratio, y. Secondly, the terms 1 and 3 and the terms
6 and 7 almost compensate for one another when y is varied,
because the sum of each pair is approximately independent
of y. Changing y, for example, may decrease term 1, but,
at the same time, term 3 will increase by approximately the
same amount. This compensation effect would not necessarily
be true if (1) the force mixture were chosen in an arbitrary
manner and not on the basis of being a combination of Serber
and symmetric type forces, and (2) if the range of the
nuclear potential were significantly different than the
1.47 F used.

We have calculated the relative importance of the
seven terms for several different sets of perturbing nuclear
potential parameters. Table II lists the four sets of para-
meters used for the nucleon-nucleon interactions. The

TABLE II

Nucleon-nucleon potential parameters used in studying the
effects of the range of the potential on the reaction
mechanism.

TABLE II

β^2 (F^{-2})	V_o (MeV)	Reference
.2669	46.8	Laskar, et al., (1960)
.3906	51.5	Baker, et al., (1962)
.4600	72.98	Thompson and Tang (1967)
.5636	86.4	Frank and Gammel (1954)

contributions from the reaction processes were calculated at 5°, 36 MeV, and at 0°, 53 MeV for a p-p center-of-mass energy of 1.0 MeV. For the 5°, 36 MeV calculation, terms 1 through 6 oscillate slightly about mean values which are approximately the values given in Figure 15. Term 7, the charge exchange process, is approximately proportional to β^2 and changes by a factor of five in magnitude over the range of β^2 calculated. For the reversed reaction, 0°, 53 MeV, the antisymmetrization terms 3 through 7 also oscillate slightly about mean values given approximately by the values in Figure 15. Terms 1 and 2 approximately double in value when β^2 varies from .2669 to .5636. Thus, the predicted spectra are not strongly dependent on the range of the force used if β^2 is within the region calculated. For very long range interactions (5-6 F), the contributions of the antisymmetrizations terms 3 through 7 increase as expected. The magnitude of the 0°, 53 MeV cross section is enhanced relative to the 5°, 36 MeV cross section. In agreement with the work of Phillips (1964), the long range interaction narrows the peak of the energy spectra. In the limit of a zero range interaction, term 1 equals term 3, and term 6 equals term 7, while all the terms are enhanced by a factor of nearly 1000. The relative ordering of the terms is the same, except for term 4, which drops below terms 6 and 7.

The calculated spectra for the data of Morton, et al., using the Irving-Gunn and Irving wave functions, are shown in Figures 20 and 21, respectively. The parameters for the nuclear potential and the force mixture is the same for the curves in these figures as for Figure 15. The Irving-Gunn prediction for the forward angle spectrum is narrower than the prediction using the Gaussian wave function. The spectrum calculated with the Irving wave function falls between the Gaussian and Irving-Gunn predicted spectra. For the reversed reaction, the three wave functions predict about the same spectrum shape.

The relative contributions of the terms to the total matrix element are plotted on the same scale in Figures 15, 20, and 21. The contributions of the terms for the Gaussian and Irving wave functions are quite similar. For the calculation with the Irving-Gunn wave function at 5°, the contribution of term 2 is comparatively greater than in the calculations with the other two wave functions. This indicates that the simple pickup process is preferentially favored if the mass-three nuclei have a spatial distribution that is neither compact (Gaussian) nor diffuse (Irving).

2. $^{3}H(d,^{3}He)2n$ Reaction

    a. Description

FIGURE 20

The PWBA (antisymmetrized) fits to the data of Morton,
et al., (1968) as in Figure 15, except that the mass-three
wave functions have the Irving-Gunn spatial dependence.
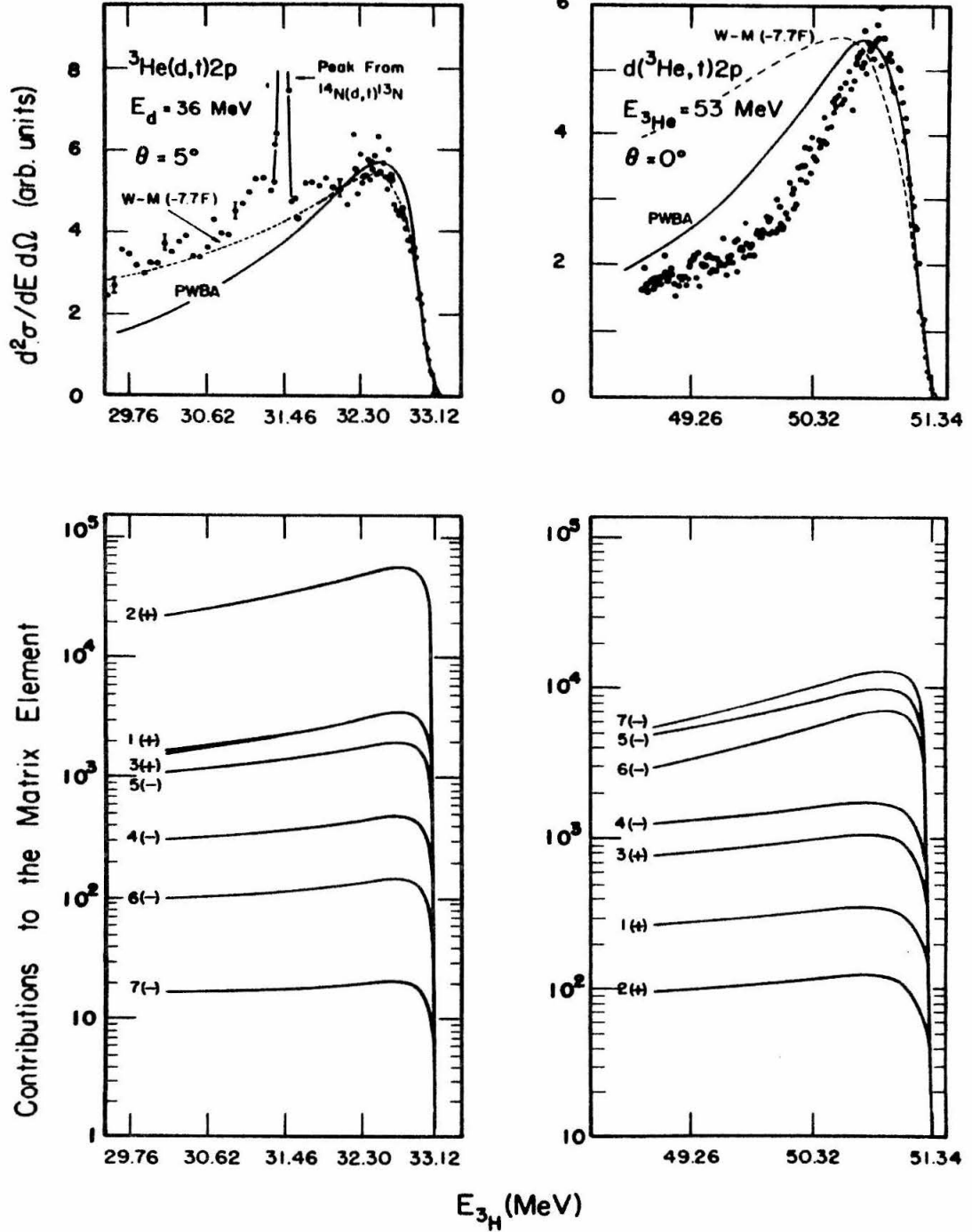
FIGURE 20

FIGURE 21

The PWBA (antisymmetrized) fits to the data of Morton,
et al., (1968) as in Figure 15, except that the mass-three
wave functions have the Irving spatial dependence.
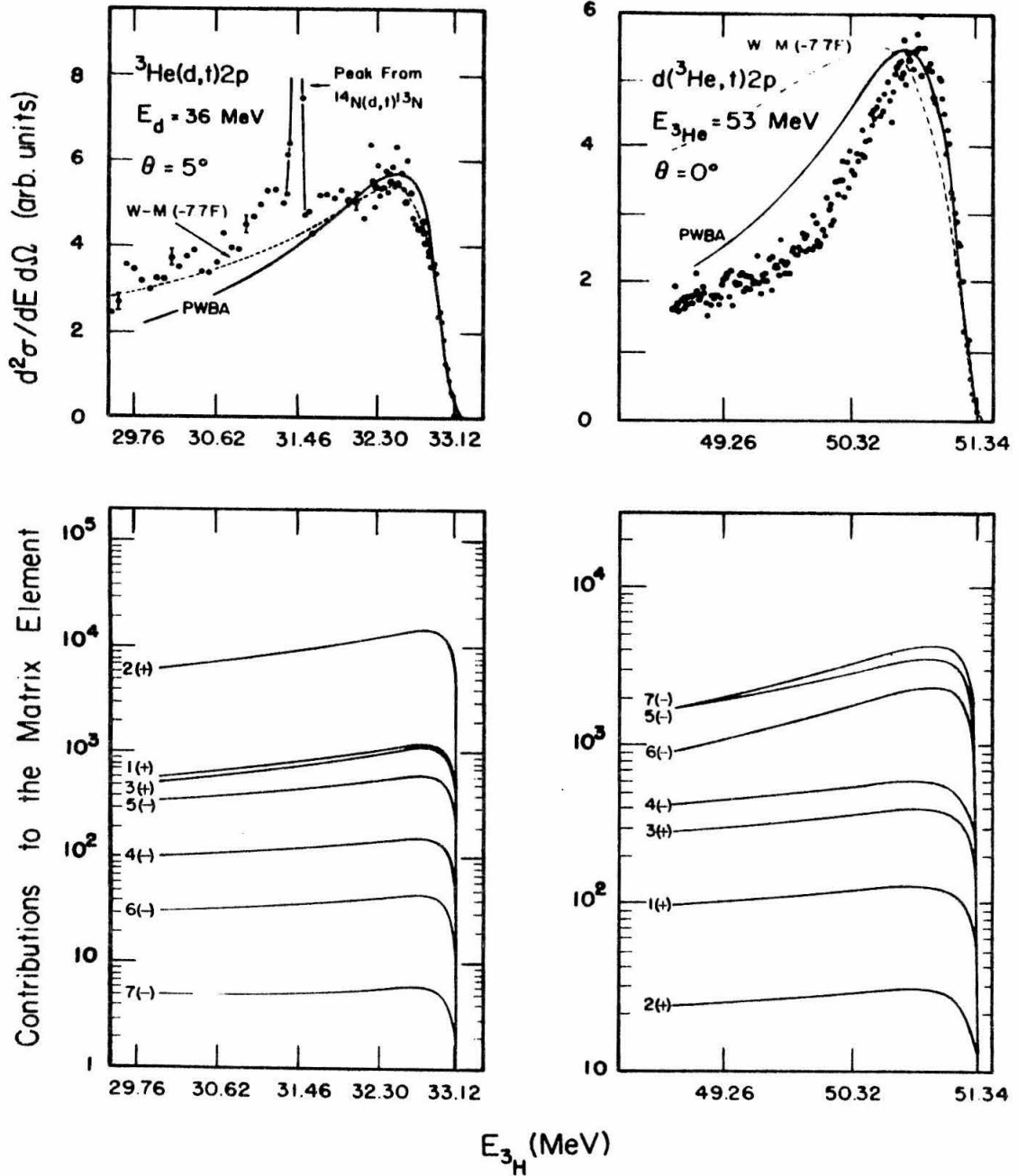
FIGURE 21

The ^{3}H(d,^{3}He)2n calculation proceeded in the same way as the ^{3}He(d,t)2p calculation except for two modifications. The first modification was to "turn off" the Coulomb interaction in the Schrodinger equation used to calculate $\Phi_{nn}(r)$, while keeping the nuclear parameters the same. Thus, by assuming the charge symmetry of nuclear forces, we directly related the results of the ^{3}He(d,t)2p calculation to those of the ^{3}H(d,^{3}He)2n reaction. The second modification was to change the Coulomb interactions among the nucleons in the perturbing interaction. Except for these modifications, the calculation was identical to the ^{3}He(d,t)2p calculation.

b. Comparison with Data

The results for our 6°, 11 MeV data are shown in Figure 22. Without the Coulomb interaction to mask its effect, the low energy nucleon-nucleon interaction markedly enhances the high energy region of the ^{3}He spectrum. The nuclear effects, of course, are the same as in the mirror reaction (compare with Figure 17). The predicted energy spectra are compared to our observed spectra in Figure 23. The results are similar to those obtained for the ^{3}He(d,t)2p reaction.

3. Relationship of the ^{3}He(d,t)2p Spectra to the ^{3}H(d,^{3}He)2n Spectra

FIGURE 22

The PWBA (antisymmetrized) fit to our 6°, $^{3}H(d,^{3}He)2n$ data.
The curves are calculated with the same assumptions used
for Figure 15.
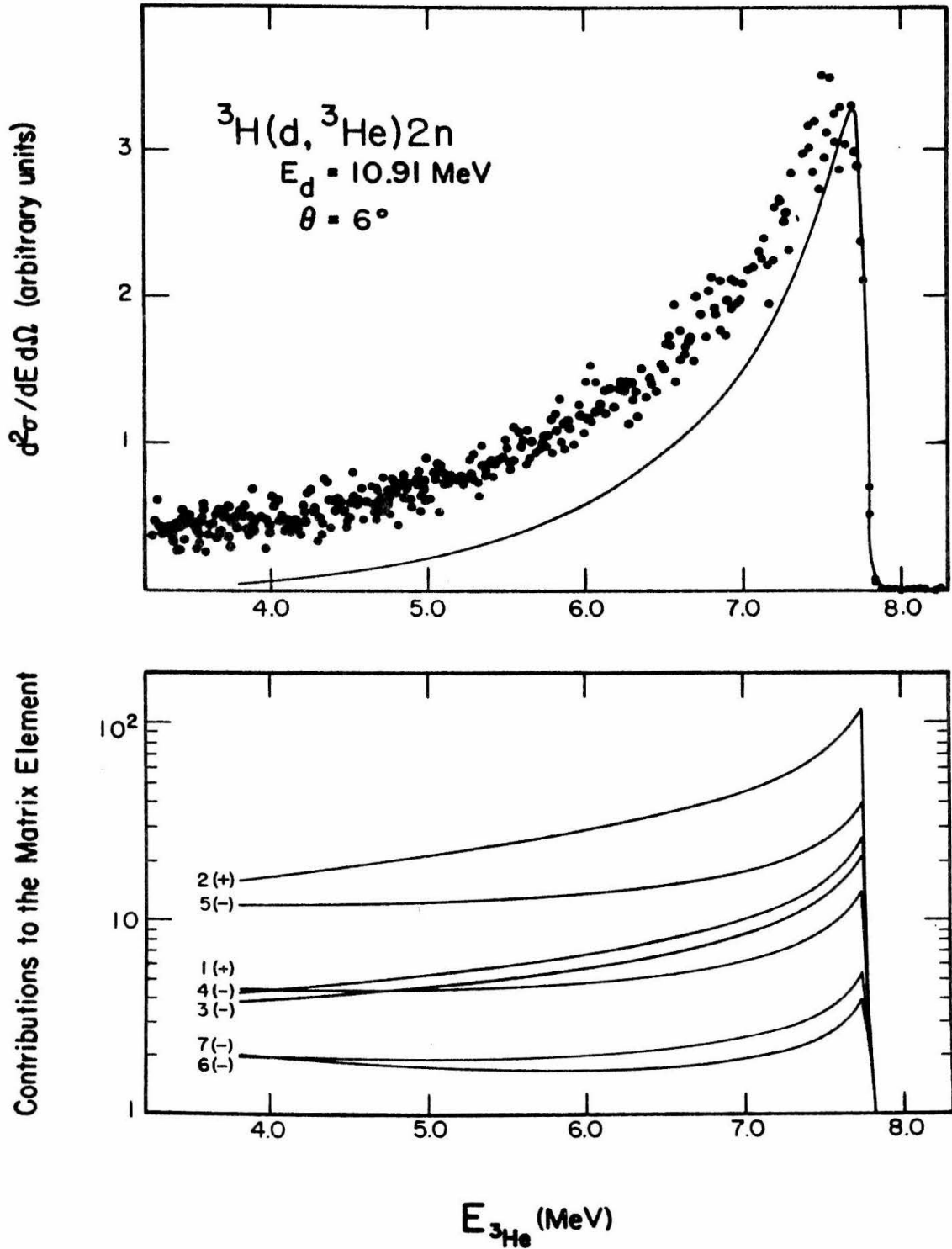
FIGURE 22

FIGURE 23

The PWBA (antisymmetrized) fit to our 6°, 10°, 15°, and 20°

$^3H(d, ^3He)2n$ data. All of the spectra are plotted on the

same scale. The curves are calculated with the same

assumptions used for Figure 15; the only arbitrary parameter

is the normalization to the data at 6°.

³H(d, ³He)2n
E_d = 10.91 MeV
θ = 6°

³H(d, ³He)2n
E_d = 10.91 MeV
θ = 10°

³H(d, ³He)2n
E_d = 10.91 MeV
θ = 15°

³H(d, ³He)2n
E_d = 10.91 MeV
θ = 20°

$d^2\sigma/dE\,d\Omega$ (arbitrary units)

$E_{^3He}$ (MeV)
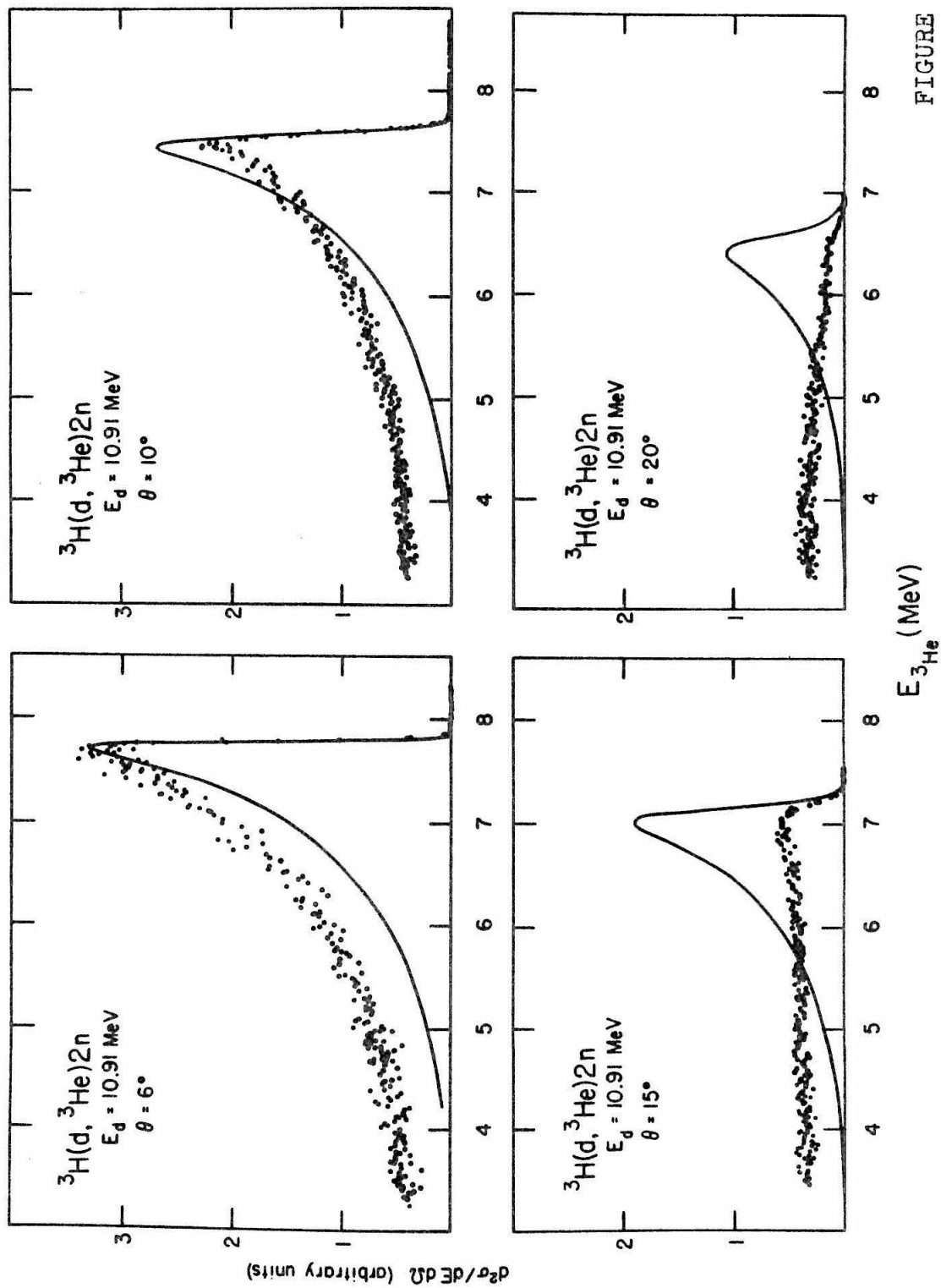
FIGURE 23

We have compared our antisymmetrized PWBA calculation with our 11 MeV data in a way that largely cancels out the effects of distortion. We integrated the area under each experimental and theoretical spectrum that corresponded to center-of-mass energies from 0 to 2 MeV in the nucleon-nucleon system. Table III lists the ratio of these areas. In determining the theoretical ratios, we folded the experimental resolution into the calculated spectra so that the ratios could be compared directly with the experimental ratios. The errors given for the experimental ratios are the r.m.s. errors arising from the determination of the area under each spectrum for both reactions. The error in determining the area under the experimental points was estimated from the data's spread. While this comparison test does not depend strongly upon the details of the reaction mechanism, the good agreement obtained between the ratios verifies the overall final state interaction process.

TABLE III

Ratio of the ^{3}H(d,^{3}He)2n differential cross section to the ^{3}He(d,t)2p differential cross section as predicted by the present PWBA calculation and as determined from the present measurements. The ratios were calculated for the portion of the spectra that corresponds to the center-of-mass energy from 0 to 2 MeV in the nucleon-nucleon system.

TABLE III

Ratio	Lab Angle			
	6°	10°	15°	20°
Theoretical	0.9564	0.9898	0.9452	0.8673
Experimental	1.1 ± 0.09	1.02 ± 0.13	0.93 ± 0.13	1.38 ± 0.35

V. COMPARATIVE ANALYSIS

We can use the calculation of the previous Part to estimate the precision with which the neutron-neutron scattering length can be determined. The results of the last Section of Part IV emphasized the interrelationship between the mirror reactions. It has been proposed (Slobodrian, et al., 1968) to exploit this interrelationship in order to aid in removing the theoretical uncertainties in the analysis.

In our expression for the transition amplitude, Equation (10), we can factor the plase shift dependence out of the integral that corresponds to the Watson-Migdal factorization. That is

$$T_{fi} = \frac{\exp(-i\delta)\sin\delta}{kC(\eta)} \langle \chi_f^{(-)} | V | \Psi_i^{(+)} \rangle$$

$$= \frac{\exp(-i\delta)\sin\delta}{kC(\eta)} T_o(\theta,k)$$

(45)

where the notation is the same as that for Equation (23).

As we have previously seen, the uncertainty of the analysis is in the evaluation of the function $T_o(\theta,k)$. The Watson-Migdal approximation assumes the $T_o(\theta,k)$ function to be constant. However, even the theoretically unsophisticated calculations made in Part III indicate that the $T_o(\theta,k)$ function cannot, a-priori, be considered constant. The calculation emphasizes the complex nature of the processes contributing to $T_o(\theta,k)$ and shows that $T_o(\theta,k)$ is not

readily evaluated with realistic wave functions and inter-
actions.

The experimental work reported here and that of
Baumgartner, et al. (1966) show that $T_o(\theta,k)$ is approxi-
mately constant as a function of k for the ^{3}He(d,t)2p
reaction at very forward angles. This has not proven to be
true for the D(p,n)2p and ^{3}He(p,d)2p reactions (van Oers,
1967) and even for the ^{3}He(d,t)2p reaction at very backward
angles (Morton, et al., 1968). Furthermore, our experi-
mental work shows that $T_o(\theta,k)$ is a very sensitive function
of θ .

Slobodrian, et al. have tried to obviate the need for
evaluating the $T_o(\theta,k)$ function by experimentally determin-
ing $\left| T_{pp}(\theta,k) \right|^2$ from the 2p final state enhancement in the
mirror reaction assuming that

$$\left| T_{nn}(\theta,k) \right|^2 = \text{Constant} \left| T_{pp}(\theta,k) \right|^2 \tag{46}$$

This method could be applied to all of the reactions listed
above, and, perhaps, the wide discrepancies in extracted
scattering lengths could be resolved.

We have used the calculation described in Section
III-B as "experimental data" to study this proposal. Our
calculation served as a useful tool in two ways: (1) The
predicted spectra are qualitatively correct at both very

forward and very backward angles without simplifying
assumptions about the reaction mechanism. All first order
reaction processes were included; thus, we expected the
$T(\theta,k)$ functions to have some semblence of reality for
these angles. (2) The interrelationship of the "data" for
the two reactions was precisely known. Thus, we could
judge the precision with which the method could determine
the scattering length and effective range.

Our procedure was to determine the $\left| T_{pp}(\theta,k) \right|^2$
function by calculating the ratio of our PWBA calculated
spectrum ("the triton data") to the Watson-Migdal spectrum
using the known p-p effective range parameters. This was
done at 25 selected points in the p-p center-of-mass system
energy range from 0 to 4 MeV. Using Equation (24), a number
of comparison spectra were then calculated corresponding to
various choices of a_{nn} and r_{nn}. In this way our comparison
spectra were generated with the equation,

$$\left[\frac{d^2\sigma}{dEd\Omega} \right]^{comp.}_{a_{nn},r_{nn}} \propto \left[\frac{\left(\frac{d^2\sigma}{dEd\Omega} \right)^{PWBA}_{PP}}{\left(\frac{d^2\sigma}{dEd\Omega} \right)^{WM}_{PP}} \right] \left[\frac{d^2\sigma}{dEd\Omega} \right]^{WM}_{a_{nn},r_{nn}} \qquad (47)$$

The normalization constant, α, for each comparison
spectrum was chosen by minimizing a measure of the goodness
of fit, defined by

$$\Omega^2 = \frac{1}{N} \sum_{i=1}^{N} \left[\frac{\left\{\frac{d^2\sigma}{dEd\Omega}\right\}_i^{PWBA} - \alpha \left\{\frac{d^2\sigma}{dEd\Omega}\right\}_{a_{nn},r_{nn},i}^{comp.}}{\left\{\frac{d^2\sigma}{dEd\Omega}\right\}_i^{PWBA}} \right]^2 \tag{48}$$

Figure 24 shows several of these spectra compared to the
PWBA calculated spectrum. The kinematic conditions in this
figure were chosen to correspond to data taken at over-all
center-of-mass energy of 20 MeV (the experimental conditions
of the data of Morton, et al.). The PWBA spectrum in this
figure and all other PWBA spectra used in studying the com-
parison method were calculated with the Irving-Gunn wave
function, the nuclear potential of Thompson and Tang, and a
pure Serber force mixture. The fits were made over those
parts of the spectrum that corresponded to 2n relative
energies up to 4 MeV.

Real data have experimental uncertainty that affects
the determination of a_{nn}. For the reaction under discussion
the scatter in the data points above and below the average
value of the spectrum tends to be uniform over most of the
spectrum. However, for simplicity, we shall discuss our
results in terms of a constant $\pm$ % deviation about the
predicted PWBA spectrum to simulate the effects of experi-
mental uncertainty. At the present time good experimental
data typically have a deviation of $\pm$ 5% in the region of the
maximum of the spectrum.

130

FIGURE 24

The solid curves are examples of ^{3}He spectra predicted with
the comparison method and the Watson-Migdal approximation for
the ^{3}H(d,^{3}He)2n reaction at 5°, 38.5 MeV. Each curve is
labeled with the scattering length used in its calculation.
For all three curves r_{nn} = 2.65 F. The dashed curve is
the corresponding PWBA (antisymmetrized) spectrum.
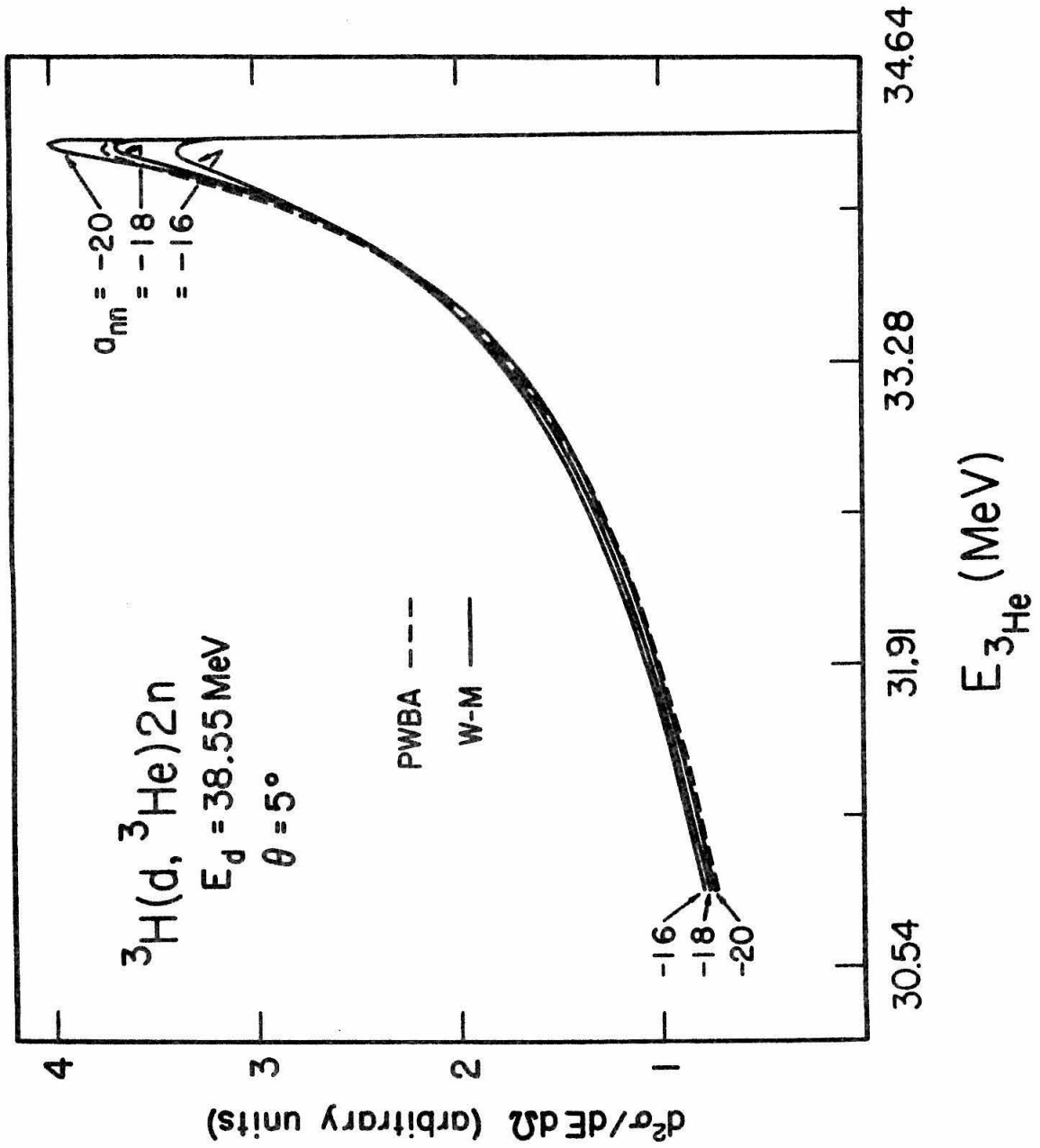
FIGURE 24

The quality of fits obtained with the comparison procedure for various combinations of a_{nn} and r_{nn} is conveniently described in terms of contour plots of the goodness of fit parameter, Ω^2. Figure 25 presents four such plots. The curves represent constant values of Ω^2 corresponding to the various combinations of a_{nn} and r_{nn} which give equally good fits to our PWBA spectrum. The contours are labeled according to the constant percentage uncertainty that corresponds to the value of Ω^2 calculated with Equation (48). All the plots in this figure are for an overall center-of-mass energy of 20 MeV. Plot a presents the results for a laboratory angle of 5° when the fitting is made over 2n relative energies from 0 to 2 MeV, while in Plot b the fitting is made for energies from 0 to 4 MeV. In Plots c and d, we have had to make a modification of our fitting procedure. We have excluded the leading edges of the spectra corresponding to 2n relative energies from 0 to 150 keV. In this region the agreement between the comparison spectra and the PWBA spectrum was poor, and very large values of Ω^2 were obtained if the region were included. Even though we have made this exclusion, the comparison of the spectra is still reasonable, since the experimental resolution is typically of the same width as the excluded region, and the discrepancy in the spectra would be difficult to observe.

In each plot of Figure 25, the position of the circled cross indicates the correct values of a_{nn} and r_{nn}. These values were obtained directly from the phase shifts of the neutron-neutron scattering wave functions. The value of $a_{nn} = -19.2$ F is a result of the use of the Yukawa potential for the nucleon-nucleon interaction; a different value would be obtained if some other potential shape were used.

The plots of Figure 25 show clearly that many combinations of a_{nn} and r_{nn} give equivalent fits to the PWBA spectrum. Even though our plots cover the region of the expected values for the effective range parameters, the contours indicate that many more combinations would give comparable fits if the range of the parameters were extended. The four plots have a similar pattern; they show a strong correlation between a_{nn} and r_{nn} for obtaining equivalent fits. The correlation pattern covers roughly the same values of the effective range parameters for both the forward and backward angles, particularly when judged with the 5% uncertainty that is typical of actual data. When made over larger 2n relative energies, equivalent fits have a tendency to become less sensitive to the value of a_{nn}, as shown by the change in pattern of the contours when Plot b is compared with Plot a and Plot d is compared with Plot c. The correct value of a_{nn} and r_{nn} is not located at the minimum point of the surface defined by the contours in any

FIGURE 25

Contour plots of the goodness-of-fit parameter Ω^2 for a_{nn} ranging from -15 to -20 F and for r_{nn} ranging from 1 to 5 F. The curves represent constant values of Ω^2 that correspond to combinations of a_{nn} and r_{nn} which give equally good fits to our PWBA calculated spectrum. The contours are labeled according to the constant percentage uncertainty assumed for the PWBA spectrum. The plots are for (a) $\theta_L = 5^\circ$, $E_{nn} = 0$ to 2 MeV; (b) $\theta_L = 5^\circ$, $E_{nn} = 0$ to 4 MeV; (c) $\theta_L = 180^\circ$, $E_{nn} = 0$ to 2 MeV; and (d) $\theta_L = 180^\circ$, $E_{nn} = 0$ to 4 MeV. The circled crosses indicate the correct values of the n-n effective range parameters for the Yukawa potential used.

SCATTERING LENGTH (fm)

EFFECTIVE RANGE (fm)
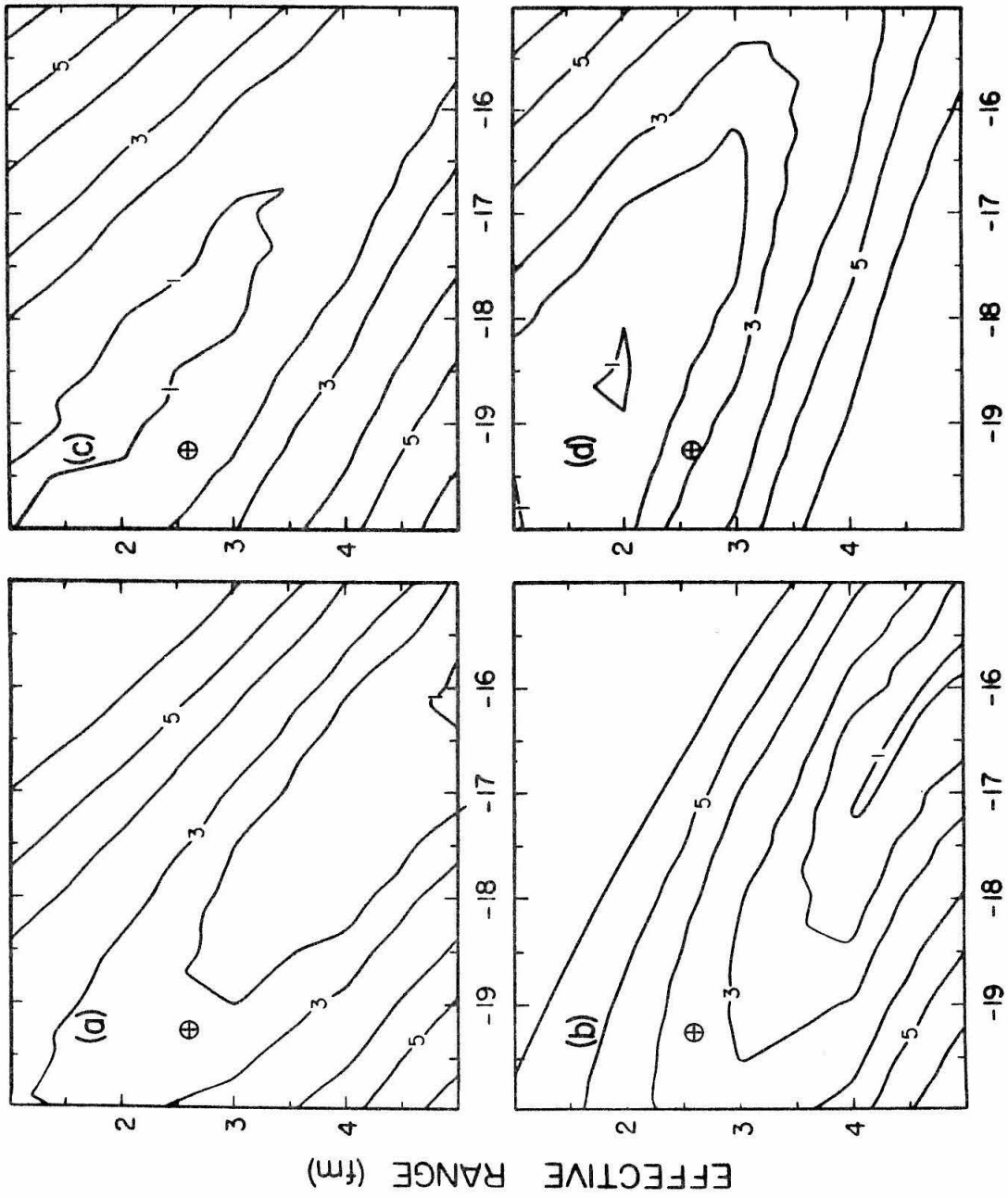
FIGURE 25

of the plots. For the 5° plots, the minimum points lie in the region of larger a_{nn} and larger r_{nn}, while, for the 180° plots, they are in the region of smaller a_{nn} and smaller r_{nn}. Contour plots made from comparison with actual data should be similar to those shown in Figure 25, because the calculated PWBA spectra are similar in form to that of the actual data.

Baumgartner, et al., in fitting their data for the $H^3(d, {}^3He)2n$ reaction, first assumed $r_{nn} = 2.65$ F and obtained a best fit with $a_{nn} = -16.1 \pm 1.0$ F. Then, using $a_{nn} = -16.1$ F, they found a best fit with $r_{nn} = 3.2 \pm 1.6$ F. (They used a χ^2 criterion for determining the best fit to their data. Our goodness of fit parameter Ω^2 differs from the usual χ^2 criterion in that all parts of the spectrum used in our fits are equally weighted.) If we use the fitting procedure of Baumgartner, et al., then, for a 5% uncertainty and $r_{nn} = 2.6$ F, we find a_{nn} from each of the plots to be:

a: -18.75 ± 2.7 F

b: -19.25 ± 2.0 F

c: -18.0 ± 3.4 F

d: -17.5 ± 3.0 F

Using the above values for a_{nn}, we find the values for r_{nn}, respectively, to be:

a: 3.0 ± 2.5 F

b: 3.2 ± 1.4 F

c: 2.5 ± 2.8 F

d: 2.3 ± 1.8 F

The four pairs of values of a_{nn} and r_{nn} obtained from the plots are in agreement within the assigned errors.

When viewed in terms of the information provided by the contour plots, the fitting procedure of Baumgartner, et al. is seen to be too limited in scope. If they had chosen the initial value of r_{nn} to be 1 or 3 F instead of 2.65 F, they would have obtained a very different value of a_{nn}. While a_{nn} has been determined from the $D(\pi,\gamma)2n$ reaction, the only experimental measurement of r_{nn} is that of Baumgartner, et al. From the above study we see that their value of r_{nn} is of little value unless a_{nn} were assumed from the $D(\pi,\gamma)2n$ reaction.

VI. SUMMARY AND CONCLUSIONS

The rapid change in shape of the measured spectra with forward laboratory angle indicates that complicated processes are involved in the ^{3}H(d,^{3}He)2n reaction. A peripheral, direct neutron pickup reaction mechanism cannot adequately explain this behavior, even in principle, because the final state interaction appears as a simple multiplicative factor. Assuming that contributions from non-central interactions are small for the direct process, other reaction modes are required to explain the observations.

By properly antisymmetrizing the five particle system and using the plane wave Born approximation, we have found that other reaction processes may significantly contribute to the transition amplitude. While the calculations are not in quantitative agreement with our measurements, they exhibit the qualitative features required to explain our data. The competing reaction processes may interfere with one another to provide the measured change in spectrum shape. The calculation provides a systematic description for both forward and backward spectra; the relative magnitudes of the differential cross section at $0°$ and $180°$ is in agreement with the data of Jakobsen, _et al._, (1965).

At higher energies, where the approximations made in our calculation are more nearly justified, better agreement

is obtained with the available data. Even at these higher energies, our calculation indicates that more than one reaction process may contribute significantly to the total matrix element. Measurements at even higher energies and at more angles are important in further establishing the validity of this calculation.

Thus, simplifying assumptions about the reaction mechanism, such as that of Henley, et al., (1967), are not adequate in analyzing the observed spectra. At the present time, the use of the Watson-Migdal approximation for extracting a_{nn} from the spectra can only be justified with an empirical knowledge of the production form factor $\left|T_{nn}(\theta,k)\right|^2$ If this form factor is determined from the mirror reaction by assuming the charge symmetry of nuclear forces, the measurement is prejudiced in determining a_{nn}. Beside this logical inconsistancy, effects due to direct breakup or other final state interactions may inadvertently be included in the form factor $\left|T_{nn}(\theta,k)\right|^2$ if it is determined empirically in the manner of Slobodrian, et al., (1968). Without a thorough understanding of the reaction mechanism, the method of Slobodrian, et al. is not adequate.

For plots a and b of Figure 25, the way in which the value of r_{nn} changes in fitting our calculated spectrum is similar to the way in which it changes for the data of Baumgartner, et al., (1966). Because of strong correlations

between a_{nn} and r_{nn} as shown in Part V, a limited fitting procedure such as used by Baumgartner, et al. gives an incomplete and misleading picture of the fits obtainable with the effective range parameters. Within the uncertainty of the experimental data, the fitting of a spectrum determines many sets of effective range parameters. Unless the uncertainty of the data is fairly small, the allowable effective range parameters may extend over a large region. If, however, a particular value of r_{nn} is assumed, our study indicates that a_{nn} can be determined to about $\pm$ 2 F with data of about $\pm$ 3% uncertainty. On the other hand, if a value for a_{nn} is taken from the $D(\pi^-,\gamma)2n$ experiments, r_{nn} can be determined to about $\pm$ 1.5 F.

APPENDIX A.   ARRAY DATA REDUCTION PROGRAM

This program, largely written by Dr. A. D. Bacher, can perform one or all of the following functions:

(1) Reduce raw spectrometer data to both momentum and energy spectra while correcting for: energy losses in the target gas and exit foil; differences in detector response and position; dead time in the electronics of the detection system; and variations in target density. The reduction of raw data is handled by the subroutine RDATA and its auxiliary subroutines.

(2) Plot reduced data for either one, several, or all of the detectors of the array. Plotting is handled by the subroutine CDATA and its auxiliary subroutines.

(3) Generate Watson-Migdal energy spectra, fold in the total experimental energy resolution, normalize calculated spectra to the data, and plot the spectra. The generation of Watson-Migdal spectra is handled by the subroutine SIGGEN and its auxiliary subroutines.

Figure A-1 is a schematic diagram of the relationship between the subroutines RDATA, CDATA, and SIGGEN and the main control program (called MAIN). The input begins with a

FIGURE A-1

An organizational diagram of the main subroutines of the
array data reduction program. The input to the main control
program is a code word which specifies what calculations
are to be made and the form of the output. The functions
of the main subroutines RDATA, CDATA, and SIGGEN are des-
cribed in Appendix A.
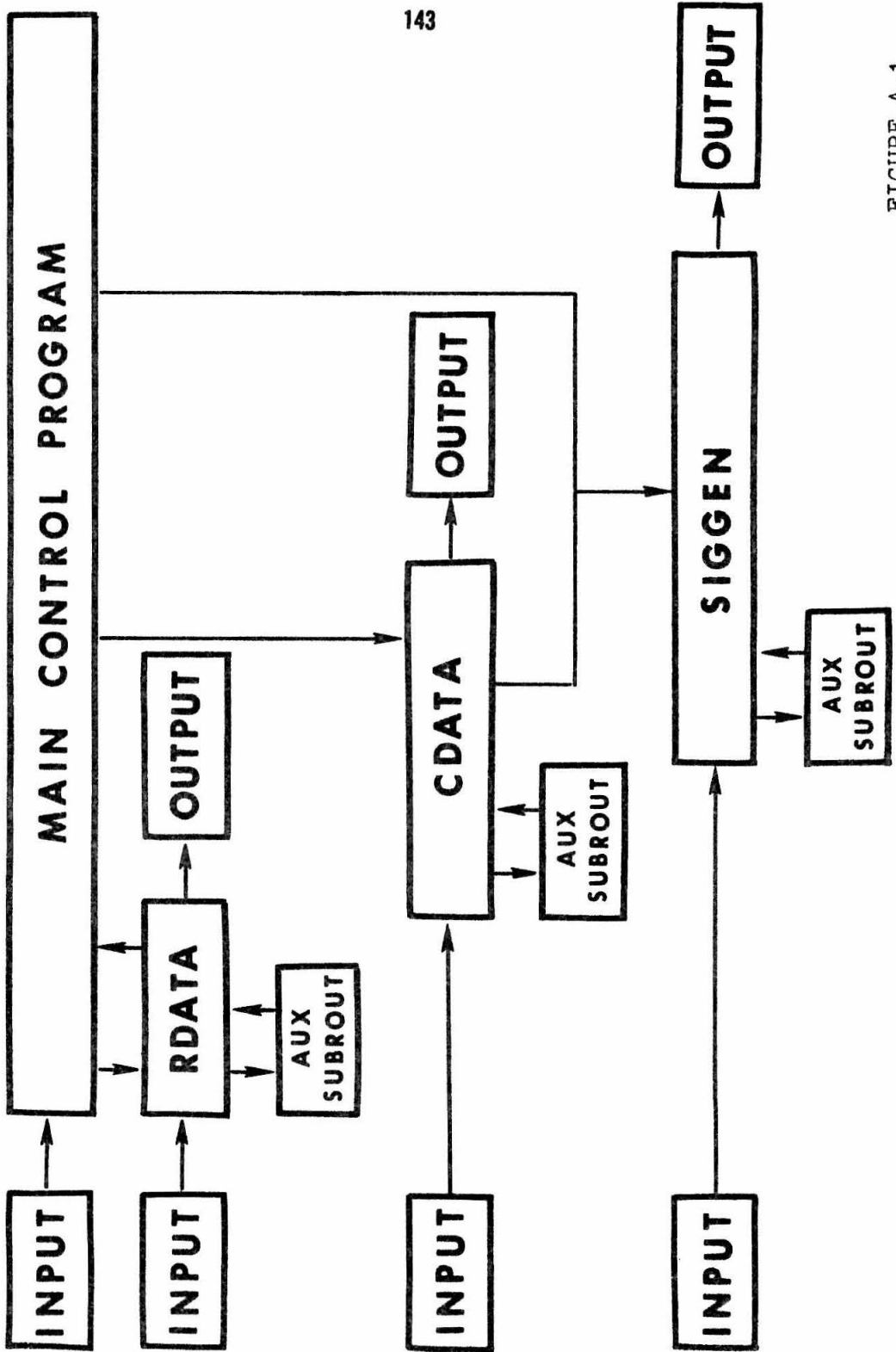
FIGURE A-1

code word, read by MAIN, which selects the functions that
are to be performed. The function subroutines, in turn,
take their input (either read from punched cards or passed
on from a previous calculation) and make their calculations.
After generating their output (in the form of listings,
punched cards, and plots), they pass control on to the
next function subroutine. The function subroutines can be
cycled through as described below.

The input consists of the following cards, grouped
according to the function routines:

 A. MAIN input:

  Card 1: KIND, NPUNCH, NPLOT, NFIT (4I2)

     A control word for selecting functions.

     If KIND = 1, raw data input

      KIND = 2, reduced data input

      KIND = 3, Watson-Migdal fits only

    If NPUNCH = 0, no cards punched

     NPUNCH = 1, cards punched

      NPLOT = n, the number of plots to be
         made

       NFIT = m, the number of Watson-Migdal
         fits to be made

 B. RDATA input (included only if KIND = 1):

  Card 1: TITLE (10A6)

     A title for the printed output.

Card 2: CORFAC(I) (16F5.0)

        Correction factors for the response of

        each detector of the array.

Card 3: Z,A (2F5.0)

        Charge and mass number of the detected

        particle.

Card 4: NRUN, FREQ8, DTCORR (I3,2F10.0)

Card 5: SUM(I) (16F5.0)

Card 6: NRUN, FREQ8, DTCORR (I3,2F10.0)

Card 7: SUM(I) (16F5.0)

   •   •

   •   •

   •   •

Blank Card

  where:

   NRUN = identifying run number

  FREQ8 = frequency of detector 8

 DTCORR = correction factor for the electronics

         dead time

  SUM(I) = array of 16 sums that correspond to

         the yields in the 16 detectors

         Cards 4 and 5 form a set which contains

         the raw data for one run. As many sets

         of these cards can be submitted as

         desired. Reading of the sets is

terminated by the blank card.

C. CDATA input (included only if KIND = 2 or
    NPLOT ≠ 0):

    1, Data Cards (included only if KIND = 2):
        Card 1: NCOUN, EN, CY (I5,2F10.0)
        Card 2: NCOUN, EN, CY (I5,2F10.0)

            .   .

            .   .

            .   .

        Blank Card

            where:

            NCOUN = number of counter in which data
                    were taken

               EN = energy of the detected particles

               CY = corrected yield of the detected
                    particles

            There are as many of these cards as
            there are data points to be plotted in
            a spectrum. Reading of the cards is
            terminated by the blank card.

    2. Plotting Cards (included only if NPLOT ≠ 0):
        Card 1: DATE, REAC, ENAG (2A6,8X,3A6,2X,5A6)
            where:
            DATE = date of run
            REAC = name of the reaction

7

ENAG = incident energy and laboratory

angle for the reaction.

This card identifies the spectrum

plot.

Card 2: XMIN, XMAX, YMIN, YMAX (4F10.0)

This card specifies the minimum and

maximum values of the energy and

yield/(freq)^2 to be plotted.

Card 3: NPC (16I1)

Card 4: NPC (16I1)

  .   .

  .   .

  .   .

Card n: NPC (16I1)

where n = (NPLOT + 2)

NPC is a binary code word that designates

which detector's data are to be plotted.

Each detector corresponds to one digit

of the code word: if that digit = 1,

the detector's data are plotted; if the

digit = 0, the data are not plotted.

The number of NPC cards equals NPLOT ---

the number of plots designated in the

MAIN program control word. Each NPC card

is followed by the SIGGEN input given

in Part D below.

D. SIGGEN input (if KIND = 2, NPLOT sets are included):

1. Plotting Cards (included only if KIND = 3):

    Card 1: GRAPH (3A6)

            This word is used to identify plots
            when they are only made by SIGGEN.

    Card 2: XMIN, XMAX, YMIN, YMAX (4F10.0)

            This card specifies the minimum and
            maximum of the energy and cross
            section values to be plotted by
            SIGGEN.

2. Reaction Cards:

    Card 1: M1, M3, M4, Z3, Z5, Z6 (6F10.0)

        where:

            M1 = mass of the incident particle

            M3 = mass of the observed particle

            M4 = sum of masses of the unobserved
                 particles

            Z3 = charge of the observed particle

            Z5 = charge of one of the unobserved
                 particles

            Z6 = charge of the other unobserved
                 particle

Card 2: E1, THETA3, Q, DEX, E3MIN (5F10.0)

where:

E1 = energy of the incident particle

THETA3 = lab angle of the observed particle

Q = the Q-value of the reaction

DEX = the increment of excitation
energy in the final state
nucleon-nucleon system

E3MIN = minimum energy in the spectrum
of the observed particle for
which calculations are to be made

3. Parameter Cards:

Card 1: SCATLN, RO, SP, R, L3, PARAM
(4F10.0,I2,8X4A6)

where:

SCATLN = nucleon-nucleon scattering length

RO = nucleon-nucleon effective range

SP = nucleon-nucleon shape parameter

R = Coulomb radius (28.8 F)

L3 = angular momentum quantum number
for the motion of the observed
particle with respect to the c.m.
of the nucleon-nucleon system
(see Tombrello and Bacher, 1965).
If L3 = -1, this effect is not

included.

    PARAM = label for identifying the effec-

           tive range parameters used

Card 2: DE3, RES, SNORM, IGMAX (3F10.0,I2)

  where:

     DE3 = increment in the observed parti-

          cle's energy used in folding in

          the experimental resolution

     RES = total experimental energy reso-

          lution (FWHM) of the Gaussian

          resolution function

  SNORM = scale height to which the maximum

          of the calculated energy spectrum

          is normalized

  IGMAX = number of points in one-half of

          the Gaussian resolution function

Card 3: SCATLN, RO, SP, R, L3, PARAM

Card 4: DE3, RES, SNORM, IGMAX

    •   •

    •   •

    •   •

Card n: SCATLN, RO, SP, R, L3, PARAM

Card m: DE3, RES, SNORM, IGMAX

    where n = 2*NFIT-1 and m = 2*NFIT

Cards 1 and 2 and each succeeding pair

form a set. A total of NFIT sets are

required.

On the following pages is a listing of the complete

program.

```
$IBFTC MAIN     DECK
C
C       SPECTROMETER DATA REDUCTION PROGRAM
C
C               MAIN CONTROL PROGRAM
C
        COMMON /MAIN/ KIND,NPUNCH,NPLOT,NFIT
     10 READ(5,1) KIND,NPUNCH,NPLOT,NFIT
      1 FORMAT(4I2)
        IF(KIND .EQ. 1) CALL RDATA
        IF(KIND .EQ. 2 .OR. NPLOT .NE. 0) CALL CDATA
        IF(KIND .EQ. 3) CALL SIGGEN
        GO TO 10
        END
$IBFTC RDATA    DECK
        SUBROUTINE  RDATA
        DIMENSION FREFAC(16),CORFAC(16),F(16),SUM(16),YIELD(16),YF(16),
       1YFF(16),E(16),TITLE(10),EN(1000),CY(1000),NCOUN(1000)
        COMMON /DATA/ EN,CY,NCOUN,IMAX
        COMMON /MAIN/ KIND,NPUNCH,NPLOT,NFIT
        DATA(FREFAC(I),I=1,16)/0.98148,0.98416,0.98693,0.98961,0.99230,
       10.99494, 0.99748, 1.0, 1.00257, 1.00504, 1.00749, 1.00984,
       21.01220, 1.01453, 1.01692, 1.01912/
C
C       INPUT-OUTPUT OF PARAMETERS
C
        READ(5,1)TITLE
      1 FORMAT(10A6)
        READ(5,2)(CORFAC(I),I=1,16)
      2 FORMAT(16F5.0)
        READ(5,3)Z,A
      3 FORMAT(2F5.0)
        WRITE(6,4)
      4 FORMAT(1H1///15X,27HSPECTROMETER DATA REDUCTION////)
        WRITE(6,5)TITLE
      5 FORMAT(5X,10A6//)
        WRITE(6,6)Z,A
      6 FORMAT(19X,4H Z =F4.1,2X 3HA =F4.1///)
        WRITE(6,7)
      7 FORMAT(19X,19H CORRECTION FACTORS/)
        WRITE(6,8) CORFAC
      8 FORMAT(26X,F6.3)
C
C       CALCULATION AND OUTPUT
C
        L=0
     13 LPAGE = 0
        WRITE(6,12)
     12 FORMAT(1H1)
     11 READ(5,9) NRUN,FREQ8,DTCORR
      9 FORMAT(I3,2F10.0)
        FREQ8=0.001*FREQ8
        IF(NRUN .EQ. 0) GO TO 18
        READ(5,10) SUM
     10 FORMAT(16F5.0)
        DO 20 I=1,16
        F(I)=FREQ8*FREFAC(I)
        FR=F(I)
        E(I)=ENER(FR,Z,A)
        YIELD(I)=SUM(I)*CORFAC(I)*DTCORR
        YF(I)=YIELD(I)/F(I)
```

```
      YFF(I)=YF(I)/F(I)
      II=L+I
      EN(II)=E(I)
      CY(II)=YFF(I)
      NCOUN(II)=I
   20 CONTINUE
      WRITE(6,14) NRUN,FREQ8,DTCORR
   14 FORMAT(//5X,5H RUN I3, 4X 7HFREQ = F7.3, 4X 17HDEAD TIME CORR =
     1F6.3//)
      WRITE(6,15)
   15 FORMAT(8H COUNTER 3X 4HFREQ 3X 6HY/FREQ 4X 3HSUM 4X 5HYIELD 3X
     16HENERGY 3X 9HY/FREQ**2)
      WRITE(6,16)(I,F(I),YF(I),SUM(I),YIELD(I),E(I),YFF(I), I=1,16)
   16 FORMAT(I5,F11.3,F8.3,F8.1,F8.1,F9.3,F10.3)
      L=L+16
      IMAX=L
      LPAGE = LPAGE+1
      IF(LPAGE .EQ. 3) GO TO 13
      GO TO 11
C
C     ORDER BY ENERGY AND PUNCH
C
   18 DO 30 J=1,IMAX
      BIG = EN(J)
      K=J
      DO 31 JJ=J,IMAX
      IF(EN(JJ) .GT. BIG) GO TO 32
      GO TO 31
   32 BIG = EN(JJ)
      K=JJ
   31 CONTINUE
      A=EN(J)
      AA=CY(J)
      NA=NCOUN(J)
      EN(J)=BIG
      CY(J)=CY(K)
      NCOUN(J)=NCOUN(K)
      EN(K)=A
      CY(K)=AA
      NCOUN(K)=NA
   30 CONTINUE
      IF(NPUNCH .NE. 1)RETURN
      DO 33 I=1,IMAX
      PUNCH 40, NCOUN(I),EN(I),CY(I)
   40 FORMAT(I5,2F10.5)
   33 CONTINUE
      RETURN
      END
$IBFTC CDATA    DECK
      SUBROUTINE CDATA
      DIMENSION EN(1000),CY(1000),NCOUN(1000),NPC(16),DATE(2),REAC(3),
     1ENAG(5),ENP(1000),CYP(1000),TT(2),TT1(2),AA(14)
      COMMON /MAIN/ KIND,NPUNCH,NPLOT,NFIT
      COMMON /DATA/ EN,CY,NCOUN,IMAX
      COMMON/PLOT/XMIN,XMAX,YMIN,YMAX,TT,TTT,TT1
      DATA(TT(I), I=1,2)/6HENERGY,6H (MEV)/
      DATA TTT/5HYIELD/
      DATA(TT1(I), I=1,2)/2*1H /
      IF(KIND .EQ. 1) GO TO 3
      I=0
    1 I=I+1
```

```
      READ(5,2)NCOUN(I),EN(I),CY(I)
    2 FORMAT(I5,2F10.0)
      IMAX=I
      IF(NCOUN(I) .NE. 0) GO TO 1
    3 IF(NPLOT .EQ. 0) RETURN
      READ(5,4) DATE,REAC,ENAG
    4 FORMAT(2A6,8X3A6,2X5A6)
      READ(5,5) XMIN,XMAX,YMIN,YMAX
    5 FORMAT(4F10.0)
C
C     PLOT DATA FOR SELECTED COUNTERS
C
      L=0
    6 READ(5,7) NPC
    7 FORMAT(16I1)
      II=1
      DO 10 I=1,IMAX
      NC=NCOUN(I)
      NCC=NPC(NC)
      IF(NCC .EQ. 0) GO TO 10
      ENP(II)=EN(I)
      CYP(II)=CY(I)
      NMAX=II
      II=II+1
   10 CONTINUE
      CALL LABEL(0.,0.,XMIN,XMAX,15.,6,TT,12,0)
      CALL LABEL(0.,0.,XMIN,XMAX,15.,-30,TT1,2,0)
      CALL LABEL(0.,0.,YMIN,YMAX,10.,4,TTT,5,1)
      CALL LABEL(0.,0.,YMIN,YMAX,10.,-20,TT1,2,1)
      CALL OUTCOR(AA,NWDS)
      WRITE(6,100)(DATE(I), I=1,2)
  100 FORMAT(2A6)
      CALL OUTCOR
      CALL SYSSYM(2.25,9.5,.25,AA,6*NWDS,0.)
      CALL OUTCOR(AA,NWDS)
      WRITE(6,101)(REAC(I), I=1,3)
  101 FORMAT(3A6)
      CALL OUTCOR
      CALL SYSSYM(1.5,8.75,.35,AA,6*NWDS,0.)
      CALL OUTCOR(AA,NWDS)
      WRITE(6,102)(ENAG(I), I=1,5)
  102 FORMAT(5A6)
      CALL OUTCOR
      CALL SYSSYM(1.0,8.25,.25,AA,6*NWDS,0.)
      CALL OUTCOR(AA,NWDS)
      WRITE(6,103) (NPC(I), I=1,16)
  103 FORMAT(16I1)
      CALL OUTCOR
      CALL SYSSYM(2.00,7.85,.12,AA,6*NWDS,0.)
      LF=1
      IF(NFIT .NE. 0) LF=0
      CALL PLOTXY(NMAX,ENP,CYP,XMIN,XMAX,YMIN,YMAX,LF,0,3,1)
      IF(NFIT .NE. 0) CALL SIGGEN
      L=L+1
      IF(L .LT. NPLOT) GO TO 6
      RETURN
      END
$IBFTC SIGGEN   DECK
      SUBROUTINE SIGGEN
      DIMENSION E3(1000),SIG(1000),EX(1000),E3INT(1000),SIGINT(1000),
     1SIGFLD(1000),GA(50),AB(14),PARAM(4),GRAPH(3),TT(2),TT1(2)
```

```
      COMMON /MAIN/ KIND,NPUNCH,NPLOT,NFIT
      COMMON /FOOL/ E3,SIG,NMAX,E3INT,SIGINT,SIGFLD,INTMAX,DE3,RES,
     1SGFM,IGMAX
      COMMON/PLOT/XMIN,XMAX,YMIN,YMAX,TT,TTT,TT1
      REAL M1,M3,M4,M34,M41,MMM
      LFIT=1
C
C     INPUT-OUTPUT OF FITTING PARAMETERS
C
      IF(KIND .NE. 3) GO TO 18
      READ(5,190) GRAPH
  190 FORMAT(3A6)
      READ(5,19) XMIN,XMAX,YMIN,YMAX
   19 FORMAT(4F10.0)
   18 READ(5,1)M1,M3,M4,Z3,Z5,Z6
    1 FORMAT(6F10.0)
      READ(5,2)E1,THETA3,Q,DEX,E3MIN
    2 FORMAT(5F10.0)
    3 READ(5,4)SCATLN,RO,SP,R,L3,PARAM
    4 FORMAT(4F10.0,I2,8X4A6)
      READ(5,5)DE3,RES,SNORM,IGMAX
    5 FORMAT(3F10.0,I2)
      WRITE(6,6)
    6 FORMAT(1H16X46HSPECTRUM FOR DINUCLEON FINAL STATE INTERACTION////)
      WRITE(6,7)M1,M3,M4,Z3,Z5,Z6
    7 FORMAT(15X6H M1 = F10.6/,16X5HM3 = F10.6/,16X5HM4 = F10.6/,16X
     15HZ3 = F5.1/,16X5HZ5 = F5.1/,16X5HZ6 = F5.1///)
      WRITE(6,8)E1,Q,THETA3,DEX,E3MIN,DE3,RES,SNORM
    8 FORMAT(10X10H E1(MEV) =F6.3,4X14HQ-VALUE(MEV) =F6.3//,20X
     112HTHETA(DEG) =F4.1//,10X 5HDEX =F6.3,4X 7HE3MIN = F4.1,
     24X 5HDE3 =F6.3//,20X 12HRESOLUTION =F6.3//,
     317X 15HNORMALIZATION =F7.4////)
      WRITE(6,10) PARAM
   10 FORMAT(20X 4A6//)
      WRITE(6,11)SCATLN,RO,SP,R,L3
   11 FORMAT(17X 20H SCATTERING LENGTH =F7.3//,20X 17HEFFECTIVE RANGE =
     1F7.3//,20X 17HSHAPE PARAMETER =F7.3//,29X 8HRADIUS =F7.3//,33X
     24HL3 =I3///)
C
C     CALCULATE KINEMATICS AND SPECTRUM SHAPE
C
      M34=M3+M4
      M41=M4-M1
      EMAX=Q+E1*(M34-M1)/M34
      TH3R=0.0174533*THETA3
      V=SQRT(M1*M3*E1)*COS(TH3R)/M34
      MMM=M3*M4/M34
      Z4 = Z5 + Z6
      Z56 = Z5*Z6
      I=0
      SIGMAX=0.0
   15 EX(I+1)=DEX*FLOAT(I)
      EE=EMAX-EX(I+1)
      ECM=EX(I+1)
      AK3=0.218738*SQRT(MMM*EE)
      ETA3=0.157481*Z3*Z4*SQRT(MMM/EE)
      WT3=1.0
      IF(L3 .GE. 0) WT3=WGT(ETA3,AK3,L3)
      U=(M4*(Q-ECM)+E1*M41)/M34
      T=V*V+U
      IF(T .LT. 0.0) GO TO 16
```

```
      SE=V+SQRT(T)
      E3(I+1)=SE*SE
      SIG(I+1) = SE*WT3*D(ECM,Z56,SCATLN,RO,SP,R)
      IF(SIGMAX .LT. SIG(I+1))SIGMAX=SIG(I+1)
      I=I+1
      NMAX=I
      IF(E3(I) .GE. E3MIN) GO TO 15
      WRITE(6,300) (EX(I),E3(I),SIG(I), I=1,NMAX)
  300 FORMAT(3F20.8)
C
C     LABEL PLOTS
C
   16 IF(LFIT.GT.1) GO TO 30
      CALL OUTCOR(AB,NWDS)
      WRITE(6,200)(PARAM(I), I=1,4)
  200 FORMAT(4A6)
      CALL OUTCOR
      CALL SYSSYM(1.75,7.50,.12,AB,6*NWDS,0.)
      CALL OUTCOR(AB,NWDS)
      WRITE(6,201)
  201 FORMAT(26H A    RO    P    R    L3    RES)
      CALL OUTCOR
      CALL SYSSYM(1.00,7.00,.25,AB,6*NWDS,0.)
      IF(KIND.NE.3) GO TO 30
      CALL LABEL(0.,0.,XMIN,XMAX,15.,6,TT,12,0)
      CALL LABEL(0.,0.,XMIN,XMAX,15.,-30,TT1,2,0)
      CALL LABEL(0.,0.,YMIN,YMAX,10.,4,TTT,5,1)
      CALL LABEL(0.,0.,YMIN,YMAX,10.,-20,TT1,2,1)
      CALL OUTCOR(AB,NWDS)
      WRITE(6,204) GRAPH
  204 FORMAT(3A6)
      CALL OUTCOR
      CALL SYSSYM(1.5,8.75,.35,AB,6*NWDS,0.)
      CALL OUTCOR(AB,NWDS)
      WRITE(6,205) E1,THETA3
  205 FORMAT(4H E =F7.3, 4H MEV 2X F4.1, 4H DEG)
      CALL OUTCOR
      CALL SYSSYM(1.0,8.0,.25,AB,6*NWDS,0.)
   30 CALL OUTCOR(AB,NWDS)
      WRITE(6,202) SCATLN,RO,SP,R,L3,RES
  202 FORMAT(F9.3,F8.3,F10.3,F8.3,4X I2,F13.3)
      CALL OUTCOR
      AY=6.90-.15*FLOAT(LFIT)
      CALL SYSSYM(0.75,AY,.12,AB,6*NWDS,0.)
      IF(RES .EQ. 0.0) GO TO 17
C
C     CALCULATE AND PLOT FOLDED SPECTRUM
C
      CALL FOLD
      WRITE(6,20)(E3INT(I),SIGINT(I),SIGFLD(I), I=1,INTMAX)
   20 FORMAT(3F20.8)
      SFAC = SNORM/SGFM
      DO 34 I = 1,INTMAX
   34 SIGFLD(I) = SFAC*SIGFLD(I)
      LF=1
      IF(LFIT .LT. NFIT) LF=0
      IP=1
      IF(LFIT.GT.1) IP = 2
      ISYS=0
      IF(LFIT.GT.1) ISYS = 3 + LFIT
      CALL PLOTXY(INTMAX,E3INT,SIGFLD,XMIN,XMAX,YMIN,YMAX,LF,IP,ISYS,50)
```

```
      GO TO 25
C
C     PLOT UNFOLDED SPECTRUM
C
   17 SIGN=SNORM/SIGMAX
      DO 35 I=1,NMAX
   35 SIG(I)=SIGN*SIG(I)
      LF = 1
      IF(LFIT .LT. NFIT) LF=0
      IP = 1
      IF(LFIT.GT.1) IP = 2
      ISYS = 0
      IF(LFIT.GT.1) ISYS = 3 + LFIT
      CALL PLOTXY(NMAX,E3,SIG,XMIN,XMAX,YMIN,YMAX,LF,IP,ISYS,50)
   25 LFIT=LFIT+1
      IF(LFIT .LE. NFIT) GO TO 3
      RETURN
      END
$IBFTC FOLD      DECK
      SUBROUTINE  FOLD
      DIMENSION E3(1000),SIG(1000),E3INT(1000),SIGINT(1000),
     1 SIGFLD(1000),GA(50)
      COMMON /FOOL/ E3,SIG,NMAX,E3INT,SIGINT,SIGFLD,INTMAX,DE3,RES,
     1SGFM,IGMAX
C
C     SET UP GAUSSIAN
C
      SD=RES/2.354
      DO 10 IG = 1,IGMAX
      AIG = IG
      EE = AIG*DE3
      GA(IG)=EXP(-EE*EE/(2.*SD*SD))
      WRITE(6,301) IGMAX,AIG,EE,GA(IG)
  301 FORMAT(I3,2F10.4,E10.2)
   10 CONTINUE
      WRITE(6,30)GA(IGMAX)
   30 FORMAT(15X 22H LAST GAUSSIAN POINT =E10.2)
C
C     INTERPOLATE TO EVENLY-SPACED SPECTRUM
C
      RIGMAX=IGMAX
      E3IMIN=E3(NMAX)-RIGMAX*DE3
      E3INT(IGMAX + 1) = E3(1)
      J=1
    1 II = IGMAX + J
      E3INT(II+1) = E3INT(II) - DE3
      IF(E3INT(II+1).LT.E3IMIN) GO TO 2
      J=J+1
      GO TO 1
    2 INTMAX = II + 1
      DO 3 I = 1,IGMAX
      IJ = IGMAX + 1 - I
    3 E3INT(IJ) = E3INT(IJ+1) + DE3
      DO 4 I = 1,INTMAX
      SIGFLD(I) = 0.0
    4 SIGINT(I) = 0.0
      SIGINT(IGMAX+1) = SIG(1)
      IM = IGMAX + 2
      IE3 = 2
      DO 5 I = IM,INTMAX
      IJM = I
```

```
      GO TO 9
    6 IE3 = IE3 + 1
    9 IF(E3INT(I).LT.E3(NMAX-1)) GO TO 14
      IF(E3INT(I).LT.E3(IE3)) GO TO 6
      X = E3INT(I)
      X1 = E3(IE3+1)
      X2 = E3(IE3)
      X3 = E3(IE3-1)
      Y1 = SIG(IE3+1)
      Y2 = SIG(IE3)
      Y3 = SIG(IE3-1)
      SIGINT(I) = (X-X2)*(X-X3)*Y1/((X1-X2)*(X1-X3)) + (X-X1)*(X-X3)*Y2/
     1((X2-X1)*(X2-X3))   +   (X-X1)*(X-X2)*Y3/((X3-X1)*(X3-X2))
    5 CONTINUE
   14 SL = (SIG(NMAX)-SIG(NMAX-1))/(E3(NMAX)-E3(NMAX-1))
      X1 = E3(NMAX)
      Y1 = SIG(NMAX)
      DO 15 J = IJM,INTMAX
   15 SIGINT(J) = Y1 + SL*(E3INT(J) - X1)
C
C     FOLD GAUSSIAN RESOLUTION INTO SPECTRUM
C
      DO 7 I = 1,IGMAX
      SIGFLD(I) = SIGINT(I)
      DO 8 IF = 1,IGMAX
      IFG = IF + I
    8 SIGFLD(I) = SIGFLD(I) + SIGINT(IFG)*GA(IF)
    7 CONTINUE
      JMIN = IGMAX + 1
      DO 11 J = JMIN,INTMAX
      SIGFLD(J) = SIGINT(J)
      DO 12 JF = 1,IGMAX
      JFP = J + JF
      JFM = J - JF
   12 SIGFLD(J) = SIGFLD(J)+(SIGINT(JFP)+SIGINT(JFM))*GA(JF)
   11 CONTINUE
      SGFM = 0.0
      DO 13 I = 1,INTMAX
   13 IF(SIGFLD(I).GT.SGFM) SGFM = SIGFLD(I)
      RETURN
      END
$IBFTC ENERGY   DECK
      FUNCTION ENER(F,Z,A)
      DIMENSION AM(4,2)
      DOUBLE PRECISION  AM,DKSP,DF,DZ,DMP,DAM
      REAL KSP
      AM(1,1)=938.21875D0
      AM(2,1)=1875.50638D0
      AM(3,1)=2808.76109D0
      AM(3,2)=2808.23198D0
      AM(4,2)=3727.16715D0
      I=IFIX(A)
      J=IFIX(Z)
      KSP=0.011381*(0.0000283*(ABS(F-22.0)**1.813)+0.9994)
      IF(F .LT. 14.0) KSP=0.011385
      DKSP=DBLE(KSP)
      DF=DBLE(F)
      DZ=DBLE(Z)
      DMP=1876.4375D0
      DAM=AM(I,J)
      EN=DSQRT(DKSP*DF*DF*DZ*DZ*DMP+DAM*DAM)-DAM
```

```
      ENER=EN+0.0780*Z*Z*((A/EN)**0.639)
      RETURN
      END
$IBFTC WGT       DECK
      FUNCTION WGT(ETA3,AK3,L3)
      WGT=1.0
      IF(ETA3 .LE. 0.0 .OR. AK3 .LE. 0.0) GO TO 1
      ETA3B=6.2831853*ETA3
      GAMOW=ETA3B/(EXP(ETA3B)-1.0)
      WGT=WGT*GAMOW
      IF(L3 .EQ. 0) GO TO 1
      WGT=WGT*(AK3**(2*L3))
      EL3=L3
      PRD=1.0
      T=1.0
    2 PRD=PRD*(1.0+(ETA3*ETA3)/(T*T))
      T=T+1.0
      IF(T .LE. EL3) GO TO 2
      WGT=WGT*PRD
    1 RETURN
      END
$IBFTC DEZ       DECK
      FUNCTION  D(E,Z,SCATLN,RO,SP,R)
      IF(E .EQ. 0.0) GO TO 2
      AK=0.10985*SQRT(2.0*E)
      IF(Z .EQ. 1.0) GO TO 1
      FN=-1.0/SCATLN + 0.5*RO*AK*AK
      D=AK/(FN*FN+AK*AK)
      RETURN
    2 D=0.0
      RETURN
    1 ETA=0.15805/SQRT(2.0*E)
      C=6.28318*ETA/(EXP(6.28318*ETA)-1.0)
      FN=-1.0/SCATLN+0.5*RO*AK*AK-SP*AK*((RO*AK)**3)-H(ETA)/R
      D=C*AK/(FN*FN+C*C*AK*AK)
      RETURN
      END
$IBFTC HOT       DECK
      FUNCTION H(ETA)
      ET=ETA*ETA
      TUM=-0.57721566-ALOG(ETA)
      AN=0.0
      TEMP=0.0
    1 AN=AN+1.0
      SUM=TEMP
      TERM=1.0/(AN*(AN*AN+ET))
      TEMP=SUM+TERM
      IF(SUM-TEMP .GT. 1.0E-8) GO TO 1
    2 H=ET*SUM+TUM
      RETURN
      END
```

APPENDIX B.   THEORETICAL SPECTRA PROGRAM

This program calculates theoretical spectra using the antisymmetrized plane wave Born approximation described in Part IV of the main text.   The program will also calculate spectra using the Watson-Migdal approximation discussed in Part II.

Each of the integrals of Equation (36) can be analytically reduced to the sum

$$\sum \left[G_1(k,i)G_2(k,i)G_3(k,j,i) \right] \exp\left\{ -\left[Q_1^2/G_1(k,i) + Q_2^2(k,i)/G_2(k,i) + Q_3^2(k,i)/G_3(k,j,i) \right] \int \exp\left\{ -G_4(k,j,i)r^2 \right\} \left\{ \sin[P(k,j,i)r]/ \right. \right. \tag{B-1}$$
$$\left. P(k,j,i) \right\} \Phi_{NN}(r)rdr$$

where the Q's and P are momentum transfers; the G's are weighting coefficients for the momentum transfers, and the integration is over the separation distance between the final state nucleons. $\Phi_{NN}(r)$ is the S-wave nucleon-nucleon scattering wave function.   The triple summation occurs because the deuteron, the mass-three initial state, and the mass-three final state wave functions are expanded in Gaussian functions.   Tables B-I and B-II list the above parameters for each of the seven terms of the transition matrix element.

161

TABLE B-I

A tabulation of the momentum transfer weighting coefficients for the

overlap integrals of the transition matrix. The α_j, γ_i, and Γ_k are

the exponents of the Gaussian expansions of the deuteron, mass-three

initial state and mass-three final state wave functions, respectively.

The subscripts, j, i, and k are their respective summation indices.

β is the inverse range of the nucleon-nucleon potential. For the

Coulomb terms of the transition matrix, β is replaced by the ζ_n,

the exponents of the Gaussian expansion of the Coulomb potential.

TABLE B-I

Term	$G_1(l,m)$	$G_2(l,m)$	$G_3(k,j,i)$	$G_4(k,j,i)$
1	$\Gamma_k + \gamma_i$	$(3\Gamma_k + \beta^2)/4 + \alpha_j$	$\Gamma_k + \beta^2 - \Gamma_k^2/G_1(k,i)$ $- \beta^4/(4G_2(k,j))$	$3\gamma_i/4 + (3\Gamma_k/4 + \alpha_j))\beta^2/$ $(4G_2(k,j))) + (3\Gamma_k/4 + \alpha_j)^2\beta^4/$ $(4G_2^2(k,j)G_3(k,j,i))$
2	γ_i	$(3\Gamma_k + \beta^2)/4 + \alpha_j$	$\Gamma_k + \beta^2 - \beta^4/(4G_2(k,j))$	$3\gamma_i/4$
3	$\Gamma_k + \gamma_i + \beta^2$	$(3\Gamma_k + 3\gamma_i + \beta^2)/4$	$\gamma_i + \beta^2 + \alpha_j - \beta^4/(4G_2(k,i))$ $- \alpha_j^2/G_1(k,j)$	$\gamma_i - \gamma_i^2/G_3(k,j,i)$
4	$\Gamma_k + \gamma_i$	$3(\Gamma_k + \gamma_i)/4$	$\Gamma_k + \beta^2 + \alpha_j - \Gamma_k^2/G_1(k,i)$	$\alpha_j + \beta^2 - \alpha_j^2/G_3(k,j,i)$
5	$\Gamma_k + \gamma_i + \beta^2$	$(3\Gamma_k + 3\gamma_i + \beta^2)/4$ $- \beta^4/(4G_1(k,i))$	$\Gamma_k + \beta^2 + \alpha_j - (\Gamma_k + \beta^2)^2/G_1(k,i)$ $- \gamma_i^2\beta^4/(4G_1^2(k,i)G_2(k,i))$	$\alpha_j - \alpha_j^2/G_3(k,j,i)$
6	$\Gamma_k + \gamma_i$	$3(\Gamma_k + \gamma_i)/4$	$\Gamma_k + \beta^2 + \alpha_j - \Gamma_k^2/G_1(k,i)$	$\alpha_j - \alpha_j^2/G_3(k,j,i)$
7	$\Gamma_k + \gamma_i$	$3(\Gamma_k + \gamma_i)/4$	β^2	α_j

163

TABLE B-II

A tabulation of the momentum transfers of the overlap integrals of

the transition matrix. The momentum transfers $\bar{Q}_n$, $\bar{Q}_d$, and $\bar{Q}_{2p}$ are

defined in terms of the initial state and final state wave vectors

($\bar{K}_i$ and $\bar{K}_f$, respectively) at the bottom of the table. The other

parameters appearing in the table are identified in Table B-I.

TABLE B-II

Term	Q_1	$Q_2(k,i)$	$Q_3(k,m)$	$P(k,j,i)$
1	Q_n	0	$\left\|\bar{Q}_d + \Gamma_k \bar{Q}_n/G_1(k,i)\right\|$	$\beta^2(3\Gamma_k/4 + \alpha_j)Q_3(k,i)/$ $(2G_2(k,j)G_3(k,j,i))$
2	Q_{2p}	0	Q_d	0
3	$Q_d/2$	0	$\left\|\Gamma_k \bar{Q}_d/(2G_1(k,j)) + 2\bar{Q}_n\right\|$	$\left\|\bar{Q}_{2p}/2 - \gamma_i \bar{Q}_3(k,j)/G_3(k,j,i)\right\|$
4	$2Q_n$	0	$\left\|\bar{Q}_d/2 + 2\Gamma_k \bar{Q}_n/G_1(k,i)\right\|$	$\left\|3\bar{Q}_n/2 - \alpha_j \bar{Q}_3(k,i)/G_3(k,j,i)\right\|$
5	$2Q_n$	$\beta^2 Q_n/G_1(k,i)$	$\left\|\bar{Q}_d/2 + (2(\Gamma_k + \beta^2) - \gamma_i \beta^4/ (G_1(k,i)G_2(k,i)))\bar{Q}_n/G_1(k,i)\right\|$	$\left\|3\bar{Q}_n/2 - \alpha_j \bar{Q}_3(k,i)/G_3(k,j,i)\right\|$
6	$2Q_n$	0	$\left\|\bar{Q}_d/2 + 2\Gamma_k \bar{Q}_n/G_1(k,i)\right\|$	$\left\|3\bar{Q}_n/2 - \alpha_j \bar{Q}_3(k,i)/G_3(k,j,i)\right\|$
7	$2Q_n$	0	$3Q_n$	$3Q_n/2$

Where: $\bar{Q}_n = -(\bar{K}_f - \bar{K}_i)/3$, $\bar{Q}_d = -(2\bar{K}_f/3 + \bar{K}_i)$, $\bar{Q}_{2p} = \bar{K}_f + 2\bar{K}_i/3$

To keep the program running time within reasonable limits, the evaluation of the matrix element was restricted to 25 points. These points corresponded to 25 preselected excitation energies in the final state nucleon-nucleon system. The energies were unevenly spaced to give a better description of the spectrum for the fixed number of points used. The points were most numerous where the spectrum changed most rapidly --- the high energy region and the region of the maximum.

The use of preselected values for the nucleon-nucleon excitation energies allowed the integrals of Equation (B-1) to be evaluated with the Gaussian integration method. The nucleon-nucleon scattering wave functions were tabulated for each standard excitation energy at radii corresponding to the zeros of the generalized Laquerre polynomials used in the Gaussian integration. The corresponding weighting functions were also tabulated.[*] Sixteen points were used in the integration. The accuracy of the Gaussian integration was checked by using Simpson's rule to evaluate the integrals at several test energies.

Figure B-1 shows the organization and major subroutines of the program. The purpose of each of the subroutines is briefly described on the following pages.

_____
[*]P. Rabinowitz, and Weiss, G., Math. Tables and Other Aids to Comp., 13, 285 (1959).

FIGURE B-1

An organizational diagram of the theoretical spectra

program.   The function of each of the major subroutines is

described on pages 168 and 169.
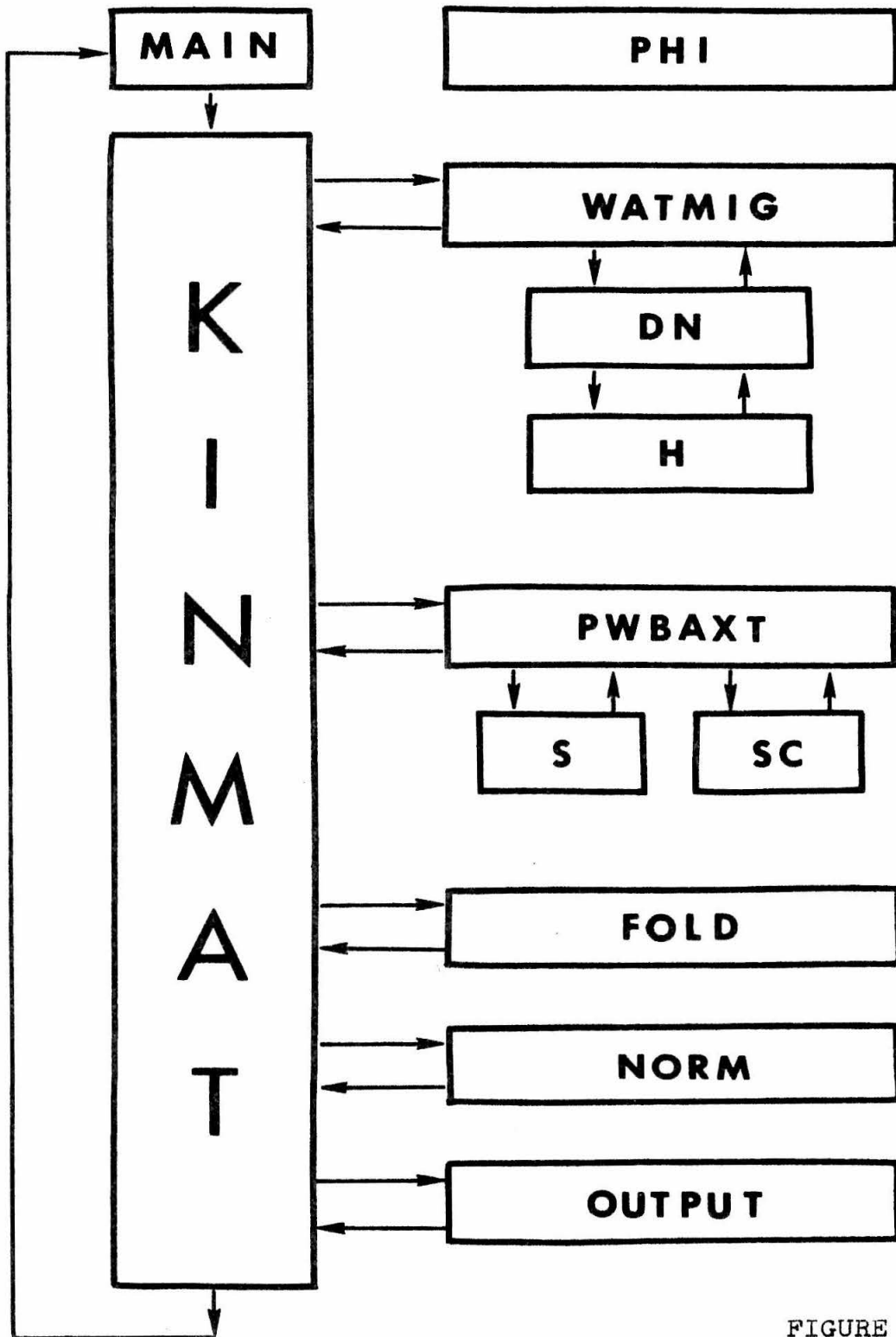
FIGURE B-1

MAIN is an entry program about which computations for different reactions can be cycled. It also has a role in normalizing spectra to a common scale.

KINMAT calculates the required kinematics for each standard excitation energy in the final state nucleon-nucleon system. It also calls the other major subroutines.

PHI is a block data subroutine that stores the tabulated nucleon-nucleon scattering wave function and the corresponding weighting functions.

WATMIG calculates the single particle spectrum using the Watson-Migdal approximation (Equation (24) of the main text). WATMIG requires the auxiliary routines DN and H.

PWBAXT calculates the single particle spectrum using the antisymmetrized plane wave Born approximation described in Part IV. PWBAXT requires the auxiliary integration routines S and SC.

FOLD interpolates a smooth energy spectrum between the points calculated either by WATMIG or PWBAXT. It then folds in the experimental energy resolution which is approximated by a

Gaussian weighting function.

NORM normalizes the spectrum generated by FOLD
in one of three ways: (a) it normalizes to a
designated value at a designated energy;
(b) it normalizes the maximum to 1.0; or
(c) it normalizes all spectra to a common
scale determined by the first spectrum.

OUTPUT handles the listing, punching, and plotting
of the calculated spectrum.

The input consists of the following cards, grouped according to the primary subroutines.

    A.   MAIN input:

            Card 1: $M1$, $M2$, $M3$, $M5$, $M6$, $Z3$, $Z5$, $Z6$

                    (8F10.0)

               where:

                 $M1$ = mass of the incident particle

                 $M2$ = mass of the target particle

                 $M3$ = mass of the observed particle

                 $M5$ = mass of one of the unobserved particles

                 $M6$ = mass of the other unobserved particle

                 $Z3$ = charge of the observed particle

                 $Z5$ = charge of one of the unobserved particles

                 $Z6$ = charge of the other unobserved particle

    B.   KINMAT input:

            Card 1: KTHRY, KOMNRM, NFIT, KOUT (412)

                    A control word for directing the calculation.

                    If KTHRY = 1, the calculation uses the Watson-Migdal approximation

KTHRY = 2, the calculation uses
the antisymmetrized PWBA

If KOMNRM = 0, each spectrum is
individually normalized to
either a preselected point
or to the maximum of the
calculated spectrum

KOMNRM = 1, the first spectrum is
normalized to a preselected
point; thereafter, each
succeeding spectrum is to
the same scale as the
first

NFIT = n, the number of calculations
to be made at each angle and
incident energy; also, n
equals the number of plots
to be made on one sheet of
paper

If KOUT = 0, the output consists only
of a listing of the calcu-
lated spectrum

KOUT = 1, the output includes both
a listing and a Calcomp plot
of the spectrum

KOUT = 2, the output includes a
listing and a punched tabu-
lation of the spectrum

KOUT = 3, the output consists of
a listing, a Calcomp plot,
and a punched tabulation
of the calculated spectrum

Card 2: VMEDIA (F10.0)

If VMEDIA > 0.0, the reaction is
assumed to occur in a nuclear potential
well of infinite range and of depth
VMEDIA. VMEDIA was included in the
program as a crude attempt at estimating
the effects of distortion. All calcu-
lations presented in this thesis were
made with VMEDIA = 0.0.

Card 3: NE1, QVAl, (E1(I), I = 1, NE1)
(I2,8X,7F10.0)

where:

NE1 = the number of incident beam
energies for which spectra are
to be calculated

QVAL = the Q value of the reaction
named by the MAIN input card

E1(I) = the beam energies for which

spectra are to be calculated

(up to a maximum of 6)

Card 4: NTHETA, (THETA3(I), I = 1.7)

(I2,8X,7F10.0)

where:

NTHETA = the number of laboratory angles

for which spectra are to be

calculated. If NTHETA $\leq$ 0,

calculationa are made for

each THETA3(I) $\geq$ 0.0 (up to a

maximum of 7). If NTHETA > 0,

then NTHETA angles are calcu-

lated starting from

THCMIN = THETA3(2) in steps of

DTHETA = THETA3(1) and the dummy

subroutine ANG is called

THETA3(I) = the values of laboratory angles

or the minimum and increment

values as discussed above under

NTHETA

Card 5: NECM, (JSTD(I), I = 1, NECM)

(8(I2,8X))

where:

NECM = the number of standard

excitation energy values

(called ECMSTD) used in the calculations. If NECM $\leq$ 0, all the standard values are used. If NECM $>$ 0, only selected values are used (designated by ᴥthe numbers JSTD(I)). A maximum of 7 ECMSTD values can be selected; otherwise, all 25 values must be used.

JSTD(I) = the identification number of the ECMSTD(I) selected. The JSTD(I) range from 1 through 25, corresponding to the 25 standard excitation energy values used by the program.

The program then requires N sets of the following cards (including the cards of Parts C or D) where N equals the total number of spectrum calculations to be made:

 1. Parameter Cards

  Card 1: WTLBL (13A6)

  Permits supplementary comments to be included in the regular calculation heading.

  Card 2: DE3, RES, IGMAX (2F10.0,I2)

  where:

DE3 = the increment in the energy
of the observed particle
(called E3) used in interpolating
a smooth spectrum and folding
in the experimental resolution.

RES = the FWHM for the single
Gaussian function used to
approximate the resolution
function

IGMAX = the number of points in one
half of the Gaussian resolution
function

Card 3: ENORM, SNORM (2F10.0)

where:

ENORM = the energy of the normalization
point

SNORM = the value of the normalization
point

Card 4: PNLBL (13A6) (included only if
KOUT ≥ 2). A punched label to go with
the punched card output.

Card 5: PTLBL (13A6) (included only if
KOUT = 1 or if KOUT > 2). A label for
identifying the plotted spectrum.

Card 6: XMIN, XMAX, YMIN, YMAX (4F10.0)

(included only if KOUT = 1 or if

KOUT > 2). This card specifies the

minimum and maximum values of the

energy and cross section to be

plotted.

2. Data Cards (included only if KOUT $\leq$ 0)

   Card 1: EXE3(I), EXD(I), EXVD(I) (3F10.0)
   Card 2: EXE3(I), EXD(I), EXVD(I) (3F10.0)

   .   .

   .   .

   .   .

   Blank Card

   where:

   EXE3(I) = the energy of the experimental
             data point

   EXD(I) = the value of the experimental
            data point

   EXVD(I) = the $\pm$ variation of EXD(I)

   There are as many of the cards as

   there are data points to be included

   in the listed spectrum. Reading of

   the cards is terminated by the blank

   card.

C. WATMIG input (included only if KTHRY = 1)

   Card 1: SCATLN, RO, SP, R, L3, PARAM

(4F10.0,I2,8X4A6)

where:

SCATLN = the nucleon-nucleon scattering
length

RO = the nucleon-nucleon effective
range

SP = the nucleon-nucleon shape
parameter

R = the Coulomb radius (28.8 F)

L3 = a dummy input that is not used

PARAM = a label array for commentary
on the parameters used.
PARAM only appears in the
calculation heading.

D. PWBAXT input (included only if KTHRY = 2)

Card 1: (GI2(I), CH(I), I = 1, IMX)

(8F10.0)

where:

GI2(I) = the Ith exponent in the
Gaussian expansion of the
initial state mass-three wave
function

CH(I) = the Ith coefficient in the
Gaussian expansion of the
initial state mass-three wave

178

function

IMX = the number of terms in the
Gaussian expansion of the
initial state mass-three wave
function. IMX is determined
by a statement in the program.

Card 2: (GF2(K), CT(K), K = 1, KMX)

(8F10.0)

where:

GF2(K) = the Kth exponent of the
Gaussian expansion of the
final state mass-three wave
function

CT(K) = the Kth coefficient in the
Gaussian expansion of the
final state mass-three wave
function

KMX = the number of terms in the
Gaussian expansion of the
final state mass-three wave
function. KMX is determined
by a statement in the program.

Card 3: (A2(J), CD(J), J = 1, JMX)

(8F10.0)

where:

$A2(J)$ = the Jth exponent in the Gaussian expansion of the deuteron wave function

$CD(J)$ = the Jth coefficient in the Gaussian expansion of the deuteron wave function

JMX = the number of terms in the Gaussian expansion of the deuteron wave function. JMK is determined by a statement in the program.

Card 4: B2, VOG, SERBER (3F10.0)

where:

B2 = the exponent of the Gaussian nucleon-nucleon potential

VOG = the strength of the Gaussian nucleon-nucleon potential (positive quantity)

SERBER = the amount of Serber-type exchange mixture in the nucleon-nucleon interaction

Card 5: IWRITE (15I2)

If IWRITE (I) $\neq$ 0, then the numerical integrals for term I will be written out for each of the 16 points in the

Gauss-Laquerre integration. This
permits checking the convergence of
the integrals. If IWRITE (15) ≠ 0,
the same wave function and interaction
parameters will be used in all sub-
sequent calculations. This eliminates
unnecessary re-calculation of the many
arrays required in PWBAXT.

On the following pages is a listing of the complete
program.

```
$IBF13 MAIN    DECK
C
C     PROGRAM TO CALCULATE THEORETICAL 3-BODY FINAL STATE INTERACTIONS
C
C     MAIN CONTROL PROGRAM FOR SUPER PROGRAM
C
      COMMON/MAIN/KTHRY,KOMNRM,NFIT,KOUT,ISAVE,SAVE
      COMMON/IN/M1,M2,M3,M5,M6,Z3,Z5,Z6
    2 READ(5,1)M1,M2,M3,M5,M6,Z3,Z5,Z6
    1 FORMAT(8F10.0)
      ISAVE=1
      CALL KINMAT
      GO TO 2
      END
$IBF13 PHI     DECK
      BLOCK DATA
C
C     P-P SCATTERING WAVE FUNCTION
C     TO BE USED IN SUPER PROGRAM
C
      COMMON/KINBLK/JSTD(25),ECMSTD(25)
      COMMON / PHII / PHIE(16,24),ZLP(16),WTE(16)
      DATA (PHIE(I,1),I=1,16) /
    X  3.7580079E 00, 2.9972505E 00, 2.1419471E 00, 1.4951218E 00,
    X  1.0904510E 00, 8.5593919E-01, 7.2225574E-01, 6.4587767E-01,
    X  6.0271083E-01, 5.7954654E-01, 5.6871609E-01, 5.6527726E-01,
    X  5.6543506E-01, 5.6548265E-01, 5.6052606E-01, 5.4095104E-01/
      DATA (PHIE(I,2),I=1,16) /
    X  5.4636709E 00, 4.3574308E 00, 3.1131139E 00, 2.1709472E 00,
    X  1.5795569E 00, 1.2339516E 00, 1.0328567E 00, 9.1240710E-01,
    X  8.3679332E-01, 7.8567640E-01, 7.4643033E-01, 7.0990427E-01,
    X  6.6801373E-01, 6.1197381E-01, 5.3000435E-01, 4.0050101E-01/
      DATA (PHIE(I,3),I=1,16) /
    X  6.4137368E 00, 5.1149008E 00, 3.6532692E 00, 2.5451823E 00,
    X  1.8474141E 00, 1.4362686E 00, 1.1924018E 00, 1.0402431E 00,
    X  9.3699669E-01, 8.5784084E-01, 7.8688568E-01, 7.1230451E-01,
    X  6.2382290E-01, 5.1134506E-01, 3.6387723E-01, 1.6711548E-01/
      DATA (PHIE(I,4),I=1,16) /
    X  7.0022175E 00, 5.5839541E 00, 3.9871882E 00, 2.7751636E 00,
    X  2.0094922E 00, 1.5547280E 00, 1.2800798E 00, 1.1024985E 00,
    X  9.7459648E-01, 8.6865047E-01, 7.6681729E-01, 6.5615854E-01,
    X  5.2655754E-01, 3.7050840E-01, 1.8473472E-01,-2.4537477E-02/
      DATA (PHIE(I,5),I=1,16) /
    X  7.3703880E 00, 5.8772796E 00, 4.1954733E 00, 2.9173352E 00,
    X  2.1073423E 00, 1.6225086E 00, 1.3246924E 00, 1.1260145E 00,
    X  9.7618721E-01, 8.4564162E-01, 7.1568567E-01, 5.7371966E-01,
    X  4.1186851E-01, 2.2826271E-01, 3.1524284E-02,-1.4724791E-01/
      DATA (PHIE(I,6),I=1,16) /
    X  7.5972824E 00, 6.0579379E 00, 4.3232322E 00, 3.0032971E 00,
    X  2.1641862E 00, 1.6581083E 00, 1.3422622E 00, 1.1256550E 00,
    X  9.5616770E-01, 8.0335877E-01, 6.4867736E-01, 4.8104277E-01,
    X  2.9646606E-01, 1.0068704E-01,-8.4424721E-02,-2.0579335E-01/
      DATA (PHIE(I,7),I=1,16) /
    X  7.7249954E 00, 6.1594809E 00, 4.3944847E 00, 3.0498713E 00,
    X  2.1924184E 00, 1.6714572E 00, 1.3414002E 00, 1.1094536E 00,
    X  9.2251699E-01, 7.5004946E-01, 5.7434795E-01, 3.8693526E-01,
    X  1.8883077E-01,-5.7482944E-03,-1.6260227E-01,-2.1437072E-01/
      DATA (PHIE(I,8),I=1,16) /
    X  7.7825151E 00, 6.2050645E 00, 4.4257809E 00, 3.0686405E 00,
    X  2.2005451E 00, 1.6693188E 00, 1.3279763E 00, 1.0828244E 00,
    X  8.8051084E-01, 6.9090784E-01, 4.9793726E-01, 2.9639413E-01,
```

```
X    9.3011528E-02,-8.9567332E-02,-2.0731013E-01,-1.8873808E-01/
     DATA (PHIE(I,9),I=1,16) /
X    7.7911294E 00, 6.2116436E 00, 4.4292436E 00, 3.0680971E 00,
X    2.1947894E 00, 1.6566341E 00, 1.3061865E 00, 1.0495811E 00,
X    8.3368208E-01, 6.2933819E-01, 4.2257012E-01, 2.1203974E-01,
X    1.0476530E-02,-1.5183715E-01,-2.2462693E-01,-1.4284310E-01/
     DATA (PHIE(I,10),I=1,16)/
X    7.7642740E 00, 6.1899512E 00, 4.4125513E 00, 3.0535967E 00,
X    2.1790699E 00, 1.6364862E 00, 1.2786785E 00, 1.0121220E 00,
X    7.8433491E-01, 5.6749697E-01, 3.5022023E-01, 1.3531663E-01,
X   -5.8523466E-02,-1.9467029E-01,-2.2075655E-01,-8.7810394E-02/
     DATA (PHIE(I,11),I=1,16)/
X    7.6434708E 00, 6.0930868E 00, 4.3410871E 00, 2.9983644E 00,
X    2.1291620E 00, 1.5827783E 00, 1.2140260E 00, 9.3115355E-01,
X    6.8386576E-01, 4.4804141E-01, 2.1825852E-01, 6.1909385E-03,
X   -1.5887173E-01,-2.3274620E-01,-1.7163904E-01, 1.9563910E-02/
     DATA (PHIE(I,12),I=1,16)/
X    7.4731563E 00, 5.9567727E 00, 4.2416162E 00, 2.9240188E 00,
X    2.0661281E 00, 1.5200976E 00, 1.1438888E 00, 8.4844493E-01,
X    5.8660410E-01, 3.3871947E-01, 1.0596636E-01,-9.1384568E-02,
X   -2.1625603E-01,-2.2475229E-01,-9.6439019E-02, 9.6178116E-02/
     DATA (PHIE(I,13),I=1,16)/
X    7.2820252E 00, 5.8038845E 00, 4.1304622E 00, 2.8418943E 00,
X    1.9981463E 00, 1.4547305E 00, 1.0733061E 00, 7.6809795E-01,
X    4.9560481E-01, 2.4121691E-01, 1.2942379E-02,-1.6139657E-01,
X   -2.4048723E-01,-1.8853069E-01,-1.8848494E-02, 1.3188462E-01/
     DATA (PHIE(I,14),I=1,16)/
X    7.0857304E 00, 5.6469232E 00, 4.0165240E 00, 2.7581601E 00,
X    1.9296020E 00, 1.3899392E 00, 1.0047934E 00, 6.9197905E-01,
X    4.1203578E-01, 1.5569997E-01,-6.2372087E-02,-2.0825391E-01,
X   -2.4029033E-01,-1.3756524E-01, 4.7572997E-02, 1.3094899E-01/
     DATA (PHIE(I,15),I=1,16)/
X    6.8920894E 00, 5.4921012E 00, 3.9042327E 00, 2.6758601E 00,
X    1.8626387E 00, 1.3272684E 00, 9.3944168E-01, 6.2074463E-01,
X    3.3599364E-01, 8.1402812E-02,-1.2212379E-01,-2.3628410E-01,
X   -2.2296661E-01,-8.1467183E-02, 9.6508344E-02, 1.0376157E-01/
     DATA (PHIE(I,16),I=1,16)/
X    6.5278707E 00, 5.2009052E 00, 3.6931159E 00, 2.5213594E 00,
X    1.7373784E 00, 1.2109202E 00, 8.1972167E-01, 4.9319232E-01,
X    2.0511119E-01,-3.7516189E-02,-2.0316288E-01,-2.5046449E-01,
X   -1.5882254E-02, 2.2578783E-01, 1.3807746E-01, 1.5643788E-02/
     DATA (PHIE(I,17),I=1,16)/
X    6.2026926E 00, 4.9409298E 00, 3.5046080E 00, 2.3833483E 00,
X    1.6255270E 00, 1.1073863E 00, 7.1442955E-01, 3.8396367E-01,
X    9.8888059E-02,-1.2367843E-01,-2.4485941E-01,-2.2779325E-01,
X   -8.0233241E-02, 9.6481811E-02, 1.1923297E-01,-6.1574749E-02/
     DATA (PHIE(I,18),I=1,16)/
X    5.9152099E 00, 4.7110585E 00, 3.3378411E 00, 2.2610743E 00,
X    1.5262189E 00, 1.0155016E 00, 6.2182919E-01, 2.9035595E-01,
X    1.2956005E-02,-1.8419982E-01,-2.5855632E-01,-1.8467768E-01,
X   -5.3348309E-03, 1.3412824E-01, 6.6776811E-02,-9.5735236E-02/
     DATA (PHIE(I,19),I=1,16)/
X    5.6619949E 00, 4.5085585E 00, 3.1908127E 00, 2.1530120E 00,
X    1.4381056E 00, 9.3383125E-01, 5.4012859E-01, 2.0989960E-01,
X   -5.6291007E-02,-2.2467278E-01,-2.5265267E-01,-1.3214536E-01,
X    5.6601120E-02, 1.3949292E-01, 5.4031788E-03,-8.5808401E-02/
     DATA (PHIE(I,20),I=1,16)/
X    5.4388706E 00, 4.3300959E 00, 3.0610896E 00, 2.0573637E 00,
X    1.3597017E 00, 8.6092577E-01, 4.6768314E-01, 1.4047536E-01,
X   -1.1182839E-01,-2.4946070E-01,-2.3340606E-01,-7.5502751E-02,
X    1.0176888E-01, 1.2067658E-01,-4.7586630E-02,-4.7041320E-02/
```

```
      DATA (PHIE(I,21),I=1,16)/
X   4.9812464E 00, 3.9639451E 00, 2.7944432E 00, 1.8596419E 00,
X   1.1961477E 00, 7.0814599E-01, 3.1798920E-01, 4.4852823F-03,
X  -2.0512058E-01,-2.6340950E-01,-1.5447412E-01, 4.1942628F-02,
X   1.4244519E-01, 2.4282754E-02,-9.7359602E-02, 5.8126268F-02/
      DATA (PHIE(I,22),I=1,16)/
X   4.6291256E 00, 3.6820439E 00, 2.5884672E 00, 1.7054460F 00,
X   1.0667176E 00, 5.8644680E-01, 2.0161769E-01,-9.1801945E-02,
X  -2.5219038E-01,-2.3515466E-01,-6.3604831E-02, 1.1623861E-01,
X   1.0773122E-01,-6.3757272E-02,-4.5795995F-02, 6.3191209E-02/
      DATA (PHIE(I,23),I=1,16)/
X   4.3496352E 00, 3.4581528E 00, 2.4242675E 00, 1.5812511E 00,
X   9.6089125E-01, 4.8649265E-01, 1.0892579E-01,-1.5996989F-01,
X  -2.6867660E-01,-1.8574782E-01, 1.7574289E-02, 1.4320736E-01,
X   3.9838341E-02,-9.8261613E-02, 3.0707759E-02,-4.3618764E-03/
      DATA (PHIE(I,24),I=1,16)/
X   4.1214113E 00, 3.2751993E 00, 2.2895804E 00, 1.4782978E 00,
X   8.7192053E-01, 4.0236065E-01, 3.3831919E-02,-2.0739187E-01,
X  -2.6459717E-01,-1.2788131E-01, 7.9816729E-02, 1.3279228E-01,
X  -2.7910435E-02,-8.0293772E-02, 7.2664366E-02,-5.6042109E-02/
      DATA(ZLP(I)   ,I=1,16)/8.7649410E-02, 4.6269633E-01, 1.1410578,
1 2.1292836, 3.4370866, 5.0780186, 7.0703385, 9.4383143,
2 1.2214223E+01, 1.5441527E+01, 1.9180157E+01, 2.3515906E+01,
3 2.8578730E+01, 3.4583399E+01, 4.1940453E+01, 5.1701160E+01 /
      DATA(WTE(I)   ,I=1,16)/2.2503631E-01, 5.2583605E-01,
1 8.3196139E-01, 1.1460992,  1.4717513, 1.8131347, 2.1755175,
2 2.5657627, 2.9932151, 3.4712345, 4.0200441, 4.6725166,
3 5.4874207, 6.5853612, 8.2763580, 1.1824278E+01/
      DATA(ECMSTD(I), I=1,25)/0.0,0.050,0.100,0.150,0.200,0.250,0.300,
10.350,0.400,0.450,0.500,0.600,0.700,0.800,0.900,1.000,1.200,1.400,
21.600,1.800,2.000,2.500,3.000,3.500,4.000/
      END
$IBF13 PHI     DECK
      BLOCK DATA
C
C     N-N SCATTERING WAVE FUNCTION
C     TO BE USED IN SUPER PROGRAM
C
      COMMON/KINBLK/JSTD(25),ECMSTD(25)
      COMMON / PHII / PHIE(16,24),ZLP(16),WTE(16)
      DATA (PHIE(I,1),I=1,16) /
X   2.0156979E 01, 1.5958350E 01, 1.1220627E 01, 7.6011437E 00,
X   5.2804517E 00, 3.8654487E 00, 2.9819131E 00, 2.3974013E 00,
X   1.9842147E 00, 1.6722098E 00, 1.4208510E 00, 1.2049416F 00,
X   1.0072946E 00, 8.1462530E-01, 6.1424273E-01, 3.8726351E-01/
      DATA (PHIE(I,2),I=1,16) /
X   1.7454110E 01, 1.3817880E 01, 9.7129056E 00, 6.5732975E 00,
X   4.5547448E 00, 3.3162676E 00, 2.5333246E 00, 2.0042370E 00,
X   1.6180267E 00, 1.3136628E 00, 1.0559528E 00, 8.2347488E-01,
X   6.0270514E-01, 3.8535491E-01, 1.6750090E-01,-4.9924797E-02/
      DATA (PHIE(I,3),I=1,16) /
X   1.5618549E 01, 1.2364158E 01, 8.6886077E 00, 5.8742977E 00,
X   4.0599603E 00, 2.9399964E 00, 2.2236363E 00, 1.7302181E 00,
X   1.3604608E 00, 1.0600659E 00, 7.9845253E-01, 5.5837508E-01,
X   3.3137110E-01, 1.1655576E-01,-7.7829431E-02,-2.2721300E-01/
      DATA (PHIE(I,4),I=1,16) /
X   1.4268344E 01, 1.1294782E 01, 7.9348941E 00, 5.3594361E 00,
X   3.6945983E 00, 2.6608073E 00, 1.9921916E 00, 1.5237041E 00,
X   1.1649727E 00, 8.6719178E-01, 6.0405545E-01, 3.6274341E-01,
X   1.4044017E-01,-5.5844773E-02,-2.0652283E-01,-2.6995416E-01/
      DATA (PHIE(I,5),I=1,16) /
```

```
X    1.3221937E 01,  1.0465897E 01,  7.3505529E 00,  4.9598554E 00,
X    3.4103287E 00,  2.4425536E 00,  1.8100307E 00,  1.3599666E 00,
X    1.0091664E 00,  7.1360667E-01,  4.5106983E-01,  2.1326622E-01,
X    3.1038337E-03,-1.6510652E-01,-2.6331295E-01,-2.4309561E-01/
     DATA (PHIE(I,6),I=1,16)  /
X    1.2380447E 01,  9.7993907E 00,  6.8805002E 00,  4.6380985E 00,
X    3.1808434E 00,  2.2655513E 00,  1.6613405E 00,  1.2254401E 00,
X    8.8070772E-01,  5.8741980E-01,  3.2733054E-01,  9.6665369E-02,
X   -9.6208302E-02,-2.3091077E-01,-2.7475591E-01,-1.8329650E-01/
     DATA (PHIE(I,7),I=1,16)  /
X    1.1684866E 01,  9.2484388E 00,  6.4918277E 00,  4.3717728E 00,
X    2.9904222E 00,  2.1180165E 00,  1.5366548E 00,  1.1119785E 00,
X    7.7214549E-01,  4.8139316E-01,  2.2534867E-01,  4.6381691E-03,
X   -1.6741042E-01,-2.6595148E-01,-2.5778786E-01,-1.1200108E-01/
     DATA (PHIE(I,8),I=1,16)  /
X    1.1097626E 01,  8.7832220E 00,  6.1635495E 00,  4.1465994E 00,
X    2.8290133E 00,  1.9924054E 00,  1.4298794E 00,  1.0143476E 00,
X    6.7866330E-01,  3.9081173E-01,  1.4018901E-01,-6.8372229E-02,
X   -2.1724527E-01,-2.7891564E-01,-2.2369539E-01,-4.1744050E-02/
     DATA (PHIE(I,9),I=1,16)  /
X    1.0593262E 01,  8.3836849E 00,  5.8815225E 00,  3.9529430E 00,
X    2.6898677E 00,  1.8836425E 00,  1.3369303E 00,  9.2899661E-01,
X    5.9698270E-01,  3.1244016E-01,  6.8424919E-02,-1.2628266E-01,
X   -2.5052961E-01,-2.7600258E-01,-1.8019463E-01,  2.0432917E-02/
     DATA (PHIE(I,10),I=1,16)/
X    1.0154210E 01,  8.0357579E 00,  5.6358532E 00,  3.7840868E 00,
X    2.5682217E 00,  1.7881575E 00,  1.2549078E 00,  8.5341806E-01,
X    5.2477816E-01,  2.4396468E-01,  7.5764671E-03,-1.7196864E-01,
X   -2.7083586E-01,-2.6177050E-01,-1.3262224E-01,  7.0971951E-02/
     DATA (PHIE(I,11),I=1,16)/
X    9.4232554E 00,  7.4566599E 00,  5.2267724E 00,  3.5024512E 00,
X    2.3645995E 00,  1.6273534E 00,  1.1158084E 00,  7.2473694E-01,
X    4.0239917E-01,  1.3027115E-01,-8.8366681E-02,-2.3490618E-01,
X   -2.8282765E-01,-2.1222843E-01,-3.8849173E-02,  1.3323881E-01/
     DATA (PHIE(I,12),I=1,16)/
X    8.8358625E 00,  6.9912066E 00,  4.8977606E 00,  3.2754633E 00,
X    2.1996839E 00,  1.4960582E 00,  1.0012720E 00,  6.1840459E-01,
X    3.0221208E-01,  4.0279488E-02,-1.5805322E-01,-2.6960932E-01,
X   -2.6879215E-01,-1.4910752E-01,  4.0338618E-02,  1.4833017E-01/
     DATA (PHIE(I,13),I=1,16)/
X    8.3506911E 00,  6.6067176E 00,  4.6258071E 00,  3.0874348E 00,
X    2.0623978E 00,  1.3859302E 00,  9.0446807E-01,  5.2841399E-01,
X    2.1850505E-01,-3.1910645E-02,-2.0813645E-01,-2.8417038E-01,
X   -2.3878987E-01,-8.3579870E-02,  9.8156334E-02,  1.2851201E-01/
     DATA (PHIE(I,14),I=1,16)/
X    7.9413612E 00,  6.2822931E 00,  4.3961841E 00,  2.9283251E 00,
X    1.9456642E 00,  1.2915949E 00,  8.2101142E-01,  4.5087072E-01,
X    1.4752871E-01,-9.0242761E-02,-2.4315977E-01,-2.8418255E-01,
X   -1.9960374E-01,-2.2247222E-02,  1.3351040E-01,  8.7756399E-02/
     DATA (PHIE(I,15),I=1,16)/
X    7.5901158E 00,  6.0038765E 00,  4.1989924E 00,  2.7913945E 00,
X    1.8447083E 00,  1.2094422E 00,  7.4792421E-01,  3.8311445E-01,
X    8.6691606E-02,-1.3749218E-01,-2.6638292E-01,-2.7367747E-01,
X   -1.5591952E-01,  3.1167263E-02,  1.4833626E-01,  3.8465072E-02/
     DATA (PHIE(I,16),I=1,16)/
X    7.0155558E 00,  5.5483671E 00,  3.8760571E 00,  2.5664064E 00,
X    1.6776773E 00,  1.0721786E 00,  6.2501284E-01,  2.6989663E-01,
X   -1.1555007E-02,-2.0639018E-01,-2.8658522E-01,-2.3237536E-01,
X   -6.7148384E-02,  1.0804966E-01,  1.3060532E-01,-5.0526582E-02/
     DATA (PHIE(I,17),I=1,16)/
X    6.5623023E 00,  5.1889544E 00,  3.6208954E 00,  2.3878414E 00,
```

```
      X   1.5438468E 00,  9.6085597E-01,  5.2468864E-01,  1.7872710F-01,
      X  -8.6301186E-02,-2.4982520E-01,-2.8235200E-01,-1.7670251E-01,
      X   1.1686209E-02,  1.4454423E-01,  7.5799712E-02,-9.6889095F-02/
          DATA (PHIE(I,18),I=1,16)/
      X   6.1932871E 00,  4.8962590E 00,  3.4128058E 00,  2.2415470F 00,
      X   1.4331855E 00,  8.6777850E-01,  4.4052179E-01,  1.0365362F-01,
      X  -1.4366008E-01,-2.7483490E-01,-2.6233916E-01,-1.1654364E-01,
      X   7.3608495E-02,  1.4705725E-01,  1.0878918E-02,-9.5185167F-02/
          DATA (PHIE(I,19),I=1,16)/
      X   5.8855215E 00,  4.6520969E 00,  3.2389684E 00,  2.1187682E 00,
      X   1.3394697E 00,  7.8816255E-01,  3.6846285E-01,  4.0891858E-02,
      X  -1.8764798E-01,-2.8617275E-01,-2.3238440E-01,-5.7948658E-02,
      X   1.1653513E-01,  1.2504467E-01,-4.5659324E-02,-5.9544864E-02/
          DATA (PHIE(I,20),I=1,16)/
      X   5.6239505E 00,  4.4445248E 00,  3.0909603E 00,  2.0137495F 00,
      X   1.2586020E 00,  7.1883667E-01,  3.0581237E-01,-1.2141468E-02,
      X  -2.2106297E-01,-2.8722472E-01,-1.9657321E-01,-4.5611103E-03,
      X   1.4111755E-01,  8.8125011E-02,-8.3833094E-02,-1.0054161E-02/
          DATA (PHIE(I,21),I=1,16)/
      X   5.1110989E 00,  4.0373678E 00,  2.7998780E 00,  1.8055612E 00,
      X   1.0959361E 00,  5.7761893E-01,  1.7919287E-01,-1.1305050E-01,
      X  -2.7054477E-01,-2.5989329E-01,-9.8673761E-02,  9.5092651E-02,
      X   1.3787187E-01,-1.8573555E-02,-8.9603107E-02,  7.3988978E-02/
          DATA (PHIE(I,22),I=1,16)/
      X   4.7314891E 00,  3.7357853E 00,  2.5834154E 00,  1.6488794E 00,
      X   9.7099260E-01,  4.6759242E-01,  8.2598666E-02,-1.8162550E-01,
      X  -2.8639710E-01,-2.0839097E-01,-7.9184964E-03,  1.4264533E-01,
      X   7.9064842E-02,-8.8166375E-02,-1.7587427E-02,  4.7128630E-02/
          DATA (PHIE(I,23),I=1,16)/
      X   4.4364982E 00,  3.5012551E 00,  2.4143852E 00,  1.5250366E 00,
      X   8.7035609E-01,  3.7816533E-01,  6.5594895F-03,-2.2775592E-01,
      X  -2.8057897E-01,-1.4726503E-01,  6.3958763E-02,  1.4610277E-01,
      X   5.4731333E-03,-9.8665496F-02,  5.2619813F-02,-2.5396720E-02/
          DATA (PHIE(I,24),I=1,16)/
      X   4.1991024E 00,  3.3123799E 00,  2.2776645E 00,  1.4236476E 00,
      X   7.8651439E-01,  3.0333852E-01,-5.4438218E-02,-2.5747647E-01,
      X  -2.6064722E-01,-8.5114082E-02,  1.1326630E-01,  1.1895849E-01,
      X  -5.5911444E-02,-6.3871624F-02,  7.6674433E-02,-6.1550766E-02/
          DATA(ZLP(I)    ,I=1,16)/8.7649410E-02,  4.6269633E-01,  1.1410578,
     1 2.1292836,  3.4370866,  5.0780186,  7.0703385,  9.4383143,
     2 1.2214223E+01,  1.5441527E+01,  1.9180157E+01,  2.3515906E+01,
     3 2.8578730E+01,  3.4583399E+01,  4.1940453E+01,  5.1701160E+01 /
          DATA(WTE(I)    ,I=1,16)/2.2503631E-01,  5.2583605E-01,
     1 8.3196139E-01,  1.1460992,  1.4717513,  1.8131347,  2.1755175,
     2 2.5657627,  2.9932151,  3.4712345,  4.0200441,  4.6725166,
     3 5.4874207,  6.5853612,  8.2763580,  1.1824278E+01 /
          DATA(ECMSTD(I), I=1,25)/0.0,0.050,0.100,0.150,0.200,0.250,0.300,
     10.350,0.400,0.450,0.500,0.600,0.700,0.800,0.900,1.000,1.200,1.400,
     21.600,1.800,2.000,2.500,3.000,3.500,4.000/
          END
$IBF13 KINMAT   DECK
          SUBROUTINE KINMAT
C
C       CALCULATES KINEMATICS AND CALLS FOR MATRIX ELEMENTS
C       CAN INCLUDE PLANE WAVES IN A NUCLEAR MEDIA
C       TO BE USED IN SUPER PROGRAM
C
          COMMON/MAIN/KTHRY,KOMNRM,NFIT,KOUT,ISAVE,SAVE
          COMMON/NORM/SNORM,SIGNRM(1000),SMAX,ENORM,SIGMAX
          COMMON/FOOL/E3INT(1000),SIGINT(1000),SIGFLD(1000),GA(50),INTMAX,
     1DE3,RES,SGFM,IGMAX
```

```
      COMMON/IN/M1,M2,M3,M5,M6,Z3,Z5,Z6
      COMMON/ALG/DTHETA,THCMIN,CTHETA(25)
      COMMON/LBL/WTLBL(13),PTLBL(13),PNLBL(13),XMIN,XMAX,YMIN,YMAX,TT(2)
     1,TT1(2),AA(14),TTT,EXE3(25),EXD(25),EXVD(25),DATAMX,NE3MAX
      COMMON/KIN/NE1,QVAL,E1(8),NTHETA,THETA3(8),THR(8),NECM,ECM(25),DEC
     1M,ECMIN,Z56,AKI2,AKF2,CKK,AKCM(25),INDEX,LFIT,SIG(25),SQRMAT,F3(25
     2),LOCKCM,INECM,JECM(25)
      COMMON/KINBLK/JSTD(25),ECMSTD(25)
      REAL M1,M2,M3,M4,M5,M6,M34,M41,M2M,M3M,M4M
C
C     READ IN CONTROL CARD
C
      READ(5,1)KTHRY,KOMNRM,NFIT,KOUT
    1 FORMAT(4I2)
      LFIT=1
      NCAL=NFIT
C
C     READ IN MEDIA POTENTIAL
C
      READ(5,70)VMEDIA
   70 FORMAT(F10.0)
C
C     READ IN KINEMATICS VARIABLES
C
      READ(5,2)NE1,QVAL,(E1(I),I=1,NE1)
    2 FORMAT(I2,8X,7F10.0)
      READ(5,2)NTHETA,(THETA3(I),I=1,7)
      IF(NTHETA .LE. 0)GO TO 12
      ITHFG=1
      DTHETA=THETA3(1)
      THCMIN=THETA3(2)
      DO 13 I=1,NTHETA
   13 CTHETA(I)=0.0174533*(THCMIN+FLOAT(I-1)*DTHETA)
      GO TO 14
   12 NTHETA = 1
      DO 16 I=1,7
      THR(I)=0.0174533*THETA3(I)
      IF(THETA3(I+1) .LT. 0.001) GO TO 14
      NTHETA=NTHETA+1
   16 CONTINUE
C
C     SELECT THE STANDARD VALUES OF ECM THAT ARE TO BE CALCULATED
C
   14 READ(5,11)NECM,(JSTD(I),I=1,NECM)
   11 FORMAT(8(I2,8X))
      IF(NECM .LE. 0) NECM=25
      DO 19 I=1,NECM
      J=JSTD(I)
      IF(NECM .EQ. 25) J=I
      ECM(I)=ECMSTD(J)
      JECM(I)=J
   19 CONTINUE
    7 IF(ITHFG .EQ. 1) CALL ANG
      DO 1000 N=1,NE1
      DO 1001 M=1,NTHETA
      LOCKCM=N+M
C
C     READ IN COMMENT CARD    WTLBL
C
      READ(5,10)WTLBL
   10 FORMAT(13A6)
```

```
      READ(5,25)DE3,RES,IGMAX
   25 FORMAT(2F10.0,I2)
      READ(5,22) ENORM,SNORM
   22 FORMAT(2F10.0)
      IF(KOUT .LE. 0) GO TO 23
      IF(KOUT .EQ. 1) GO TO 20
      READ(5,10)PNLBL
      IF(KOUT .EQ. 2) GO TO 9
   20 READ(5,10)PTLBL
      READ(5,21) XMIN,XMAX,YMIN,YMAX
   21 FORMAT(4F10.0)
      GO TO 9
   23 DATAMX=0.0
      IE3=1
    8 READ(5,3) EXE3(IE3),EXD(IE3),EXVD(IE3)
    3 FORMAT(3F10.0)
      IF(EXE3(IE3) .EQ. 0.0) GO TO 9
      IF(EXD(IE3) .GT. DATAMX) DATAMX=EXD(IE3)
      NE3MAX=IE3
      IE3=IE3+1
      GO TO 8
C
C     WRITE OUT KINEMATICS VARIABLES
C
    9 WRITE(6,4)WTLBL
    4 FORMAT(1H1,30X45HDINUCLEON FINAL STATE INTERACTION CALCULATION////
     1,20X13A6///)
      WRITE(6,5)M1,M2,M3,M5,M6,Z3,Z5,Z6
    5 FORMAT(4X5H M1 =F10.6,5X4HM2 =F10.6,5X4HM3 =F10.6,5X4HM5 =F10.6,5X
     14HM6 =F10.6//,15X4HZ3 =F5.1,15X4HZ5 =F5.1,15X4HZ6 =F5.1//)
      WRITE(6,6)E1(N),QVAL,THETA3(M)
    6 FORMAT(20X10H E1(MEV) =F6.3,10X14HQ-VALUE(MEV) =F8.3,10X12HTHETA(D
     1EG) =F6.1///)
      WRITE(6,60)VMEDIA
   60 FORMAT(10X34HPOTENTIAL DEPTH OF NUCLEAR MEDIA =F10.6///)
C
C     CALCULATE  RAW,UNNORMALIZED XSECTION--SIG
C
      M4=M5+M6
      M34=M3+M4
      M41=M4-M1
      M2M=M2/M34
      M3M=M3/M34
      M4M=M4/M34
      Z56=Z5*Z6
      P1=2.0*M1*E1(N)
      VUM=2.0*M1*M2M*VMEDIA
      PK=M2M*M2M*P1
      PJ=M3M*M3M*P1
      AKI2=0.0239231*(PK+VUM)
      CTHR=COS(THR(M))
      V=SQRT(M1*M3*E1(N))*CTHR/M34
      EMAX=M4M*QVAL+M41*E1(N)/M34
      NF=0
  100 WRITE(6,101)
  101 FORMAT(1H0,25X26HMATRIX ELEMENT CALCULATION//)
      SIGMAX=0.0
C
C     PUNCH CALCULATION LABEL
C
      PUNCH 75, M1,M2,M3,M5,M6,Z3,Z5,Z6
```

```
    75 FORMAT(8F10.6)
       PUNCH 76, E1(N),QVAL,THETA3(M),VMEDIA
    76 FORMAT(4F10.6)
       INDEX=1
       DO 15 I=1,NECM
       IF(ECM(I) .LT. 0.0) GO TO 50
       U=EMAX-M4M*ECM(I)
       T=V*V+U
       IF(T .LT. 0.0) GO TO 51
       SRE3    =V+SQRT(T)
    31 E3(I)=SRE3*SRE3
       IF(ECM(I) .EQ. 0.0) GO TO 50
       P3=2.0*M3*E3(I)
       W=4.0*M3*V*SRE3
       AKF2=0.0239231*(PJ+P3-W)
       CKK=-0.0239231*SQRT((PK+VUM)*(PJ+P3*CTHR*CTHR-W))
       IF(M1 .GT. M2)CKK=-CKK
       AKCM(I)=0.10985*SQRT(2.0*ECM(I))
       INECM=I
       IF(KTHRY .EQ.1)CALL WATMIG
       IF(KTHRY .EQ. 2) CALL PWBAXT
       SIG(I)=SRE3*AKCM(I)*SQRMAT/SQRT(E1(N))
       INDEX=INDEX+1
       IF(SIGMAX .LT. SIG(I)) SIGMAX=SIG(I)
       GO TO 15
    51 WRITE(6,52)
    52 FORMAT(1H ,10X,42HTHE REACTION IS NOT ENERGETICALLY POSSIBLE//)
    50 SIG(I)=0.0
    15 CONTINUE
       CALL FOLD
       CALL NORMLZ
       CALL OUTPUT
       IF(KOMNRM .EQ. 1) GO TO 55
    56 NF=NF+1
       IF(NCAL .GT. NF) GO TO 100
       GO TO 1001
    55 IF(ISAVE .EQ. 2) GO TO 56
       SAVE=SNORM/SIGMAX
       ISAVE=2
       GO TO 56
  1001 CONTINUE
  1000 CONTINUE
       RETURN
       END
$IBF13 ANGLE    DECK
       SUBROUTINE ANG
C
C      DUMMY SUBROUTINE THAT HAS NO FUNCTION
C      THIS SUBROUTINE WAS INTENDED TO GENERATE ANGULAR DISTRIBUTIONS
C
       RETURN
        END
$IBF13 WATMIG   DECK
       SUBROUTINE WATMIG
C
C      WATSON-MIGDAL A LA TOMBRELLO AND BACHER
C      L3 IS A DUMMY VARIABLE--NOT USED
C      TO BE USED IN SUPER PROGRAM
C
       COMMON/KIN/NE1,QVAL,E1(8),NTHETA,THETA3(8),THR(8),NECM,ECM(25),DEC
      1M,ECMIN,Z56,AKI2,AKF2,CKK,AKCM(25),INDEX,LFIT,SIG(25),SQRMAT,E3(25
```

```
      2),LOCKCM,INECM,JECM(25)
        IF(INDEX .GT. 1) GO TO 100
      3 READ(5,4)SCATLN,RO,SP,R,L3,PARAM
      4 FORMAT(4F10.0,I2,8X4A6)
        WRITE(6,10) PARAM
     10 FORMAT(20X 4A6//)
        WRITE(6,11)SCATLN,RO,SP,R,L3
     11 FORMAT(17X 20H SCATTERING LENGTH =F7.3//,20X 17HEFFECTIVE RANGE =
       1F7.3//,20X 17HSHAPE PARAMETER =F7.3//,29X 8HRADIUS =F7.3//,33X
       24HL3 =I3///)
    100 SQRMAT=DN(ECM(INECM),Z56,SCATLN,RO,SP,R)/AKCM(INECM)
        RETURN
        END
$IBF13 DEZ      DECK
        FUNCTION DN(E,Z,SCATLN,RO,SP,R)
C
C       TO BE USED IN SUPER PROGRAM
C
        IF(E .EQ. 0.0) GO TO 2
        AK=0.10985*SQRT(2.0*E)
        IF(Z .EQ. 1.0) GO TO 1
        FN=-1.0/SCATLN + 0.5*RO*AK*AK
        DN=AK/(FN*FN+AK*AK)
        RETURN
      2 DN=0.0
        RETURN
      1 ETA=0.15805/SQRT(2.0*E)
        C=6.28318*ETA/(EXP(6.28318*ETA)-1.0)
        FN=-1.0/SCATLN+0.5*RO*AK*AK-SP*AK*((RO*AK)**3)-H(ETA)/R
        DN= AK/(FN*FN+C*C*AK*AK)*C
        RETURN
        END
$IBFTC HOT       DECK
        FUNCTION H(ETA)
C
C       TO BE USED IN SUPER PROGRAM
C
        IF(ETA .EQ. 0.0) GO TO 3
        ET=ETA*ETA
        TUM=-0.57721566-ALOG(ETA)
        AN=0.0
        TEMP=0.0
      1 AN=AN+1.0
        SUM=TEMP
        TERM=1.0/(AN*(AN*AN+ET))
        TEMP=SUM+TERM
        IF(SUM-TEMP .GT. 1.0E-8) GO TO 1
      2 H=ET*SUM+TUM
        RETURN
      3 H=0.0
        RETURN
        END
$IBF13 PWBA      DECK
        SUBROUTINE PWBAXT
C
C       CALCULATES ALL TERMS WITH A FINITE RANGE INTERACTION
C       3HE(D,T)2P VERSION
C       SINGLE GAUSSIAN 3-BODY WAVE FUNCTION
C       TO BE USED IN SUPER PROGRAM
C
        COMMON/KIN/NE1,QVAL,E1(8),NTHETA,THETA3(8),THR(8),NECM,ECM(25),DEC
```

```
    1M,ECMIN,Z56,AKI2,AKF2,CKK,AKCM(25),INDEX,LFIT,SIG(25),SQRMAT,F3(25
    2),LOCKCM,INECM,JECM(25)
     COMMON/PWB/
    1GI2(4),GI4(4),GF2(4), GF4(4),A2(4),A4(4),CH(4),CT(4),CD(4),G1(7,4,
    24),G2(7,4,4),G3(7,4,4,4),G4(7,4,4,4),GB(4),GB2(4),GGG(4,4),GA(4,4)
    3,GAG(4,4),GBA(4,4),D(7,4,4),DD(1,4,4,4),DA(6,4,4,4),DB(6,4,4,4),Q1
    4(7),Q2(7,4,4),Q3(7,4,4),P(7,4,4,4),CO(7),IWRITE(15),C(4,4,4)
     COMMON/CLINT/ZT2(5),  ZT24(5),   ZT44(5),  GC1(3,4,4),GC2(3,5,4,4),
    1GC3(3,5,4,4,4),DC(3,4,4),QC1(3),QC2(3,4,4),QC3(3,4,4),GAGC(3,5,4,4
    2),GC4(3,5,4,4,4),DDC(1,5,4,4,4),DAC(3,5,4,4,4),DBC(3,5,4,4,4),
    3PC(3,5,4,4,4),CCO(3),CC(5,4,4,4),VOC(5)
     COMMON/MATS/ZMAT(10)
     DATA (ZT2(I),VOC(I),I=1,4)/5.8174E-04, 8.5499E-02, 8.1899E-03,
    11.3780E-01, 4.7414E-02, 3.2466E-01, 2.8663E-01, 7.5095F-01/
     DATA VWS,VBS,VMS,VHS,VWY,VBY,VMY,VHY/0.4075,0.0925,0.4075,0.0925,
    1-0.14833,0.48167,+0.96334,-0.29666/
     QFUN(A,B)=0.33333334*SQRT((2.0*A+B)*(2.0*A+B)*AKF2+(3.0*A-B)*
    1(3.0*A-B)*AKI2+2.0*(2.0*A+B)*(3.0*A-B)*CKK)
     GFUN(G1,Q1,G2,Q2,G3,Q3)=1.0/(G1*G2*G3*SQRT(G1*G2*G3))*EXP(-0.25*(Q
    11*Q1/G1+Q2*Q2/G2+Q3*Q3/G3))
     KMX=1
     JMX=3
     IMX=1
     MMX=4
C
C     READ IN AND WRITE OUT PARAMETERS
C
     IF(INDEX .GT. 1) GO TO 100
     IF(IWRITE(15) .NE. 0) GO TO 100
     READ(5,5)(GI2(I),CH(I),I=1,IMX)
   5 FORMAT(8F10.0)
     READ(5,5)(GF2(K),CT(K), K=1,KMX)
     READ(5,5)(A2(J),CD(J),J=1,JMX)
     READ(5,4) B2,VOG,SERBER
   4 FORMAT(3F10.0)
     READ(5,507)IWRITE
 507 FORMAT(15I2)
     WRITE(6,11)B2,VOG,SERBER
  11 FORMAT(25X9HBETASQR =F9.5/,25X26HGAUSSIAN POTENTIAL DEPTH =F9.5/,
    125X24HSERBER-SYMETRIC MIXING =F9.5/)
     WRITE(6,12)(I,GI2(I),I,CH(I),I=1,IMX)
  12 FORMAT(25X19HHELIUM-3 PARAMETERS/,(30X4HGI2(I1,3H) =F9.5,5X3HCH(I1
    1,3H) =F9.5/))
     WRITE(6,13)(K,GF2(K),K,CT(K), K=1,KMX)
  13 FORMAT(25X17HTRITON PARAMETERS/,(30X4HGF2(I1,3H) =F9.5,5X3HCT(I1,
    13H) =F9.5/))
     WRITE(6,14)(J,A2(J),J,CD(J), J=1,JMX)
  14 FORMAT(25X19HDEUTERON PARAMETERS/,(30X3HA2(I1,3H) =F9.5,5X3HCD(I1,
    13H) =F9.5/))
     WRITE(6,515)(IWRITE(I), I=1,15)
 515 FORMAT(25X12HWRITE CODE =15I2/)
C
C     CALCULATE MOMENTUM TRANSFERS AND CONVIENT TERMS
C
     SYMT=1.0-SERBER
     B24=0.25*B2
     B44=B24*B2
     DO 21 I=1,IMX
     GI4(I)=GI2(I)*GI2(I)
  21 CONTINUE
     DO 22 J=1,JMX
```

```
    A4(J)=A2(J)*A2(J)
 22 CONTINUE
    DO 31 M=1,MMX
    ZT24(M)=0.25*ZT2(M)
    ZT44(M)=ZT24(M)*ZT2(M)
 31 CONTINUE
    DO 23 K=1,KMX
    GB(K)=GF2(K)+B2
    GB2(K)=GB(K)*GB(K)
    GF4(K)=GF2(K)*GF2(K)
    DO 24 I=1,IMX
    G1(1,K,I)=GF2(K)+GI2(I)
    G1(2,K,I)=GI2(I)
    G1(4,K,I)=G1(1,K,I)
    G1(5,K,I)=G1(1,K,I)+B2
    G1(6,K,I)=G1(1,K,I)
    G1(7,K,I)=G1(1,K,I)
    G2(4,K,I)=0.75*G1(1,K,I)
    G2(3,K,I)=G2(4,K,I)+B24
    G2(5,K,I)=G2(3,K,I)-B44/G1(5,K,I)
    G2(6,K,I)=G2(4,K,I)
    G2(7,K,I)=G2(4,K,I)
    GGG(K,I)=G1(5,K,I)*G1(5,K,I)*G2(5,K,I)
    D(1,K,I)=GF2(K)/G1(1,K,I)
    D(2,K,I)=0.0
    D(4,K,I)=4.0*GF2(K)/G1(4,K,I)
    D(5,K,I)=4.0*GB(K)/G1(5,K,I)-4.0*GI2(I)*B44/GGG(K,I)
    D(6,K,I)=D(4,K,I)
    GC1(1,K,I)=G1(1,K,I)
    GC1(3,K,I)=G1(4,K,I)
    QC2(1,K,I)=0.0
    QC2(2,K,I)=0.0
    QC2(3,K,I)=0.0
    DO 28 L=1,7
    Q2(L,K,I)=0.0
 28 CONTINUE
    DO 32 M=1,MMX
    GC2(2,M,K,I)=G2(4,K,I)+ZT24(M)
    GC2(3,M,K,I)=G2(4,K,I)
 32 CONTINUE
 24 CONTINUE
    DO 25 J=1,JMX
    G1(3,K,J)=GF2(K)+A2(J)
    GA(K,J)=0.75*GF2(K)+A2(J)
    G2(1,K,J)=GA(K,J)+B24
    G2(2,K,J)=G2(1,K,J)
    GAG(K,J)=GA(K,J)/G2(1,K,J)
    GBA(K,J)=GB(K)+A2(J)
    D(3,K,J)=4.0*G1(3,K,J)/GF2(K)
    GC1(2,K,J)=G1(3,K,J)
    DC(2,K,J)=D(3,K,J)
    DO 33 M=1,MMX
    GC2(1,M,K,J)=GA(K,J)+ZT24(M)
    GAGC(1,M,K,J)=GA(K,J)/GC2(1,M,K,J)
 33 CONTINUE
 25 CONTINUE
    DO 26 I=1,IMX
    DO 27 J=1,JMX
    C(K,J,I)=2169.6231366*VOG*CT(K)*CD(J)*CH(I)
    G3(1,K,J,I)=GB(K)-GF4(K)/G1(1,K,I)-B44/G2(1,K,J)
    G3(2,K,J,I)=GB(K)-B44/G2(2,K,J)
```

```
    G3(3,K,J,I)=GI2(I)+B2+A2(J)-B44/G2(3,K,I)-A4(J)/G1(3,K,J)
    G3(4,K,J,I)=G1(3,K,J)-GF4(I)/G1(4,K,I)
    G3(5,K,J,I)=GBA(K,J)-GB2(K)/G1(5,K,I)-B44*GI4(I)/GGG(K,I)
    G3(6,K,J,I)=GBA(K,J)-GF4(K)/G1(6,K,I)
    G3(7,K,J,I)=B2
    G4(2,K,J,I)=0.75*GI2(I)
    G4(1,K,J,I)=G4(2,K,J,I)+B24*GAG(K,J)-B44*GAG(K,J)*GAG(K,J)/G3(1,K,
   1J,I)
    G4(3,K,J,I)=GI2(I)-GI4(I)/G3(3,K,J,I)
    G4(4,K,J,I)=B2+A2(J)-A4(J)/G3(4,K,J,I)
    G4(5,K,J,I)=A2(J)-A4(J)/G3(5,K,J,I)
    G4(6,K,J,I)=A2(J)-A4(J)/G3(6,K,J,I)
    G4(7,K,J,I)=A2(J)
    DD(1,K,J,I)=0.5*B2*GA(K,J)/(G2(1,K,J)*G3(1,K,J,I))
    P(2,K,J,I)=1.0E-6
    DA(3,K,J,I)=1.0-GI2(I)*GF2(K)/(G1(3,K,J)*G3(3,K,J,I))
    DB(3,K,J,I)=1.0-4.0*GI2(I)/G3(3,K,J,I)
    DO 29 L=4,6
    DA(L,K,J,I)=A2(J)/G3(L,K,J,I)
    DB(L,K,J,I)=D(L,K,I)*DA(L,K,J,I)-3.0
 29 CONTINUE
    DO 34 M=1,MMX
    GC3(1,M,K,J,I)=GF2(K)-GF4(K)/GC1(1,K,I)+ZT2(M)   -ZT44(M)/GC2(1,M
   1,K,J)
    GC3(2,M,K,J,I)=GI2(I)+A2(J)-A4(J)/GC1(2,K,J)+ZT2(M)-ZT44(M)/GC2(2,
   1M,K,I)
    GC3(3,M,K,J,I)=G3(4,K,J,I)
    GC4(1,M,K,J,I)=G4(2,K,J,I)   +ZT24(M)*GAGC(1,M,K,J)-ZT44(M)*GAGC(1,
   1M,K,J)*GAGC(1,M,K,J)/GC3(1,M,K,J,I)
    GC4(2,M,K,J,I)=GI2(I)-GI4(I)/GC3(2,M,K,J,I)
    GC4(3,M,K,J,I)=A2(J)-A4(J)/GC3(3,M,K,J,I)+ZT2(M)
    DDC(1,M,K,J,I)=  2.0*ZT24(M)*GAGC(1,M,K,J)/GC3(1,M,K,J,I)
    DAC(2,M,K,J,I)=1.0-4.0*GI2(I)/(GC3(2,M,K,J,I)*DC(2,K,J))
    DBC(2,M,K,J,I)=1.0-4.0*GI2(I)/(GC3(2,M,K,J,I))
    CC(M,K,J,I)=2169.6231366*VOC(M)*CT(K)*CD(J)*CH(I)
 34 CONTINUE
 27 CONTINUE
 26 CONTINUE
 23 CONTINUE
100 QD=SQRT(0.444444*AKF2+AKI2+1.333333*CKK)
    Q2P= SQRT(AKF2+0.444444*AKI2+1.333333*CKK)
    QN=0.333333*SQRT(AKF2+AKI2-2.0*CKK)
    Q1(1)=QN
    Q1(2)=Q2P
    Q1(3)=0.5*QD
    Q1(4)=2.0*QN
    Q1(5)=Q1(4)
    Q1(6)=Q1(4)
    Q1(7)=Q1(4)
    QC1(1)=Q1(1)
    QC1(2)=Q1(3)
    QC1(3)=Q1(4)
    DO 40 K=1,KMX
    DO 41 J=1,JMX
    Q3(3,K,J)=2.0/D(3,K,J)*QFUN(1.0,D(3,K,J))
    QC3(2,K,J)=Q3(3,K,J)
 41 CONTINUE
    DO 42 I=1,IMX
    Q2(5,K,I)=B2/G1(5,K,I)*QN
    Q3(1,K,I)=QFUN(1.0,D(1,K,I))
    Q3(2,K,I)=QD
```

```
       Q3(4,K,I)=0.5*QFUN(1.0,D(4,K,I))
       Q3(5,K,I)=0.5*QFUN(1.0,D(5,K,I))
       Q3(6,K,I)=Q3(4,K,I)
       Q3(7,K,I)=3.0*QN
       QC3(1,K,I)=Q3(1,K,I)
       QC3(3,K,I)=Q3(4,K,I)
       DO 43 J=1,JMX
       P(1,K,J,I)=DD(1,K,J,I)*Q3(1,K,I)
       P(7,K,J,I)=1.5*QN
       DO 44 L=3,6
       P(L,K,J,I)=.5*QFUN(DA(L,K,J,I),DB(L,K,J,I))
   44 CONTINUE
       DO 35 M=1,MMX
       PC(1,M,K,J,I)=DDC(1,M,K,J,I)*QC3(1,K,I)
       PC(2,M,K,J,I)=0.5*QFUN(DAC(2,M,K,J,I),DBC(2,M,K,J,I))
       PC(3,M,K,J,I)=P(4,K,J,I)
   35 CONTINUE
   43 CONTINUE
   42 CONTINUE
   40 CONTINUE
       WRITE(6,98)ECM(INECM),QD,Q2P,QN
   98 FORMAT(25X26HMATRIX ELEMENT CALCULATION//,25X5HECM =F7.3/,25X4HQD
      1=F9.5/,25X5HQ2P =F9.5/,25X4HQN =F9.5/)
       DO 50 L=1,7
       CO(L)=0.0
   50 CONTINUE
       CCO(1)=0.0
       CCO(2)=0.0
       CCO(3)=0.0
       DO 51 K=1,KMX
       DO 52 J=1,JMX
       DO 53 I=1,IMX
       CO(1)=CO(1)+C(K,J,I)*GFUN(G1(1,K,I),Q1(1),G2(1,K,J),Q2(1,K,I),G3(1
      1,K,J,I),Q3(1,K,I))*S(1,K,J,I)
       CO(2)=CO(2)+C(K,J,I)*GFUN(G1(2,K,I),Q1(2),G2(2,K,J),Q2(2,K,I),G3(2
      1,K,J,I),Q3(2,K,I))*S(2,K,J,I)
       CO(3)=CO(3)+C(K,J,I)*GFUN(G1(3,K,J),Q1(3),G2(3,K,I),Q2(3,K,I),G3(3
      1,K,J,I),Q3(3,K,J))*S(3,K,J,I)
       DO 54 L=4,7
       CO(L)=CO(L)+C(K,J,I)*GFUN(G1(L,K,I),Q1(L),G2(L,K,I),Q2(L,K,I),G3(L
      1,K,J,I),Q3(L,K,I))*S(L,K,J,I)
   54 CONTINUE
C
C      CALCULATE COULOMB OVERLAPS CCO(N)
C
       DO 57 M=1,MMX
       CCO(1)=CCO(1)+CC(M,K,J,I)*GFUN(GC1(1,K,I),QC1(1),GC2(1,M,K,J),QC2(
      11,K,I),GC3(1,M,K,J,I),QC3(1,K,I))*SC(1,M,K,J,I)
       CCO(2)=CCO(2)+CC(M,K,J,I)*GFUN(GC1(2,K,J),QC1(2),GC2(2,M,K,I),QC2(
      12,K,I),GC3(2,M,K,J,I),QC3(2,K,J))*SC(2,M,K,J,I)
       CCO(3)=CCO(3)+CC(M,K,J,I)*GFUN(GC1(3,K,I),QC1(3),GC2(3,M,K,I),QC2(
      13,K,I),GC3(3,M,K,J,I),QC3(3,K,I))*SC(3,M,K,J,I)
   57 CONTINUE
   53 CONTINUE
   52 CONTINUE
   51 CONTINUE
C
C      CACULATE TERMS OF THE MATRIX ELEMENT
C
       ZMAT(1)=2.*((2.*VWS+VBS-VMS-VHS)*SERBER+(2.*VWY+VBY-VMY-VHY)*SYMT)
      1*CO(1)-2.0*CCO(1)
```

```
      ZMAT(2)=((2.*VWS-VBS+2.*VMS-VHS)*SERBER+(2.*VWY-VBY+2.*VMY-VHY)*SY
     1MT)*CO(2)
      ZMAT(3)=-2.*((VWS+VBS-2.*VMS-VHS)*SERBER+(VWY+VBY-2.0*VMY-VHY)*SYM
     1T)*CO(3)+CCO(2)
      ZMAT(4)=-((VWS-VBS+VMS-VHS)*SERBER+(VWY-VBY+VMY-VHY)*SYMT)*CO(4)
     1+CCO(3)
      ZMAT(5)=-2.*((VWS+VMS)*SERBER+(VWY+VMY)*SYMT)*CO(5)
      ZMAT(6)=-(VWS*SERBER+VWY*SYMT)*CO(6)
      ZMAT(7)=-(VMS*SERBER+VMY*SYMT)*CO(7)
C
C     SUM THE TERMS OF THE MATRIX ELEMEMENT
C
      ZMATT=0.0
      DO 60 L=1,7
      ZMATT=ZMATT+ZMAT(L)
   60 CONTINUE
      WRITE(6,61)(L,CO(L),L=1,7)
   61 FORMAT(1H ,24X3HCO(I1,3H) =E15.6)
   62 FORMAT(1H ,24X4HCCO(I1,3H) =E15.6)
      WRITE(6,62)(N,CCO(N), N=1,3)
      PUNCH 65, (AKCM(INECM),AKI2,AKF2,CKK,L,CO(L), L=1,7)
      PUNCH 65, (AKCM(INECM),AKI2,AKF2,CKK,N,CCO(N),N=1,3)
   65 FORMAT(4E15.6,I5,E15.6)
      WRITE(6,70)ZMATT,(L,ZMAT(L), L=1,7)
   70 FORMAT(1H0,24X22HTOTAL MATRIX ELEMENT =E15.6/,(25X5HTERM(I2,3H) =E
     113.6))
      SQRMAT=ZMATT*ZMATT
      RETURN
      END
$IBF13 PWBA      DECK
      SUBROUTINE PWBAXT
C
C     CALCULATES ALL TERMS WITH A FINITE RANGE INTERACTION
C     T(D,3HE)2N VERSION
C     TRIPLE GAUSSIAN 3-BODY WAVE FUNCTION
C     TO BE USED IN SUPER PROGRAM
C
      COMMON/KIN/NE1,QVAL,E1(8),NTHETA,THETA3(8),THR(8),NECM,ECM(25),DEC
     1M,ECMIN,Z56,AKI2,AKF2,CKK,AKCM(25),INDEX,LFIT,SIG(25),SQRMAT,E3(25
     2),LOCKCM,INECM,JECM(25)
      COMMON/PWB/
     1GI2(4),GI4(4),GF2(4), GF4(4),A2(4),A4(4),CH(4),CT(4),CD(4),G1(7,4,
     24),G2(7,4,4),G3(7,4,4,4),G4(7,4,4,4),GB(4),GB2(4),GGG(4,4),GA(4,4)
     3,GAG(4,4),GBA(4,4),D(7,4,4),DD(1,4,4,4),DA(6,4,4,4),DB(6,4,4,4),Q1
     4(7),Q2(7,4,4),Q3(7,4,4,4),P(7,4,4,4),CO(7),IWRITE(15),C(4,4,4)
      COMMON/CLINT/ZT2(5),  ZT24(5),  ZT44(5),GC1(2,5,4,4),GC2(2,5,4,4),
     1GC3(2,5,4,4,4),DC(2,5,4,4), QC2(2,5,4,4),QC3(2,5,4,4),GGGC(5,4,4)
     2, GC4(2,5,4,4,4),QC1(2),          DAC(2,5,4,4,4),DBC(2,5,4,4,4),
     3PC(2,5,4,4,4),CCO(3),CC(5,4,4,4),VOC(5),GCB(5,4),GCB2(5,4)
      COMMON/MATS/ZMAT(10)
      DATA (ZT2(I),VOC(I),I=1,4)/5.8174E-04, 8.5499E-02, 8.1899E-03,
     11.3780E-01, 4.7414E-02, 3.2466E-01, 2.8663E-01, 7.5095E-01/
      DATA VWS,VBS,VMS,VHS,VWY,VBY,VMY,VHY/0.4075,0.0925,0.4075,0.0925,
     1-0.14833,0.48167,+0.96334,-0.29666/
      QFUN(A,B)=0.33333334*SQRT((2.0*A+B)*(2.0*A+B)*AKF2+(3.0*A-B)*
     1(3.0*A-B)*AKI2+2.0*(2.0*A+B)*(3.0*A-B)*CKK)
      GFUN(G1,Q1,G2,Q2,G3,Q3)=1.0/(G1*G2*G3*SQRT(G1*G2*G3))*EXP(-0.25*(Q
     11*Q1/G1+Q2*Q2/G2+Q3*Q3/G3))
      KMX=3
      JMX=3
      IMX=3
```

```
      MMX=4
C
C     READ IN AND WRITE OUT PARAMETERS
C
      IF(INDEX .GT. 1) GO TO 100
      IF(IWRITE(15) .NE. 0) GO TO 100
      READ(5,5)(GI2(I),CH(I),I=1,IMX)
    5 FORMAT(8F10.0)
      READ(5,5)(GF2(K),CT(K), K=1,KMX)
      READ(5,5)(A2(J),CD(J),J=1,JMX)
      READ(5,4) B2,VOG,SERBER
    4 FORMAT(3F10.0)
      READ(5,507)IWRITE
  507 FORMAT(15I2)
      WRITE(6,11)B2,VOG,SERBER
   11 FORMAT(25X9HBETASQR =F9.5/,25X26HGAUSSIAN POTENTIAL DEPTH =F9.5/,
     125X24HSERBER-SYMETRIC MIXING =F9.5/)
      WRITE(6,12)(I,GI2(I),I,CH(I),I=1,IMX)
   12 FORMAT(25X19HHELIUM-3 PARAMETERS/,(30X4HGI2(I1,3H) =F9.5,5X3HCH(I1
     1,3H) =F9.5/))
      WRITE(6,13)(K,GF2(K),K,CT(K), K=1,KMX)
   13 FORMAT(25X17HTRITON PARAMETERS/,(30X4HGF2(I1,3H) =F9.5,5X3HCT(I1,
     13H) =F9.5/))
      WRITE(6,14)(J,A2(J),J,CD(J), J=1,JMX)
   14 FORMAT(25X19HDEUTERON PARAMETERS/,(30X3HA2(I1,3H) =F9.5,5X3HCD(I1,
     13H) =F9.5/))
      WRITE(6,515)(IWRITE(I), I=1,15)
  515 FORMAT(25X12HWRITE CODE =15I2/)
C
C     CALCULATE MOMENTUM TRANSFERS AND CONVIENT TERMS
C
      SYMT=1.0-SERBER
      B24=0.25*B2
      B44=B24*B2
      DO 21 I=1,IMX
      GI4(I)=GI2(I)*GI2(I)
   21 CONTINUE
      DO 22 J=1,JMX
      A4(J)=A2(J)*A2(J)
   22 CONTINUE
      DO 31 M=1,MMX
      ZT24(M)=0.25*ZT2(M)
      ZT44(M)=ZT24(M)*ZT2(M)
   31 CONTINUE
      DO 23 K=1,KMX
      GB(K)=GF2(K)+B2
      GB2(K)=GB(K)*GB(K)
      GF4(K)=GF2(K)*GF2(K)
      DO 37 M=1,MMX
      GCB(M,K)=GF2(K)+ZT2(M)
      GCB2(M,K)=GCB(M,K)*GCB(M,K)
   37 CONTINUE
      DO 24 I=1,IMX
      G1(1,K,I)=GF2(K)+GI2(I)
      G1(2,K,I)=GI2(I)
      G1(4,K,I)=G1(1,K,I)
      G1(5,K,I)=G1(1,K,I)+B2
      G1(6,K,I)=G1(1,K,I)
      G1(7,K,I)=G1(1,K,I)
      G2(4,K,I)=0.75*G1(1,K,I)
      G2(3,K,I)=G2(4,K,I)+B24
```

```
      G2(5,K,I)=G2(3,K,I)-B44/G1(5,K,I)
      G2(6,K,I)=G2(4,K,I)
      G2(7,K,I)=G2(4,K,I)
      GGG(K,I)=G1(5,K,I)*G1(5,K,I)*G2(5,K,I)
      D(1,K,I)=GF2(K)/G1(1,K,I)
      D(2,K,I)=0.0
      D(4,K,I)=4.0*GF2(K)/G1(4,K,I)
      D(5,K,I)=4.0*GB(K)/G1(5,K,I)-4.0*GI2(I)*B44/GGG(K,I)
      D(6,K,I)=D(4,K,I)
      DO 28 L=1,7
      Q2(L,K,I)=0.0
   28 CONTINUE
      DO 32 M=1,MMX
      GC1(1,M,K,I)=G1(2,K,I)
      GC1(2,M,K,I)=G1(1,K,I) +ZT2(M)
         GC2(2,M,K,I)=G2(4,K,I)+ZT24(M)-ZT44(M)/GC1(2,M,K,I)
      GGGC(M,K,I)=GC1(2,M,K,I)*GC1(2,M,K,I)*GC2(2,M,K,I)
      QC2(1,M,K,I)=0.0
      DC(2,M,K,I)=4.0*GCB(M,K)/GC1(2,M,K,I)-4.0*GI2(I)*ZT44(M)/GGGC(M,K,
     1I)
   32 CONTINUE
   24 CONTINUE
      DO 25 J=1,JMX
      G1(3,K,J)=GF2(K)+A2(J)
      GA(K,J)=0.75*GF2(K)+A2(J)
      G2(1,K,J)=GA(K,J)+B24
      G2(2,K,J)=G2(1,K,J)
      GAG(K,J)=GA(K,J)/G2(1,K,J)
      GBA(K,J)=GB(K)+A2(J)
      D(3,K,J)=4.0*G1(3,K,J)/GF2(K)
      DO 33 M=1,MMX
      GC2(1,M,K,J)=GA(K,J)+ZT24(M)
   33 CONTINUE
   25 CONTINUE
      DO 26 I=1,IMX
      DO 27 J=1,JMX
      C(K,J,I)=2169.6231366*VOG*CT(K)*CD(J)*CH(I)
      G3(1,K,J,I)=GB(K)-GF4(K)/G1(1,K,I)-B44/G2(1,K,J)
      G3(2,K,J,I)=GB(K)-B44/G2(2,K,J)
      G3(3,K,J,I)=GI2(I)+B2+A2(J)-B44/G2(3,K,I)-A4(J)/G1(3,K,J)
      G3(4,K,J,I)=G1(3,K,J)-GF4(I)/G1(4,K,I)
      G3(5,K,J,I)=GBA(K,J)-GB2(K)/G1(5,K,I)-B44*GI4(I)/GGG(K,I)
      G3(6,K,J,I)=GBA(K,J)-GF4(K)/G1(6,K,I)
      G3(7,K,J,I)=B2
      G4(2,K,J,I)=0.75*GI2(I)
      G4(1,K,J,I)=G4(2,K,J,I)+B24*GAG(K,J)-B44*GAG(K,J)*GAG(K,J)/G3(1,K,
     1J,I)
      G4(3,K,J,I)=GI2(I)-GI4(I)/G3(3,K,J,I)
      G4(4,K,J,I)=B2+A2(J)-A4(J)/G3(4,K,J,I)
      G4(5,K,J,I)=A2(J)-A4(J)/G3(5,K,J,I)
      G4(6,K,J,I)=A2(J)-A4(J)/G3(6,K,J,I)
      G4(7,K,J,I)=A2(J)
      DD(1,K,J,I)=0.5*B2*GA(K,J)/(G2(1,K,J)*G3(1,K,J,I))
      P(2,K,J,I)=1.0E-6
      DA(3,K,J,I)=1.0-GI2(I)*GF2(K)/(G1(3,K,J)*G3(3,K,J,I))
      DB(3,K,J,I)=1.0-4.0*GI2(I)/G3(3,K,J,I)
      DO 29 L=4,6
      DA(L,K,J,I)=A2(J)/G3(L,K,J,I)
      DB(L,K,J,I)=D(L,K,I)*DA(L,K,J,I)-3.0
   29 CONTINUE
      DO 34 M=1,MMX
```

```
      GC3(1,M,K,J,I)=GCB(M,K)-ZT44(M)/GC2(1,M,K,J)
      GC3(2,M,K,J,I)=GCB(M,K)+A2(J)-GCB2(M,K)/GC1(2,M,K,I)-ZT44(M)*GI4(I
     1)/GGGC(M,K,I)
      GC4(1,M,K,J,I)=G4(2,K,J,I)
      GC4(2,M,K,J,I)=A2(J)-A4(J)/GC3(2,M,K,J,I)
      DAC(2,M,K,J,I)=A2(J)/GC3(2,M,K,J,I)
      DBC(2,M,K,J,I)=DC(2,M,K,I)*DAC(2,M,K,J,I)-3.0
      CC(M,K,J,I)=2169.6231366*VOC(M)*CT(K)*CD(J)*CH(I)
   34 CONTINUE
   27 CONTINUE
   26 CONTINUE
   23 CONTINUE
  100 QD=SQRT(0.444444*AKF2+AKI2+1.333333*CKK)
      Q2P= SQRT(AKF2+0.444444*AKI2+1.333333*CKK)
      QN=0.333333*SQRT(AKF2+AKI2-2.0*CKK)
      Q1(1)=QN
      Q1(2)=Q2P
      Q1(3)=0.5*QD
      Q1(4)=2.0*QN
      Q1(5)=Q1(4)
      Q1(6)=Q1(4)
      Q1(7)=Q1(4)
      QC1(1)=Q1(2)
      QC1(2)=Q1(5)
      DO 40 K=1,KMX
      DO 41 J=1,JMX
      Q3(3,K,J)=2.0/D(3,K,J)*QFUN(1.0,D(3,K,J))
   41 CONTINUE
      DO 42 I=1,IMX
      Q2(5,K,I)=B2/G1(5,K,I)*QN
      Q3(1,K,I)=QFUN(1.0,D(1,K,I))
      Q3(2,K,I)=QD
      Q3(4,K,I)=0.5*QFUN(1.0,D(4,K,I))
      Q3(5,K,I)=0.5*QFUN(1.0,D(5,K,I))
      Q3(6,K,I)=Q3(4,K,I)
      Q3(7,K,I)=3.0*QN
      DO 38 M=1,MMX
      QC2(2,M,K,I)=ZT2(M)/GC1(2,M,K,I)*QN
      QC3(1,M,K,I)=Q3(2,K,I)
      QC3(2,M,K,I)=0.5*QFUN(1.0,DC(2,M,K,I))
   38 CONTINUE
      DO 43 J=1,JMX
      P(1,K,J,I)=DD(1,K,J,I)*Q3(1,K,I)
      P(7,K,J,I)=1.5*QN
      DO 44 L=3,6
      P(L,K,J,I)=.5*QFUN(DA(L,K,J,I),DB(L,K,J,I))
   44 CONTINUE
      DO 35 M=1,MMX
      PC(1,M,K,J,I)= P(2,K,J,I)
      PC(2,M,K,J,I)=0.5*QFUN(DAC(2,M,K,J,I),DBC(2,M,K,J,I))
   35 CONTINUE
   43 CONTINUE
   42 CONTINUE
   40 CONTINUE
      WRITE(6,98)ECM(INECM),QD,Q2P,QN
   98 FORMAT(25X26HMATRIX ELEMENT CALCULATION//,25X5HECM =F7.3/,25X4HQD
     1=F9.5/,25X5HQ2P =F9.5/,25X4HQN =F9.5/)
      DO 50 L=1,7
      CO(L)=0.0
   50 CONTINUE
      CCO(1)=0.0
```

198

```
      CCO(2)=0.0
      CCO(3)=0.0
      DO 51 K=1,KMX
      DO 52 J=1,JMX
      DO 53 I=1,IMX
      CO(1)=CO(1)+C(K,J,I)*GFUN(G1(1,K,I),Q1(1),G2(1,K,J),Q2(1,K,I),G3(1
     1,K,J,I),Q3(1,K,I))*S(1,K,J,I)
      CO(2)=CO(2)+C(K,J,I)*GFUN(G1(2,K,I),Q1(2),G2(2,K,J),Q2(2,K,I),G3(2
     1,K,J,I),Q3(2,K,I))*S(2,K,J,I)
      CO(3)=CO(3)+C(K,J,I)*GFUN(G1(3,K,J),Q1(3),G2(3,K,I),Q2(3,K,I),G3(3
     1,K,J,I),Q3(3,K,J))*S(3,K,J,I)
      DO 54 L=4,7
      CO(L)=CO(L)+C(K,J,I)*GFUN(G1(L,K,I),Q1(L),G2(L,K,I),Q2(L,K,I),G3(L
     1,K,J,I),Q3(L,K,I))*S(L,K,J,I)
   54 CONTINUE
C
C     CALCULATE COULOMB OVERLAPS CCO(N)
C
      DO 57 M=1,MMX
      CCO(1)=CCO(1)+CC(M,K,J,I)*GFUN(GC1(1,M,K,I),OC1(1),GC2(1,M,K,J),OC
     12(1,M,K,I),GC3(1,M,K,I),OC3(1,M,K,I))*SC(1,M,K,J,I)
      CCO(2)=CCO(2)+CC(M,K,J,I)*GFUN(GC1(2,M,K,I),OC1(2),GC2(2,M,K,I),OC
     12(2,M,K,I),GC3(2,M,K,I),OC3(2,M,K,I))*SC(2,M,K,J,I)
   57 CONTINUE
   53 CONTINUE
   52 CONTINUE
   51 CONTINUE
C
C     CACULATE TERMS OF THE MATRIX ELEMENT
C
      ZMAT(1)=2.*((2.*VWS+VBS-VMS-VHS)*SERBER+(2.*VWY+VBY-VMY-VHY)*SYMT)
     1*CO(1)
      ZMAT(2)=((2.*VWS-VBS+2.*VMS-VHS)*SERBER+(2.*VWY-VBY+2.*VMY-VHY)*SY
     1MT)*CO(2)-CCO(1)
      ZMAT(3)=-2.*((VWS+VBS-2.*VMS-VHS)*SERBER+(VWY+VBY-2.0*VMY-VHY)*SYM
     1T)*CO(3)
      ZMAT(4)=-((VWS-VBS+VMS-VHS)*SERBER+(VWY-VBY+VMY-VHY)*SYMT)*CO(4)
      ZMAT(5)=-2.*((VWS+VMS)*SERBER+(VWY+VMY)*SYMT)*CO(5)+CCO(2)
      ZMAT(6)=-(VWS*SERBER+VWY*SYMT)*CO(6)
      ZMAT(7)=-(VMS*SERBER+VMY*SYMT)*CO(7)
C
C     SUM THE TERMS OF THE MATRIX ELEMEMENT
C
      ZMATT=0.0
      DO 60 L=1,7
      ZMATT=ZMATT+ZMAT(L)
   60 CONTINUE
      WRITE(6,61)(L,CO(L),L=1,7)
   61 FORMAT(1H ,24X3HCO(I1,3H) =E15.6)
   62 FORMAT(1H ,24X4HCCO(I1,3H) =E15.6)
      WRITE(6,62)(N,CCO(N), N=1,3)
      PUNCH 65, (AKCM(INECM),AKI2,AKF2,CKK,L,CO(L), L=1,7)
      PUNCH 65, (AKCM(INECM),AKI2,AKF2,CKK,N,CCO(N),N=1,3)
   65 FORMAT(4E15.6,I5,E15.6)
      WRITE(6,70)ZMATT,(L,ZMAT(L), L=1,7)
   70 FORMAT(1H0,24X22HTOTAL MATRIX ELEMENT =E15.6/,(25X5HTFRM(I2,3H) =E
     113.6))
      SQRMAT=ZMATT*ZMATT
      RETURN
      END
$IBF13 SIT      DECK
```

```
      FUNCTION S(L,K,J,I)
C
C     OVERLAP OF NUCLEON-NUCLEON SCATTERING WAVE FUNCTION
C     NUCLEAR INETERATION
C     TO BE USED IN SUPER PROGRAM
C
      COMMON/KIN/NE1,QVAL,E1(8),NTHETA,THETA3(8),THR(8),NECM,ECM(25),DEC
     1M,ECMIN,Z56,AKI2,AKF2,CKK,AKCM(25),INDEX,LFIT,SIG(25),SQRMAT,E3(25
     2),LOCKCM,INECM,JECM(25)
      COMMON/PWB/
     1GI2(4),GI4(4),GF2(4), GF4(4),A2(4),A4(4),CH(4),CT(4),CD(4),G1(7,4,
     24),G2(7,4,4),G3(7,4,4,4),G4(7,4,4,4),GB(4),GB2(4),GGG(4,4),GA(4,4)
     3,GAG(4,4),GBA(4,4),D(7,4,4),DC(1,4,4,4),DA(6,4,4,4),DB(6,4,4,4),Q1
     4(7),Q2(7,4,4),Q3(7,4,4),P(7,4,4,4),CO(7),IWRITE(15),C(4,4,4)
      COMMON / PHII / PHIE(16,24),ZLP(16),WTE(16)
      FG(R,FI,PP,GG)= R*FI*SIN(PP*R)*EXP(-GG*R*R)/PP
      IF(L .EQ. 1  .AND. IWRITE(L) .NE. 0) WRITE(6,1)
    1 FORMAT(1H0)
      S = 0.0
      JJ=JECM(INECM)-1
      DO 20 JZ=1,16
   20 S=S+WTE(JZ)*FG(ZLP(JZ),PHIE(JZ,JJ),P(L,K,J,I),G4(L,K,J,I))
      IF(IWRITE(L) .NE. 0 ) WRITE(6,5)L,L,K,J,I,P(L,K,J,I),L,K,J,I,G4(L,
     1K,J,I),S
    5 FORMAT(10H INTEGRAL I1,3X2HP(I1,1H,I1,1H,I1,1H,I1,3H) =E13.6,5X3HG
     14(I1,1H,I1,1H,I1,1H,I1,3H) =E13.6,5X3HS =E13.6)
      RETURN
      END
$IBF13 SIC     DECK
      FUNCTION SC(L,M,K,J,I)
C
C     OVERLAP OF NUCLEON-NUCLEON SCATTERING WAVE FUNCTION
C     COULOMB INTERACTION
C     3HE(D,T)2P VERSION
C     TO BE USED IN SUPER PROGRAM
C
      COMMON/KIN/NE1,QVAL,E1(8),NTHETA,THETA3(8),THR(8),NECM,ECM(25),DEC
     1M,ECMIN,Z56,AKI2,AKF2,CKK,AKCM(25),INDEX,LFIT,SIG(25),SQRMAT,E3(25
     2),LOCKCM,INECM,JECM(25)
      COMMON/PWB/
     1GI2(4),GI4(4),GF2(4), GF4(4),A2(4),A4(4),CH(4),CT(4),CD(4),G1(7,4,
     24),G2(7,4,4),G3(7,4,4,4),G4(7,4,4,4),GB(4),GB2(4),GGG(4,4),GA(4,4)
     3,GAG(4,4),GBA(4,4),D(7,4,4),DD(1,4,4,4),DA(6,4,4,4),DB(6,4,4,4),Q1
     4(7),Q2(7,4,4),Q3(7,4,4),P(7,4,4,4),CO(7),IWRITE(15),C(4,4,4)
      COMMON / PHII / PHIE(16,24),ZLP(16),WTE(16)
      COMMON/CLINT/ZT2(5),  ZT24(5),   ZT44(5),  GC1(3,4,4),GC2(3,5,4,4),
     1GC3(3,5,4,4,4),DC(3,4,4),QC1(3),QC2(3,4,4),QC3(3,4,4),GAGC(3,5,4,4
     2),GC4(3,5,4,4,4),DDC(1,5,4,4,4),DAC(3,5,4,4,4),DBC(3,5,4,4,4),
     3PC(3,5,4,4,4),CCO(3),CC(5,4,4,4),VOC(5)
      FG(R,FI,PP,GG)= R*FI*SIN(PP*R)*EXP(-GG*R*R)/PP
      IF(L .EQ. 1  .AND. IWRITE(L)   .NE. 0) WRITE(6,1)
    1 FORMAT(1H0)
      SC=0.0
      JJ=JECM(INECM)-1
      DO 20 JZ=1,16
   20 SC=SC+WTE(JZ)*FG(ZLP(JZ),PHIE(JZ,JJ),PC(L,M,K,J,I),GC4(L,M,K,J,I))
      IF(IWRITE(L)   .NE. 0)WRITE(6,5)L, L,M,K,J,I,PC(L,M,K,J,I),L,M,K,J,
     1I,GC4(L,M,K,J,I),SC
    5 FORMAT(10H INTEGRAL I2,3X3HPC(I1,1H,I1,1H,I1,1H,I1,1H,I1,3H) =E13.
     16,5X4HGC4(I1,1H,I1,1H,I1,1H,I1,1H,I1,3H) =E13.6,5X4HSC =E13.6)
      RETURN
```

```
         END
$IBF13 SIC    DECK
       FUNCTION SC(L,M,K,J,I)
C
C      OVERLAP OF NUCLEON-NUCLEON SCATTERING WAVE FUNCTION
C      COULOMB INTERACTION
C      T(D,3HE)2N VERSION
C      TO BE USED IN SUPER PROGRAM
C
       COMMON/KIN/NE1,QVAL,E1(8),NTHETA,THETA3(8),THR(8),NECM,ECM(25),DEC
      1M,ECMIN,Z56,AKI2,AKF2,CKK,AKCM(25),INDEX,LFIT,SIG(25),SQRMAT,E3(25
      2),LOCKCM,INECM,JECM(25)
       COMMON/PWB/
      1GI2(4),GI4(4),GF2(4), GF4(4),A2(4),A4(4),CH(4),CT(4),CD(4),G1(7,4,
      24),G2(7,4,4),G3(7,4,4,4),G4(7,4,4,4),GB(4),GB2(4),GGG(4,4),GA(4,4)
      3,GAG(4,4),GBA(4,4),D(7,4,4),DD(1,4,4,4),DA(6,4,4,4),DB(6,4,4,4),Q1
      4(7),Q2(7,4,4),Q3(7,4,4),P(7,4,4,4),CO(7),IWRITE(15),C(4,4,4)
        COMMON / PHII / PHIE(16,24),ZLP(16),WTE(16)
       COMMON/CLINT/ZT2(5),  ZT24(5),  ZT44(5),GC1(2,5,4,4),GC2(2,5,4,4),
      1GC3(2,5,4,4,4),DC(2,5,4,4), QC2(2,5,4,4),QC3(2,5,4,4),GGGC(5,4,4)
      2, GC4(2,5,4,4,4),QC1(2),          DAC(2,5,4,4,4),DBC(2,5,4,4,4),
      3PC(2,5,4,4,4),CCO(3),CC(5,4,4,4),VOC(5),GCB(5,4),GCB2(5,4)
       FG(R,FI,PP,GG)= R*FI*SIN(PP*R)*EXP(-GG*R*R)/PP
       IF(L .EQ. 1  .AND. IWRITE(L)   .NE. 0) WRITE(6,1)
     1 FORMAT(1H0)
       SC=0.0
       JJ=JECM(INECM)-1
       DO 20 JZ=1,16
    20 SC=SC+WTE(JZ)*FG(ZLP(JZ),PHIE(JZ,JJ),PC(L,M,K,J,I),GC4(L,M,K,J,I))
       IF(IWRITE(L)   .NE. 0)WRITE(6,5)L, L,M,K,J,I,PC(L,M,K,J,
      1I,GC4(L,M,K,J,I),SC
     5 FORMAT(10H INTEGRAL I2,3X3HPC(I1,1H,I1,1H,I1,1H,I1,1H,I1,3H) =E13.
      16,5X4HGC4(I1,1H,I1,1H,I1,1H,I1,1H,I1,3H) =E13.6,5X4HSC =E13.6)
       RETURN
       END
$IBF13 FOLD    DECK
       SUBROUTINE  FOLD
C
C      FOLDS IN EXPERIMENTAL ENERGY RESOLUTION
C      TO BE USED IN SUPER PROGRAM
C
       COMMON/MAIN/KTHRY,KOMNRM,NFIT,KOUT,ISAVE,SAVE
       COMMON/KIN/NE1,QVAL,E1(8),NTHETA,THETA3(8),THR(8),NECM,ECM(25),DEC
      1M,ECMIN,Z56,AKI2,AKF2,CKK,AKCM(25),INDEX,LFIT,SIG(25),SQRMAT,E3(25
      2),LOCKCM,INECM,JECM(25)
       COMMON/FOOL/E3INT(1000),SIGINT(1000),SIGFLD(1000),GA(50),INTMAX,
      1DE3,RES,SGFM,IGMAX
C      INTERPOLATE TO EVENLY-SPACED SPECTRUM
C
       NMAX=NECM
       WRITE(6,26)RES,IGMAX,DE3
    26 FORMAT(42X19H GAUSSIAN PRAMETERS///,10X13H RESOLUTION =F7.4,
      15X26HPOINTS PER HALF-GAUSSIAN =I3,10X18HENERGY INCREMENT =F6.3//)
       IF(RES .EQ. 0.0) IGMAX = 0.0
       RIGMAX=IGMAX
       E3IMIN=E3(NMAX)-RIGMAX*DE3
       E3INT(IGMAX + 1) = E3(1)
       J=1
     1 II = IGMAX + J
       E3INT(II+1) = E3INT(II) - DE3
       IF(E3INT(II+1).LT.E3IMIN) GO TO 2
```

```
      J=J+1
      GO TO 1
    2 INTMAX = II + 1
      DO 3 I = 1,IGMAX
      IJ = IGMAX + 1 - I
    3 E3INT(IJ) = E3INT(IJ+1) + DE3
      DO 4 I = 1,INTMAX
      SIGFLD(I) = 0.0
    4 SIGINT(I) = 0.0
      SIGINT(IGMAX+1) = SIG(1)
      IM = IGMAX + 2
      IE3 = 2
      DO 5 I = IM,INTMAX
      IJM = I
      GO TO 9
    6 IE3 = IE3 + 1
    9 IF(E3INT(I).LT.E3(NMAX-1)) GO TO 14
      IF(E3INT(I).LT.E3(IE3)) GO TO 6
      X = E3INT(I)
      X1 = E3(IE3+1)
      X2 = E3(IE3)
      X3 = E3(IE3-1)
      Y1 = SIG(IE3+1)
      Y2 = SIG(IE3)
      Y3 = SIG(IE3-1)
      SIGINT(I) = (X-X2)*(X-X3)*Y1/((X1-X2)*(X1-X3)) + (X-X1)*(X-X3)*Y2/
     1((X2-X1)*(X2-X3))  +   (X-X1)*(X-X2)*Y3/((X3-X1)*(X3-X2))
    5 CONTINUE
   14 SL = (SIG(NMAX)-SIG(NMAX-1))/(E3(NMAX)-E3(NMAX-1))
      X1 = E3(NMAX)
      Y1 = SIG(NMAX)
      DO 15 J = IJM,INTMAX
   15 SIGINT(J) = Y1 + SL*(E3INT(J) - X1)
      IF(RES .EQ. 0.0) GO TO 50
      WRITE(6,30)
   30 FORMAT(20X5HPOINT,7X6HENERGY,8X5HVALUE//)
C
C     SET UP GAUSSIAN
C
      SD=RES/2.354
      DO 10 IG = 1,IGMAX
      AIG = IG
      EE = AIG*DE3
      GA(IG)=EXP(-EE*EE/(2.*SD*SD))
      WRITE(6,301)AIG,EE,GA(IG)
  301 FORMAT(19XF6.3,8XF6.3,5XE10.2)
   10 CONTINUE
C
C     FOLD GAUSSIAN RESOLUTION INTO SPECTRUM
C
      DO 7 I = 1,IGMAX
      SIGFLD(I) = SIGINT(I)
      DO 8 IF = 1,IGMAX
      IFG = IF + I
    8 SIGFLD(I) = SIGFLD(I) + SIGINT(IFG)*GA(IF)
    7 CONTINUE
      JMIN = IGMAX + 1
      DO 11 J = JMIN,INTMAX
      SIGFLD(J) = SIGINT(J)
      DO 12 JF = 1,IGMAX
      JFP = J + JF
```

```
        JFM = J - JF
     12 SIGFLD(J) = SIGFLD(J)+(SIGINT(JFP)+SIGINT(JFM))*GA(JF)
     11 CONTINUE
        SGFM = 0.0
        DO 13 I = 1,INTMAX
     13 IF(SIGFLD(I).GT.SGFM) SGFM = SIGFLD(I)
        RETURN
     50 SGFM=0.0
        DO 51 I=1,INTMAX
        SIGFLD(I)=SIGINT(I)
        IF(SIGFLD(I) .GT. SGFM)SGFM=SIGFLD(I)
     51 CONTINUE
        RETURN
        END
$IBF13 NORMLZ   DECK
        SUBROUTINE NORMLZ
C
C       TO BE USED IN SUPER PROGRAM
C
        COMMON/MAIN/KTHRY,KOMNRM,NFIT,KOUT,ISAVE,SAVE
        COMMON/FOOL/E3INT(1000),SIGINT(1000),SIGFLD(1000),GA(50),INTMAX,
       1DE3,RES,SGFM,IGMAX
        COMMON/NORM/SNORM,SIGNRM(1000),SMAX,ENORM,SIGMAX
        SMAX=0.0
        IF(KOMNRM .EQ. 1 .AND. ISAVE .EQ. 2) GO TO 25
        DO 4 I=1,INTMAX
        J=I
        IF(ABS(E3INT(J)-ENORM) .LT. DE3 ) GO TO 5
      4 CONTINUE
        SFAC=SNORM/SGFM
        WRITE(6,20)SGFM
     20 FORMAT(1HO 10X20HNORMALIZED TO SGFM =E13.6//)
        GO TO 6
      5 SFAC=SNORM/SIGFLD(J)
        WRITE(6,15) SNORM,ENORM
     15 FORMAT(1HO 29X17HNORMALIZATION IS E13.6,4H AT F7.3,4H MEV//)
      6 DO 7 I=1,INTMAX
        SIGNRM(I)=SFAC*SIGFLD(I)
        IF(SIGNRM(I) .GT. SMAX)SMAX=SIGNRM(I)
      7 CONTINUE
        RETURN
     25 WRITE(6,26)SAVE
     26 FORMAT(1HO 29X54HNORMALIZATION IS COMMON TO PREVIOUS CALCULATION
       1SAVE=E15.6//)
        SFAC=SAVE*SIGMAX/SGFM
        GO TO 6
        END
$IBF13 OUT      DECK
        SUBROUTINE OUTPUT
C
C       OUTPUT SUBROUTINE TO BE USED WITH SUPER PROGRAM
C
        DIMENSION LINE(50)
        COMMON/MAIN/KTHRY,KOMNRM,NFIT,KOUT,ISAVE,SAVE
        COMMON/KIN/NE1,QVAL,E1(8),NTHETA,THETA3(8),THR(8),NECM,ECM(25),DEC
       1M,ECMIN,Z56,AKI2,AKF2,CKK,AKCM(25),INDEX,LFIT,SIG(25),SORMAT,E3(25
       2),LOCKCM,INECM,JECM(25)
        COMMON/NORM/SNORM,SIGNRM(1000),SMAX,ENORM,SIGMAX
        COMMON/FOOL/E3INT(1000),SIGINT(1000),SIGFLD(1000),GA(50),INTMAX,
       1DE3,RES,SGFM,IGMAX
        COMMON/LBL/WTLBL(13),PTLBL(13),PNLBL(13),XMIN,XMAX,YMIN,YMAX,TT(2)
```

```
     1,TT1(2),AA(14),TTT,EXE3(25),EXD(25),EXVD(25),DATAMX,NE3MAX
       REAL MINUS,LINE
       DATA BLANK,POINT,BAR,STAR,MINUS,PLUS/1H ,1H.,1HI,1H*,1H-,1H+/
C
C      WRITE OUT RAW CROSS SECTION CALCULATED IN KINMAT
C
       WRITE(6,40)
    40 FORMAT(20X23H RAW OUTPUT FROM KINMAT//10X2HE3,20X3HECM,18X3HSIG//)
       WRITE(6,41)(E3(I),ECM(I),SIG(I),I=1,NECM)
    41 FORMAT(3E20.6)
C
C      CHOOSE MODE OF OUTPUT AS GIVEN BY CONTROL CARD
C
       IF(KOUT .NE. 0) GO TO 18
C
C      GENERATE WRITE--PLOT
C
    19 SCALE=1.25*SMAX
       SF=50.0/SCALE
       WRITE(6,1)SCALE
     1 FORMAT(2HOXE8.2,2H 29X1H49X1H69X1H88X2H1028H      E3          EXP
     1    THRY)
       WRITE(6,2)
     2 FORMAT(53H .--------+--------+--------+--------+-------+.)
       L=0
       DO 10 II=1,INTMAX
       J=0
       KP=0
       KM=0
       K=0
       NN=0
     4 DO 3 IK=1,50
     3 LINE(IK)=BLANK
       I=INTMAX+1-II
       J=SIGNRM(I)*SF+0.99
       DO 9 N=1,NE3MAX
       IF(ABS(EXE3(N)-E3INT(I)) .GT. RES) GO TO 9
       K=EXD(N)*SF+0.99
       KP=(EXD(N)+EXVD(N))*SF+0.99
       KM=(EXD(N)-EXVD(N))*SF+0.99
       NN=N
       GO TO 7
     9 NN=25
       CONTINUE
     7 L=L+1
       J=MOD(J,50)
       KP=MOD(KP,50)
       KM=MOD(KM,50)
       K=MOD(K,50)
       LINE(J)=POINT
       LINE(KP)=BAR
       LINE(KM)=BAR
       LINE(K)=STAR
       END = BAR
       IF(L .EQ. 1) END=PLUS
       IF(L .EQ. 1) L=-4
     6 WRITE(6,5)END,LINE,END,E3INT(I),EXD(NN),SIGNRM(I)
     5 FORMAT(1H 52A1,F6.2,5X,F7.3,3X,F9.5)
    10 CONTINUE
       WRITE(6,2)
       RETURN
```

```
    18 IF(KOUT .EQ. 2) GO TO 20
C
C      PLOTTING OF OUTPUT OF PROGRAM ON CALCOMP
C
       IF(LFIT.GT.1) GO TO 30
       WRITE(6,28)PTLBL
    28 FORMAT(10X,13A6/)
       CALL OUTCOR(AA,NWDS)
       WRITE(6,200) (PTLBL(I), I=1,13)
   200 FORMAT(13A6)
       CALL OUTCOR
       CALL SYSSYM(1.00,9.00,.12,AA,6*NWDS,0.)
       CALL LABEL(0.,0.,XMIN,XMAX,15.,6,TT,12,0)
       CALL LABEL(0.,0.,XMIN,XMAX,15.,-30,TT1,2,0)
       CALL LABEL(0.,0.,YMIN,YMAX,10.,4,TTT,5,1)
       CALL LABEL(0.,0.,YMIN,YMAX,10.,-20,TT1,2,1)
    30 LF=-1
       IF(LFIT .LT. NFIT) LF=0
       IP=1
       IF(LFIT.GT.1) IP=2
       ISYS=0
       IF(LFIT.GT.1)ISYS=3+LFIT
       CALL PLOTXY(INTMAX,E3INT,SIGNRM,XMIN,XMAX,YMIN,YMAX,LF,IP,ISYS,25)
    25 LFIT=LFIT+1
       IF(KOUT .EQ. 1) GO TO 21
C
C      PUNCH OUTPUT OF CALCULATION
C
    20 WRITE(6,53)
    53 FORMAT(1H0,5X34HE3INT AND SIGNRM HAVE BEEN PUNCHED//)
       PUNCH 200,(PNLBL(I), I=1,13)
       PUNCH 54, (E3INT(I),SIGNRM(I), I=1,INTMAX)
    54 FORMAT(2E20.6)
C
C      LISTING OF OUTPUT OF PROGRAM
C
    21 WRITE(6,51)
    51 FORMAT(1H0,5X5HE3INT8X6HSIGNRM//)
       WRITE(6,50) (E3INT(I),SIGNRM(I), I=1,INTMAX)
    50 FORMAT(5XF7.3,5XF9.5)
       RETURN
       END
```

205

REFERENCES

Bacher, A. D., Ph.D. Thesis, California Institute of
        Technology (1966).

Baker, G. A., Gammel, J. L., Hill, B. J., and Wills, J. G.,
        Phys. Rev. $\underline{125}$, 1754 (1962).

Bander, M., Phys. Rev. $\underline{134}$, 5B (1964).

Banerjee, M. K., "The Theory of Stripping and Pickup
        Reactions", in Nuclear Spectroscopy, Part B, ed. by
        Fay Ajzenberg-Selove, New York: Academic Press,
        1960.

Baumgartner, E., Conzett, H. E., Shield, E., and Slobodrian,
        R. J., Phys. Rev. Letters $\underline{16}$, 3 (1966).

Bilaniuk, O. M., and Slobodrian, R. J., Phys. Letters $\underline{7}$,
        77 (1963).

Brolley, J. E., Jr., Hall, W. S., Rosen, L., and Stewart,
        L., Phys. Rev. $\underline{109}$, 1277 (1958).

Brueckner, K. A., Phys. Rev. $\underline{82}$, 598 (1951).

Butler, P. G., Cohen, N., James, A. N., and Nicholson, J. P.,
        Phys. Rev. Letters $\underline{21}$, 470 (1968).

Conzett, H. E., Shield, E., Slobodrian, R. J., and Yamabe,
        S., Phys. Rev. Letters $\underline{13}$, 625 (1964).

Fadeev, L. D. Zh. Eksperim. i Theor. Fiz. $\underline{39}$, 1459 (1960)
        (English transl.: Soviet Phys. - JETP $\underline{12}$, 1014 (1961).

Frank, R. M., and Gammel, J. L., Phys. Rev. $\underline{93}$, 463 (1954).

Gell-Mann, M., and Goldberger, M. L., Phys. Rev. $\underline{91}$, 398,
        (1953).

Gillespie, J., Final-State Interactions, San Francisco:
        Holden-Day, Inc., 1964.

Gluckstern, R. L., and Bethe, H. A., Phys. Rev. $\underline{81}$, 5 (1951).

Goldberger, M. L., and Watson, K. M., Collision Theory,
        New York: John Wiley and Sons, Inc., 1964.

Griffy, T. A., and Oakes, R. J., Phys. Rev. $\underline{135}$, B1161,
        (1964).

Groce, D. E., Ph.D. Thesis, California Institute of
    Technology (1963).

Haddock, R. P., Salter, R. M., Zeller, M., Czirr, J. B.,
    and Nygren, D. R., Phys. Rev. Letters $\underline{14}$, 318 (1965).

Haybron, R. M., Nucl. Phys. $\underline{A112}$, 594 (1968).

Heckrotte, W., and MacGregor, M., Phys. Rev. $\underline{111}$, 593
    (1958).

Heller, L., Signell, P., and Yoder, N. R., Phys. Rev.
    Letters $\underline{13}$, 577 (1964).

Henley, E. M., "Charge Independence and Charge Symmetry of
    Nuclear Forces", to be published.

Henley, E. M., Richards, F. C., and Yu, D. U. L., Nucl.
    Phys. $\underline{A103}$, 361 (1967); Phys. Letters $\underline{15}$, 331 (1965).

Ilakovac, K., Kuo, L. G., Petravic, M., and Slaus, I.,
    Phys. Rev. $\underline{124}$, 6 (1961).

Jackson, J. D., and Blatt, J. M., Rev. Mod. Phys. $\underline{22}$, 77,
    (1950).

Jakobson, M., Manley, J. H., and Stokes, R. H., Nucl. Phys.
    $\underline{70}$, 97 (1965).

Koehler, D. R., Phys. Rev. $\underline{138}$, 3B (1965).

Koehler, D. R., and Mann, R. A., Phys. Rev. $\underline{135}$, 1B (1964).

McNally, J. H., Ph.D. Thesis, California Institute of
    Technology (1966).

Malanify, J. J., Gross, E. E., and Woods, R., Bull. Am.
    Phys. Soc. $\underline{12}$, 1175 (1967).

Migdal, A. B., J. Exper. Theoret. Phys. USSR $\underline{28}$, 3 (1955)
    [English translation: Soviet Physics JETP $\underline{1}$, 2
    (1955)].

Moravcsik, M. J., Phys. Rev. $\underline{136}$, B624 (1964).

Morton, B. J., Gross, E. E., Hungerford, E. V., Malanify,
    J. J., and Zucker, A., Phys. Rev. $\underline{169}$, 825 (1968).

Moss, C. E., Ph.D. Thesis, California Institute of
    Technology (1968).

Nygren, D. R., Ph.D. Thesis, University of Washington (1968).

Phillips, R. H., and Crowe, K. M., Phys. Rev. 96, 484 (1954).

Phillips, R. J. N., Nucl. Phys. 53, 650 (1964).

Preston, M. A., Physics of the Nucleus, Massachusetts: Addison-Wesley Publishing Co., 1962.

Rose, P. H., and Galejs, A., "The Production and Acceleration of Ion Beams in the Tandem Accelerator", in Progress in Nuclear Techniques and Instrumentation, ed. by F. J. M. Farley. Amsterdam: North-Holland Publishing Co., 1967.

Ryan, J. W., Phys. Rev. Letters 12, 564 (1964).

Silverstein, E. A., Nucl. Inst. and Meth. 4, 53 (1959).

Slobodrian, R. J., Conzett, H. E., and Resmini, F. G., Phys. Letters 27B, 405 (1968).

Spiger, R. J., Ph.D. Thesis, California Institute of Technology (1967).

Thompson, D. R., and Tang, Y. C., Phys. Rev. 159, 806 (1967).

Tombrello, T. A., and Bacher, A. D., Phys. Letters 17, 37 (1965).

Tombrello, T. A., Spiger, R. J., and Bacher, A. D., Phys. Rev. 154, 935 (1967).

van Oers, W. T. H., and Slaus, I., Phys. Rev. 160, 853 (1967).

van Oers, W. T. H., Slaus, I., and Tombrello, T. A., Bull. Am. Phys. Soc. 10, 693 (1965).

Watson, K. M., Phys. Rev. 88, 1163 (1952).

Watson, K. M., and Brueckner, K. A., Phys. Rev. 83, 1 (1951).

Watson, K. M., and Stuart, R. N., Phys. Rev. 82, 738 (1951).

Whaling, W., Handbuch der Physik 34, 193 (1958).

Wu, T. Y., and Ashkin, J., Phys. Rev. 73, 986 (1948).

Yu, D. U. L., and Meyerhof, W. B., Nucl. Phys. 80, 481
    (1966).